Republic of Iraq
Ministry of Higher Education
And Scientific Research
University of Babylon

Theoretical and Experimental Investigation of Conduction Heat Transfer in Porous Media

A Thesis

Submitted to the College of Engineering ,University of Babylon in Partial Fulfillment of the Requirement for the Award of Degree of Master of Science in Mechanical Engineering

BY

Hussein Mahmood Jassim Lilu
B.Sc., (Mech. Eng.)

Supervised By

Dr. Adil Abbas Al-Moosawy

Assistant Professor

July 2008

جمهوريـــــــــــــة الـــعـراق
وزارة التعليم العالي و البحث العلمي
جامـــعـــــة بابل
كلية الهندســـة

دراسه نظريه وعمليه لانتقال الحرارة بالتوصيل في الأوساط المسامية

رساله
مقدمه إلى جامعة بابل كلية الهندســـة كجزء من متطلبات نيل شهادة الماجستير في الهندسة الميكانيكية

أعدت من قبل

حسين محمود جاسم ليلو

بكالوريوس

بإشراف

أ.م.د.عادل عباس علوان الموسوي

2008

بِسْمِ اللَّهِ الرَّحْمَٰنِ الرَّحِيمِ

يَرفَعِ ٱللَّهُ ٱلَّذِينَ ءَامَنُواْ مِنكُم وَٱلَّذِينَ أُوتُواْ ٱلعِلمَ دَرَجَٰتٍ وَٱللَّهُ بِمَا تَعمَلُونَ خَبِيرٞ

المجادلة (11)

صَدَقَ اللَّهُ العَظِيمُ

الخلاصه

في هذا البحث تم دراسة الانتشار الحراري وتأثير تغير الخواص الحراريه للمواد المساميه (Porous Media) والتي ِتركيبها يتألف من طورين مختلفين 0تم بناء ا نموذج رياضي بالأبعاد الكارتيزيه وبالحالة غير المستقره مع الزمن (Unsteady steady state) للمحاور الثلاث0من خلال هذا النموذج تم حساب التوزيع الحراري بالأبعاد الثلاث وبتغير الزمن 0تم استخدام الحل العددي في حل المعادلات ألمستخدمه لنموذج الانتشار الحراري حيث تم استخدام طريقة الفرو قات ألحديه (Finite Difference Method) باستخدام تقنية الحل البائن (Explicit Technique) حيث إن هذه ألطريقه أعطت تنبأ للنتائج بشكل جيد وعملت على تقليل الخطأ المدور 0خلال النموذج تم افتراض الطورين الصلب والمائع في حالة سكون 0كذلك تم حساب معامل يعبر عن متوسط قيمة ألموصليه الحرارية لهذين الطورين والذي يدعى بالموصليه الحراريه المؤثره (Conductivity Effective Thermal)0تم حساب هذا المعامل بالأعتماد على معادلتين تجريبيتين معتمده منالدراسات السابقه

تضمن العمل جانب الاختبارات ألعمليه لغرض اثبات صحة النموذج الرياضي الذي تم بناءه خلال هذا العمل حيث تم قياس درجات الحراره باتجاهات مختلفة للمواد المسامية ألمستخدمه في هذا البحث وهي اوكسيد المغنيسيوم (MgO-air)و (Chrome steel –air) بتركيبتين مختلفتين بنسبة المسامية (Porosity) تم استخدام اجهزه حديثه لعملية القياس مثل جهاز (Interface)الذي ياخذ الاستجابة نتيجة تسليط الحرارة وخزنها وثم معالجتها بواسطة برامجيات بنيت لهذا الغرض حيث تحول هذه الاستجابة إلى درجات حراره مع تغير الزمن 0

أثبتت النتائج ألعمليه دقة وتطابق الانموذج النظري مع العملي وهذا بسبب استخدام الاجهزه الحديثه التي تم بها القياس بزمن مشابه لزمن التحليل النظري0

ايضا خلال البحث تم قياس الموصليه الحراريه المؤثره وذلك بالاعتماد على قيم عمليه تمت بقياس اختلاف درجات الحراره لمواقع مختلفة السمك0تم حساب بعض العوامل الاخرى بعد الحصول على هذه النتائج مثل نسبة الموصليات الحراريه وكذلك تم قياس الموصليه الحراريه للمعدن الصلب الخالص (Pure Dense Material) 0

كذلك تم خلال البرنامج العملي قياس المساميه لنموذجي الكروم ستيل الذين تم بناءهما خلال العمل0

Abstract

Heat transfer mechanism was explained the heat diffusion through porous media, which its structure was combined by different phases .In the present work, a model in Cartesian coordinates with three dimensional unsteady state condition was built .The spatial and temporal temperature distributions within porous media have been determined by solving the unsteady state Fourier's heat conduction equation The model was solved by using explicit finite difference numerical method which would minimize the solutions errors. This model assumed that the two phases inside the materials (solid and fluid phases) are in case of stagnation .Also this model was estimated the two thermal conductivities of two phases by factor called effective thermal conductivity k_e .It was calculated by using two empirical equations which were published by literature .

Experimental work was done to prove that the theoretical results are more consistent .A computerize temperature meter (CTMO1) is used to record the temperature readings at different positions on the samples and with different time intervals .These advanced equipments were given a good experimental results in present work and gave reliable evidence for prediction results by theoretical model .

Also experimental work was included to measure the temperature distribution at different locations of thickness material in order to calculate the effective thermal conductivity numerically.

Two samples of porous media materials were used .These are MgO-air and Chrome steel –air system with two values of porosity .The porosity of two type of a Chrome steel –air system was measured through this work.

Due to the different structure of porous media material than normal material .It was found the better way to explain the response of porous media properties by calculating the thermal conductivity ratio (k) ,and dense thermal conductivity (k_{dense}).

Appendix A

A.1.Thermal Conductivity Correlation

Thermal conductivities for the solid and fluid phases are varied with a temperature (as a function of temperature) ,so this variation must be included in calculation of temperature distribution in porous media.

For the fluid phase (air) Perry and Chilton [A.1] gives a linear function of temperature,

$$k_{air} = b_o + b_1 T \qquad \text{.....(A.1)}$$

where

k_{air} = thermal conductivity, W/(m . K);

T = temperature, °C;

b_1 = adjustable constants of the model.

The results for dry air are :

b_o = 0.024042,

$b1$ = 7.4316 x 10-5

For MgO the studies showed that its thermal conductivity varied with temperature , Barry .B.Spencer et al [A.2] shows the flowing value of Mgo thermal conductivity at different temperature table (3-1).Kingery [A.3] et al shows a polynomial relation for MgO thermal conductivity and temperature at range (100-1200) c which is :

$$ks = a + bT + cT^2 + dT^3 + gT^5 (w/m.c) \qquad \text{...(A.2)}$$

and the constants are :

a=-2.523E+01

b=2.356 E-02

C=-2.108E-05

d =7.493E-09

g=7.012E+02

These values for Mgo and some other ceramics are showed by [A.3] in fig (A -1)

Table (A-1) Mgo thermal conductivity at different temperature.Ref. [A.2]

Component	Molecular weight	Density (g/cm^3)	Thermal conductivity [W/(m · K)]	Temperature (°C)
SiO_2	60.08	2.19 (amorph)	5.88[b]–11.07[c]	37.8
		2.26[d] at 25°C	5.19[b]–9.34[c]	93.3
			4.50[b]–9.00[c]	148.9
TiO_2	79.88	4.17[d] (white)	6.53 (refractory)	100.0
			5.54[b]–9.69[c]	37.8
			5.54[b]–8.30[c]	93.3
			5.54[b]–7.61[c]	148.9
Na_2O	61.98	2.27		
Al_2O_3	101.96	3.965[d] at 25°C	30.3 (refractory)	100.0
			32.35[b]–34.95[c]	37.8
			25.95[b]–27.68[c]	93.3
			22.32[b]–24.22[c]	148.9
CuO	79.55	6.3 – 6.49		
CaO	56.08	3.25 – 3.38[d]		
Cr_2O_3	151.99	5.21[d]		
MgO	40.30	3.58[d] at 25°C	36.0 (refractory)	100.0
			36.7	37.8
			31.8	93.3
			27.7	148.9

[a]*Source*: Weast, 1989, pp. D-40, E-7. Temperatures in the right-most column are

These values are used in this study to calculate effective thermal conductivity at any temperature .

for the second solid phase (Chrome steel 1.3-1.67%Cr) Eckert and Drake [A.4] present the following thermal properties

$$k_s = 61 \frac{W}{mK} \qquad \text{and} \qquad C_P = 460 \text{ (J/kg. K)}$$

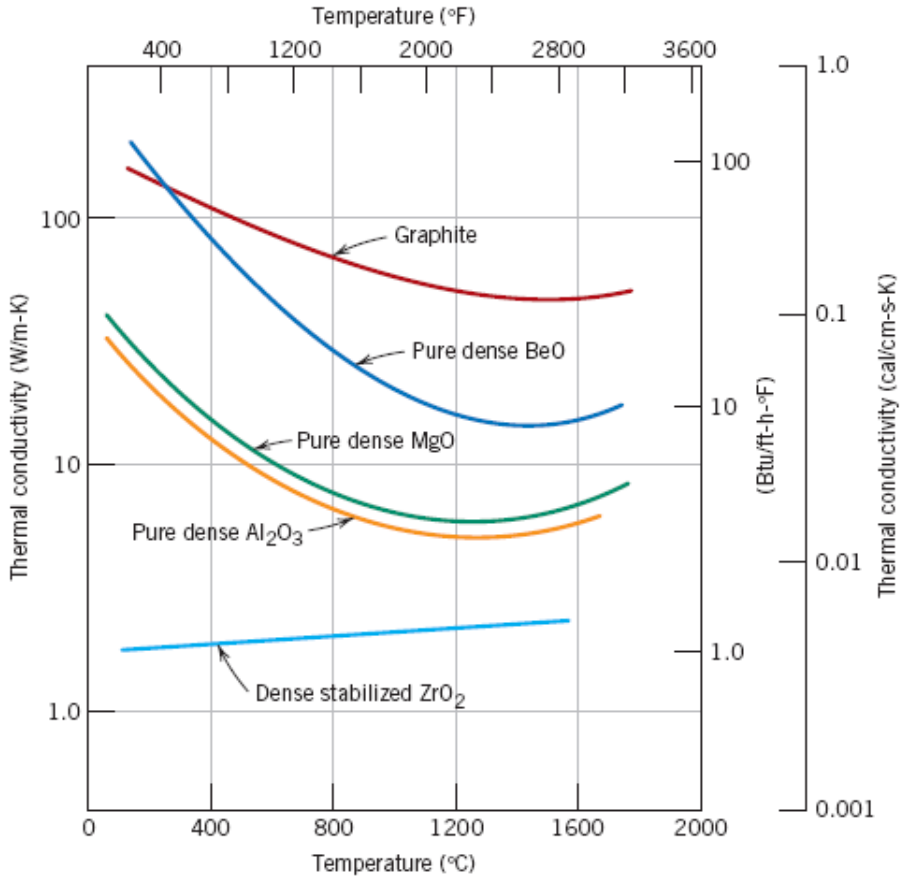

Fig (A-1)Thermal conductivity variation with temperature for selected ceramics .[A.3]

A.2. Convection Heat Transfer Coefficient

Convection heat transfer coefficient can be calculated according to the method for external flow over a flat plate Incropera & DeWitt [A.5] with knowledge of the fluid properties, conditions and flow geometry. The flow medium is dry air. Properties of air for calculating the heat convection coefficient (h)can be obtained from Table A.4 in Incropera & DeWitt (1981). For the air at a temperature of 100C (373K) and under 1 *atm* pressure, the required properties are:

$v = 23.665\times10^{-6}$ (m^2/s);

$k = 0.0319$ (W/m.K);

Pr = 0.695;

Where, ν ------- kinematic viscosity of air;

k ---- thermal conductivity of air;

Pr ---- the Prandtl's number;

then the average convection coefficients were:

$$h_{top} = 6.92 \text{ (w/m}^2\text{.K)}$$

$$h_{side} = 8.47 \text{ (w/m}^2\text{.K)}$$

References

[A.1] Perry and C.H. Chilton , Chemical Engineer s Handbook ,5th ed., McGraw-Hill Book Company, New York,1973

[A.2] Barry B. Spencer ,Hsin Wang and Kimberly K. Anderson "**Thermal Conductivity of IONSIV® IE-911™ Crystalline Silicotitanate and Savannah River Waste Stimulant Solutions**" Metals and Ceramics Division, ORNL Date Published , November 2000.

[A.3] W.D. Kingery "**Dependence of thermal conductivity on temperature for several ceramic materials**" book 2nd edition John Wily & Sons New York 1976.

[A.4] Eckert, E. R. G., and R. M. Drake Jr., "**Analysis of Heat and Mass Transfer**", McGraw -Hill, New York. (1972)

[A.5] Incropera ,F.P. and D.P. DeWitt." Analysis of heat and Mass Transfer " .4th Ed. school of Mechanical Engineering ,Purdue University .Jon Willey Sons, New York .1981

Appendix B

Temperature Readings

Table (B-1) temperature readings for Chrome steel-air matrix with heat flux 70000W/m^2

P1	P2	P3	P4	P5	P6	P7	P8	P9	P10	Time(sec)
63.3	51.2	55	32.1	35.6	40	39.9	63	37.8	41.2	0.769
65.6	51.7	51.5	32.1	35.4	39.4	39.8	56.9	35.7	40	6.417
65.9	52.2	51.2	32.1	35.5	39.8	39.9	57.2	35.8	40.4	12.078
66.6	52.8	51.6	32.2	35.5	39.8	39.8	57.7	35.8	40.6	17.738
66.9	53.4	53	32.2	35.5	39.7	40.1	57.7	36.2	40.8	23.449
67.2	54.2	52.7	32.2	35.6	39.9	39.9	57.4	36.6	41.2	29.160
66.5	54.9	53.6	32.2	35.7	40	40.2	57.5	36.9	41.7	34.878
67.4	55.5	54.3	32.2	35.8	40.1	40	57.3	37.4	42.2	40.640
74.5	56.2	54.4	32.2	35.9	40.1	40.3	57.2	38	42.7	46.300
85.7	56.9	55.4	32.2	35.6	39.8	43.4	60.9	39	43	51.960
82.2	57.3	56	32.2	35.8	39.5	41.1	57.9	38.3	43.2	57.617
75.2	58.2	56.3	32.2	35.5	39.7	40.6	58.1	38.3	43.4	63.328
74.1	58.8	57.6	32.3	35.8	40.1	40.2	57.9	39	43.8	69.039
74.5	59.5	57.8	32.3	35.9	40.1	40.4	57.7	38.7	44.1	74.750
75.6	60.1	59	32.3	35.8	40	40.1	57.8	39.3	44.7	80.460
76.5	60.7	59.3	32.3	35.9	40.4	40.2	57.9	39.4	44.8	86.179
77.4	61.5	60.2	32.3	35.7	40.2	40.3	58	39.8	45.2	91.890
77.5	62.2	60.3	32.3	35.8	40.6	40	57.5	39.9	45.8	97.550
78.4	62.9	61.9	32.3	35.7	40.4	39.9	57.5	40.1	46.4	103.257
79.1	63.7	62.8	32.3	36	40.3	40.1	57.6	40.4	46.5	108.917
81.6	64.1	63.5	32.3	35.8	40.6	40	57.8	40.7	47	114.679
82.6	65	64.2	32.3	35.9	40.8	40	57.8	40.9	47.3	120.398
83.3	65.7	64.7	32.4	35.8	40.5	40.3	57.1	41.9	47.8	126.160
84.2	66.4	65.2	32.4	36.1	40.3	40.6	57.3	41.6	48.2	131.867
85.3	66.9	65.7	32.4	35.9	40.8	40.4	57.6	41.6	48.8	137.527
86.4	67.5	67.1	32.4	35.9	40.5	40.2	58.1	43	49.4	143.187
87.7	68.1	66.4	32.4	35.8	40.5	40.6	57.8	42.6	49.6	148.847
90.4	68.7	67.7	32.4	35.7	39.9	40.5	58.2	42.9	50.1	154.558
90.4	69.3	68.6	32.5	35.8	39.9	40.5	58.1	44.4	50.8	160.218
94.6	70.2	68.9	32.5	35.7	39.8	41.2	58.8	43.5	51	165.980
94.3	70.7	69.1	32.5	35.9	39.8	40.8	58.4	44.9	51.6	171.699
97.5	71.5	69.1	32.5	35.8	39.9	41	58.7	44.2	52.1	177.460
102.6	72.4	70.9	32.6	35.7	40.1	41.4	58.6	45.1	52.4	183.117
98.6	73.2	72.1	32.6	35.6	39.9	40.8	58.3	45.6	53	188.777

106.5	74.2	73.1	32.6	35.5	40.1	41.6	59.2	45.2	53.3	194.429
99.2	75	74.9	32.6	35.6	39.7	41.5	59.5	45.5	54	200.089
105.6	75.6	73.6	32.7	35.7	40.1	41.3	58.3	45.7	54.5	205.750
116.3	76.1	76.3	32.7	35.9	39.8	41.8	59.7	46.8	54.9	211.460
120.2	77.2	76.6	32.6	35.7	40.1	42.2	59.3	47.2	55.5	217.167
107.1	77.8	76	32.7	35.6	40.3	41.2	59.9	47.8	56	222.890
121.2	78.9	77.3	32.7	35.7	40	42.3	60.6	47.4	56.7	228.597
122.9	79.5	77.5	32.7	35.6	40	42	59.5	49	57.2	234.257
112.4	80.1	77	32.7	35.6	40	41.6	59.6	49.6	57.8	239.968
114.2	81.1	78.1	32.7	35.8	40.1	41.7	58.6	49.4	58.6	245.628
147.3	82	79.8	32.7	36	39.9	43.2	61.5	50.2	59.4	251.339
115.6	82.2	79.5	32.8	35.7	40.1	41.6	59.8	49.2	59.5	257.050
115.6	83	81	32.8	35.7	40.3	41.3	58.4	50.4	60.3	262.757
114.4	83.5	81.3	32.8	35.6	40.1	41.8	59.5	50.9	60.7	268.468
130.5	84.6	81.4	32.8	35.9	40	42.2	60.2	51	61.7	274.238
122.7	84.8	81.8	32.8	35.5	40	41.7	59.7	51.2	61.9	279.898
121.3	85.6	82.9	32.8	35.7	40.2	41.8	59.2	51.7	62.6	285.558
124.5	86.4	82.8	32.8	35.9	40.1	41.9	59.1	52.4	63.5	291.269
122	87	82.7	32.8	35.6	40.1	42.3	59.9	53.7	63.7	296.929
122.5	87.6	82.5	32.9	35.7	40.4	41.7	58.8	53.4	64.5	302.687
124.8	88.3	84.6	32.9	35.6	40.3	41.5	59.4	53.1	64.9	308.410
126.9	88.8	85	32.9	35.6	40.2	41.9	59.8	53.8	65.5	314.167
128.1	89.9	85.2	32.9	35.8	40.3	41.6	59	53.2	66.3	319.828
127	90.3	86.8	32.9	35.7	40.3	41.7	59.1	54.8	66.8	325.488
130.5	91	87.9	32.9	35.9	40.1	42	59.9	53.7	67.4	331.140
137.9	91.5	88.7	32.9	35.7	40.3	43.1	61.2	55.9	67.7	336.800
147.3	92.4	89.5	32.9	35.6	40.5	43.2	60.8	56.4	68.2	342.460
130.2	93.1	88.6	33	36	40.3	41.8	59.1	55.2	68.7	348.167
143.6	93.6	90.5	33	35.7	40.1	43	60.2	55.3	69.2	353.878
143.1	94.4	91.1	33	35.7	40.3	42.5	59.8	56.5	69.7	359.597
133.5	95.1	90.8	33	35.8	40.3	41.8	59.2	57.6	70.3	365.308
131.8	95.8	90.9	33.1	35.8	40.3	41.6	60	57.9	70.7	370.968
130	96	91.8	33.1	35.6	40.4	42.1	59.3	58.1	71.2	376.679
131.2	96.5	91.7	33.1	35.6	40.4	41.9	59.1	58.1	71.7	382.328
130.6	97.2	92.1	33.1	35.8	40.6	41.6	58.6	59.8	72.5	387.988
134.2	97.8	91.5	33.1	35.6	40.2	42.6	60.2	60.3	73.5	393.699
135.6	98.6	90.9	33.1	35.7	40.3	42	60	61.2	74	399.417
149.6	99.1	92.4	33.1	35.6	40.1	42.8	61.1	61.6	74.8	405.179
136	99.7	92.9	33.2	35.8	40.3	41.5	59.9	60.1	75.4	410.839
146.2	100.1	94.3	33.2	35.9	40.7	42.4	60.1	61.2	76	416.500
133.3	100.7	94.2	33.2	36.1	40.7	41.4	58.8	61.7	76.5	422.160
136.4	101.1	95.4	33.2	35.8	40.6	41.7	59.6	60.6	77	427.917
138	101.7	94.9	33.2	35.8	40.5	41.6	60	62.3	77.6	433.578

138.2	102.1	95.2	33.3	35.8	40.7	41.5	59	61.9	78.3	439.289
138.8	102.9	96.3	33.3	35.7	40.6	41.9	59.8	61.4	78.7	445.000
140.7	103.1	97.5	33.3	35.7	40.9	42.3	59	62	79.2	450.718
138.3	103.8	98	33.3	36	40.5	41.5	59.6	62.7	79.6	456.367
141	104.2	98.7	33.3	36	40.7	41.7	59.3	63.7	80.2	462.027
141.5	104.9	97.9	33.3	36	40.8	42.2	59.1	64.2	80.8	467.687
143.9	105.6	99.1	33.3	36	40.6	41.8	60.2	62	81.3	473.347
142.9	106.2	98.9	33.3	35.9	40.7	41.8	59.9	64.2	81.7	479.058
147.3	106.7	100.1	33.3	35.8	40.8	42.1	60.3	63	82.2	484.769
144	107.2	101.1	33.4	35.8	40.8	42.7	60.1	63.4	82.8	490.480
143.6	107.6	100.9	33.4	35.8	40.8	42.6	59.3	64.8	83.3	496.199
147	108.1	101.5	33.4	35.8	40.7	42.7	59.6	64.8	83.9	501.910
146.7	108.6	100.1	33.4	35.8	40.9	42.9	59.2	66.5	84.4	507.558
147.6	109.3	99.4	33.4	35.8	41.2	41.9	59.3	68	84.9	513.218
150.2	109.9	101.1	33.4	35.7	40.9	42.6	60.1	67.2	85.5	518.878
153.6	110.3	101.6	33.4	35.7	40.9	42.6	59.9	67.9	86.1	524.539
149.2	110.8	102.5	33.5	35.8	41	42.3	59.8	66	86.5	530.250
148.1	111.1	103.1	33.5	35.9	40.9	41.9	59.5	66	87.1	535.960
151.6	111.6	103.1	33.4	35.7	40.8	42.1	60.3	68.6	87.7	541.668
153.5	111.8	102.8	33.5	36	41.1	42.4	59.5	67.5	88.6	547.328
154.7	112.6	103.9	33.5	35.9	40.9	42.8	60.5	65.9	88.9	552.988
150	113	104.1	33.6	35.8	41	42.6	60.4	69	89.4	558.648
153.9	113.4	102.2	33.5	35.9	41	42.3	60.4	69.8	89.7	564.359
153.7	113.9	102.9	33.6	35.7	41	42.4	60.6	69.6	90.2	570.019
153.7	114	103	33.6	35.8	41.2	42.2	60.1	69.9	90.7	575.890
154.6	114.4	104	33.6	35.8	41.4	42.4	59.3	70.1	91.2	581.597
157.2	115	102.6	33.6	35.7	41.4	42.3	59.3	70.9	91.6	587.320
159.5	115.4	103.8	33.6	35.7	41.2	43.1	60.8	72.1	92.2	593.027
163.9	115.7	104.6	33.6	35.8	41	43.3	60.2	72	92.9	598.687
164.8	116.1	104.4	33.6	35.9	41.1	43.1	60.2	73	93.5	604.398
161.7	116.7	104.3	33.6	35.8	41.2	42.6	60.8	71.9	93.8	610.058
162.1	117.3	104.5	33.7	35.8	41.1	42.7	60.9	72.5	94.2	615.769
162.8	117.6	105.3	33.7	36.1	41	42.6	61	72.6	94.9	621.539
162.2	117.9	105.2	33.7	36	41.1	42.6	61	73.9	95.4	627.300
162.4	118.4	105.4	33.7	36	41.2	42.7	61.1	73.7	96.1	633.007
162.2	118.8	106.4	33.7	35.8	41.1	42.7	60.9	72.8	96.3	638.668
164.5	119.1	106.6	33.8	35.8	41.2	42.7	60.6	72.5	96.6	644.328
162.4	119.5	106.7	33.8	35.9	41.3	42.2	60.8	72.6	97	649.988
163.4	119.8	107.1	33.8	35.9	41.4	42.4	59.5	73.3	97.4	655.750
163.6	120.3	107.4	33.9	35.8	41.3	42.6	60.4	73.6	97.6	661.410
165.8	120.6	106.9	33.8	35.9	41.6	42.5	59.9	76.2	98.3	667.117
166.1	121.3	105.9	33.8	35.9	41.5	42.8	60.6	76.3	98.6	672.839
165.3	121.3	107.2	33.8	35.8	41.4	42.8	60	73.5	98.8	678.597

161.8	121.4	107.5	33.8	35.9	41.4	42	60.1	76.1	99	684.257
162	121.9	108.5	33.8	36.1	41.4	42.6	59.6	75.4	99.7	689.918
155.8	122.3	108.9	33.9	36	41.5	41.7	59.2	73.2	99.9	695.570
161.9	122.5	108.4	33.9	35.9	41.6	42.4	59.3	77.3	100.4	701.230
160.5	123.2	108.8	33.9	35.9	41.4	42	60.4	76.3	100.6	706.890
164.2	123.4	108.8	33.9	35.9	41.3	42.4	60.4	76.9	101	712.597
193.7	124	110.3	33.8	36.1	41.5	44	62.7	78.6	101.4	718.308
172.2	124	109.7	33.9	35.7	41.6	42.4	60	78.5	101.3	724.027
177.3	124.3	110.1	33.9	35.8	41.4	42.8	61	79.8	101.3	729.738
159.6	124.4	107.7	33.9	35.9	41.6	41.8	59	82.6	101.5	735.398
160.2	124.8	109	33.9	36	41.8	41.7	58.8	82.7	101.9	741.109
157.3	125.1	109.6	33.9	36.2	41.8	41.4	58.7	82.2	102	746.769
178	125.2	111.3	33.9	35.9	41.6	42.8	59.7	82.6	102.3	752.480
164.8	125.5	111.4	33.9	36.1	41.6	42	60.2	84.2	102.5	758.187
156.9	125.9	112	33.9	36.1	41.7	41.1	59.3	84.3	102.1	763.898
156.8	126.1	111.7	33.9	35.9	41.6	41.2	59.2	83.6	102.5	769.609
157.4	126.6	112	34	35.9	42	41.2	59.4	82.3	102.8	775.269
155.3	126.7	112	34	36.1	41.7	40.8	59.1	84.5	103.1	780.929
157.8	126.6	112	34	36	42.1	41.4	58.4	84.9	103.8	786.589
155.7	126.8	112.3	34	36	42.4	41.1	58	84.9	104	792.300
154.7	127.3	112.6	34	36	42.2	41.5	58	84.3	104.7	797.960
156.7	127.8	112.7	34	36.2	42.2	40.9	58.5	85.2	105.2	803.718
156	127.8	111.1	34.1	35.9	42.4	41.2	58.3	85.8	105.3	809.437
156.5	128.3	112.4	34	35.9	42.1	41.6	59.2	85.8	105.6	815.199
159	128.3	112.6	34	35.7	42.3	40.8	59	86	106	820.859
157.1	128.4	112.7	34	36	42.5	41.5	58.5	85.1	106.5	826.519
155.8	128.7	112.5	34.1	36	42.7	40.4	57.9	87.2	106.8	832.168
157.6	129.1	111.8	34	35.9	42.1	41.5	59	85.2	107.3	837.828
156.9	129.4	111.9	34	36.2	42.4	41.3	58.3	85.7	107.8	843.488
158.4	129.5	111.3	34.1	35.7	42	41.8	59	85.7	107.9	849.199
154.9	129.7	112	34.1	35.9	42.3	41.5	58	84	108.2	854.910
158.1	130.2	112.6	34.1	36	42.1	41.3	59.3	84.7	108.7	860.628
157.1	130.2	112.9	34.1	36	42.3	41.4	58.1	84.5	109.2	866.339
154.8	130.5	113.1	34.1	36	42	41.7	59.9	85.6	109.4	872.000
161.9	130.8	113.2	34.1	36.1	41.9	41.7	59.4	88.5	109.6	877.710
154.8	130.9	112.8	34.1	36.1	42.5	40.8	58.2	86	110.1	883.527
154.4	131.1	112.7	34.1	36.2	43.1	40.9	57.5	85.8	110.4	889.187
157.5	131.4	113.3	34.1	36	42.3	41.2	59.5	86.3	110.7	894.898
156.3	131.5	113.1	34.2	36.2	42.4	40.8	58.9	85.8	110.9	900.609
155.6	131.6	112.6	34.2	36.1	42.7	41.7	58.2	88.4	111.1	906.320
155.9	131.7	112.4	34.2	35.9	42.5	41.3	58.4	89	111.2	911.980
155.9	132.1	112	34.2	36.1	42.7	40.8	57.9	89.2	111.4	917.640
155.6	132.2	111.8	34.2	36.2	42.7	41	58.3	91.3	111.5	924.390

155.9	132.4	111.8	34.2	36.1	42.7	41.2	58.4	91.2	111.8	930.050
155.5	132.6	111.7	34.2	36.2	43.2	41.1	57.6	90	112	935.710
156.1	132.8	112.4	34.2	36.3	42.7	41	58.5	87.7	112.3	941.480
156.7	133.1	111.7	34.2	36.2	42.9	41	57.9	91	112.7	947.238
157.7	132.9	112.3	34.2	35.8	42.9	41.2	58.1	89.1	112.7	952.960
159.7	133.4	112.2	34.2	36.3	42.7	41.2	58	86.5	113.2	958.668
158.7	133.5	112.1	34.2	36	42.8	41.2	58.7	87.9	113.1	964.328
159.2	133.5	112.5	34.2	36.1	42.8	41.7	58.2	89.6	113.5	970.039
160	133.9	112.5	34.2	36.2	42.7	41.3	58.8	88.8	113.8	975.687
160.1	134	112.1	34.3	36.2	42.7	41.2	59.1	90.9	114	981.347
159.7	134.1	112.2	34.2	36	43.1	41.6	58.3	87.9	114.1	987.117
160	134.5	111.9	34.2	36	42.9	40.7	58.2	90.9	114.4	992.828
160.5	134.7	111.4	34.2	36	43.1	41.3	58.3	91	114.9	998.539
160	134.6	112.7	34.3	36	43.1	41.6	58.5	90.1	115	1004.199
160.2	134.6	111.7	34.3	36.1	42.9	41.9	58.2	90.2	115.2	1009.859
160.7	134.6	112.9	34.3	36	42.8	41.6	58.7	90.9	115.3	1015.519
160.7	135	113.2	34.3	36.1	42.8	41.3	58.7	89.7	115.7	1021.230
161.4	135	112.8	34.3	36.2	42.8	41.6	59.2	92.3	115.6	1026.890
160.6	135.2	112.6	34.3	36	42.9	41.6	58.9	92	115.8	1032.648
160.2	135.4	112.8	34.3	35.9	43.3	41.3	58.8	90.4	116.1	1038.359
160.7	135.4	113.5	34.3	36.1	43.1	41.2	58.3	92.4	116.1	1044.078
161.5	135.8	113.7	34.3	36.3	42.9	41.4	58.5	91.2	116.5	1049.730
161.5	135.9	113.8	34.3	36	43.1	41.3	58.8	93.5	116.5	1055.390
160.6	136.1	112.9	34.4	36.2	43	41.2	58.8	93.5	116.7	1061.050
160.6	136.2	113.4	34.4	36.1	43.4	41.3	58.4	92	116.8	1066.711
160.9	136	113.3	34.4	36.1	43.3	41.2	58.3	94.2	116.8	1072.418
160.5	136.2	113.6	34.3	36.2	43.1	41.3	59	92.4	117	1078.128
161.1	136.3	113.4	34.4	36.3	43.2	41.7	58.6	92.2	117	1083.839
162.4	136.5	113.3	34.4	36.1	43.4	41.2	58.1	92.3	117.3	1089.558
166.3	136.8	112.5	34.4	36.1	43.1	42.3	59.1	92.1	117.4	1095.269
167.1	136.7	112.5	34.4	36.1	43.3	41.5	58.3	92.5	117.8	1100.929
163.4	137	112.1	34.4	36.1	43.2	41.7	58.4	91.3	117.9	1106.640
163.5	136.9	112.6	34.4	36.1	43.4	41.6	58.2	91.5	117.8	1112.289
163.6	137.1	112.6	34.4	36.3	43.4	41.2	58	90.9	118.1	1117.949
162.9	137.1	112.1	34.4	36.3	43.4	41.2	58.3	93.7	118.2	1123.660
161.3	136.9	111.5	34.4	36.1	43.2	41.2	58.6	93.6	118.4	1129.378
162.1	137.2	112.2	34.4	36.2	43.8	41.1	57.8	92.6	118.8	1135.140
164.7	137.4	112.7	34.4	36	43.5	41.3	58.3	90.7	119.2	1140.800
161.1	137.5	112	34.4	36.1	43.3	40.9	58.8	93.4	119.4	1146.461
161.3	137.6	111.2	34.4	36.2	43.7	41.4	58.2	93.5	119.5	1152.117
161	137.8	111.6	34.4	36.3	43.3	40.9	58.4	94	119.7	1157.828
161.2	138.1	111.2	34.4	36.5	43.5	41.1	57.8	94.3	119.7	1163.488
160.8	137.9	112	34.4	36.4	43.5	40.7	57.8	94.8	119.6	1169.250

161.5	137.8	111.2	34.5	36.2	43.7	41.4	58.1	95.6	119.5	1174.961
162.2	138	111.7	34.4	36.1	43.3	41.5	58.7	94.5	119.9	1180.679
162.6	138.5	111.1	34.5	36.3	43.5	41.2	57.9	93.1	120	1186.390
163.8	138.4	111.2	34.5	36	43.8	41.4	58.1	93.3	120.4	1192.050
164.8	138.6	110.9	34.5	36.1	43.6	41.4	58.3	93.3	120.6	1197.757
161.8	138.7	111.4	34.5	36.1	43.8	40.6	58.5	94	120.7	1203.418
161.1	138.7	110.6	34.5	36.3	44.1	41	57.9	94.9	120.8	1209.128
161.5	138.8	110.9	34.5	36.2	43.7	41.2	58.1	93.8	120.9	1214.839
161.5	139	111	34.5	36.3	43.8	40.8	57.6	93.7	121.4	1220.550
161.8	138.8	110.9	34.5	36.2	44	41.3	57.9	94.4	121.5	1226.269
162.5	138.8	111.3	34.5	36.2	43.7	40.9	58.3	93.9	121.3	1231.980
161.9	138.9	111.3	34.5	36.5	43.8	40.9	57.4	93.1	121.6	1237.628
161.8	138.8	111.6	34.5	36.2	43.9	40.9	57.6	92.3	121.7	1243.289
162.4	138.9	112.1	34.6	36.3	43.6	41	58.2	93.4	121.8	1248.949
162	139	111.9	34.6	36.1	43.5	41.2	58.3	93.6	121.8	1254.609
161.9	139.1	111	34.5	36.5	43.9	41	57.8	93.9	122.1	1260.367
161.6	139	110.9	34.5	36.3	43.9	40.9	57.5	94.6	122	1266.089
162.2	139	110.3	34.5	36.2	43.7	40.9	58	95.6	122.2	1271.847
162	139.2	110.6	34.6	36.3	43.6	40.8	58.4	94.6	122.4	1277.507
161.7	139.1	111.2	34.6	36.2	44.2	41.3	57.7	95.3	122.3	1283.168
161.7	139.2	111.3	34.6	36.2	43.7	41.2	58.2	95.6	122.3	1288.828
161.6	139.2	110.2	34.6	36.2	43.8	41.4	58.4	96.3	122.4	1294.539
161.8	139.3	110.5	34.6	36.2	43.9	41.4	58	96.5	122.7	1300.187
162	139.7	110.6	34.6	36.5	43.7	41	57.9	98.7	122.9	1305.910
162	139.6	110.2	34.6	36.2	43.7	41	58.8	97.2	122.9	1311.617
161.8	139.7	110.5	34.6	36.2	44	41.1	58.5	97.5	123.1	1317.328
162.2	139.9	109.7	34.6	36.4	44	41.3	57.4	98.1	123.1	1322.988
162.8	139.9	109.8	34.6	36.2	43.8	41.5	58.3	97.3	123.3	1328.648
180.5	140	110.7	34.6	35.8	43.3	42.6	60.4	96.8	123.3	1334.359
182.9	140.3	111	34.6	35.9	43.2	43.2	60.3	97.6	123.4	1340.019
183.7	140.4	110.8	34.6	35.9	43.3	43.2	60.3	95.8	123.5	1345.730
186	140.3	110.2	34.6	35.9	43.5	42.9	60.6	96.3	123.5	1351.437
187	140.4	110.7	34.6	35.7	43.2	42.8	60.5	96.9	123.7	1357.148
189.4	140.7	110.4	34.6	36.1	43.2	42.7	60.1	97.1	123.8	1362.859
187.4	140.3	110.3	34.6	36	43.3	43	60.7	97.1	123.6	1368.519
188.9	140.3	110	34.7	36	43.5	43.1	60.3	96.7	123.6	1374.179
188.6	140.5	111	34.7	36	43.6	43.1	60.5	95.9	123.8	1379.839
188	140.2	111.5	34.7	36	43.3	43	61	96.6	123.6	1385.550
189	140.2	111.4	34.7	36.1	43.3	43.5	60.6	97.8	123.7	1391.211
190.7	140.3	111.2	34.7	36	43.5	43	60.2	97.7	123.5	1396.968
189.4	140.1	111.1	34.7	35.9	43.4	43	61	97.9	123.7	1402.687
189.5	140.3	110.6	34.7	36	43.3	43.2	60.9	97.2	123.8	1408.449
189.2	140.2	110.7	34.7	35.9	43.2	43.1	60.8	96	123.8	1414.109

190.7	140	111.4	34.7	36.1	43.5	42.9	60.1	95	123.5	1419.769
189.2	140.1	110.8	34.7	36.2	43.4	43.1	60.4	95.6	123.7	1425.418
188.5	140.2	111	34.8	36.1	43.6	42.9	60.4	95.2	123.7	1431.078
188.7	140.1	111.1	34.8	36	43.6	43.4	60.5	94.1	123.5	1436.738
190	140.3	111.2	34.8	36.1	43.5	43.8	61.1	94.7	123.4	1442.449
192.3	140.3	111.1	34.8	36.1	43.4	43.6	60.6	95.8	123.6	1448.160
190.7	140.2	111.2	34.8	36	43.4	43	60.9	95.7	123.4	1453.878
191.1	140.1	109.9	34.8	35.9	43.5	43	60.7	96.2	123.5	1459.589
191.6	140.2	109.4	34.7	36	43.6	43.3	60.5	97.1	123.5	1465.250
191.4	140.2	109.7	34.8	36	43.5	43.1	60.5	96.5	123.4	1470.961
189.2	140	109.2	34.8	35.8	43.3	43.2	60.6	96.3	123.6	1476.617
190.3	140.2	108.9	34.7	36.1	43.7	43.2	60.5	96.5	123.7	1482.328
190.6	140.1	109.2	34.8	36.2	43.4	43.3	60.5	95.3	123.9	1488.039
189.6	140.1	109.7	34.8	36	43.6	43.4	60.6	96.1	124	1493.918
191.2	140.1	109.2	34.9	36.1	43.5	42.8	60.6	96.1	124.2	1499.628
190.9	140.1	108.7	34.9	36.1	43.8	43.2	60.2	95.5	124.1	1505.289
191.2	140.2	109.2	34.9	36.2	43.6	43.2	60.4	96.3	124.2	1511.000
189.2	139.9	110.1	34.9	36	43.7	43.2	61	97.6	123.9	1516.660
190.5	139.6	110.6	34.9	36	43.8	43.1	60.5	98	123.8	1522.367
190.5	139.7	110.3	34.9	36	43.5	43.2	60.5	98.3	123.9	1528.027
188.8	139.9	109.9	34.9	36	43.5	43.4	60.6	98	124.1	1533.789
188.9	139.8	108.9	34.9	36.2	43.6	43.2	60.5	96.9	124.4	1539.507
189.1	140	109.3	35	36.1	43.6	42.9	60	95.9	124.6	1545.269
189.4	139.9	109.8	34.9	36	43.9	43.5	60.4	96.6	124.7	1550.929
188.1	139.9	109.4	35	36	43.7	43	60.2	96	124.7	1556.589
189.5	140.4	108.9	35	36.2	43.8	43.4	60.4	98	124.9	1562.238
188.4	140.2	108	34.9	36.1	43.7	43.4	60.6	97	124.9	1567.898
191	140	108.4	34.9	36.1	43.9	43.4	60.5	96.6	125	1573.558
189.5	140.1	107.4	34.9	35.9	44	43.3	60.5	96.5	125	1579.269
189.4	139.9	107.5	35	36	43.9	43.4	61	95.7	124.9	1584.980
188.9	140	107.8	35	36.2	43.7	43.1	60.4	95.6	125	1590.699
190.4	139.9	108.4	35	36	43.9	43.2	60.3	96	124.9	1596.410
190.4	140	108.4	35	36.2	43.8	43.5	60.5	92.8	125.1	1602.070
188.5	140	109.4	35	36.1	43.8	43.2	60.3	93.3	125.2	1607.777
188.4	139.9	108.7	35	36.2	43.8	43.4	60.4	96.1	125.1	1613.429
187.5	139.9	108.7	35	36.1	43.5	43	60.2	94.7	125.1	1619.089
187.8	140	108.1	35	36	43.7	43.6	60.6	95.7	124.9	1624.800
187.8	139.9	107.8	35	36	43.6	42.7	60.7	94	125.1	1630.519
187.9	140	107.9	35	35.9	43.9	43.1	60.6	95.4	124.9	1636.277
186.5	140.1	108.4	35	36	43.8	42.8	60.8	92.9	125.3	1641.937
186.7	140.1	109	35	36	43.8	42.7	60.6	94.6	125.2	1647.597
187.4	140	108.6	35	36.1	43.9	43.2	60.6	95.8	125.1	1653.257
186.4	139.9	107.9	35	36	43.7	43.2	60.6	95.7	125.1	1658.968

187.2	140	106.3	35	36	43.7	43.4	60.9	96.1	125.1	1664.628
187.3	139.9	106.7	35	36.1	43.6	43.5	60.5	95.3	125.1	1670.390
188.7	139.9	106.6	35	36.2	43.8	43.5	60.4	95.5	125	1676.097
186.4	139.7	107.1	35	36.2	43.6	43.1	60.1	94.1	125.2	1681.820
186.8	139.8	106.9	35	36.1	43.7	43.1	60.9	95.5	125.3	1687.468
187.6	139.7	107.5	35	36	43.7	43.3	60.7	96.2	125.3	1693.128
186.5	139.7	106.9	35	36.2	43.8	43.3	60.9	96.5	125.3	1698.789
187.8	140	105	35	36.3	43.9	43.5	60.5	96.6	125.4	1704.449
186.8	139.8	106.7	35	36	44	43.1	60.4	94.9	125.3	1710.160
186.8	139.8	107	35	36.1	44.2	43.3	60.2	95.1	125.1	1715.867
186.3	139.7	106.9	35	36.1	43.8	43.2	60.9	93.6	125	1721.578
186	139.6	106.6	35	36.2	43.7	43.1	60.5	94.1	124.7	1727.300
186	139.6	104.9	35	36.1	43.9	43.1	59.7	95.4	124.7	1733.007
184.5	139.5	105.8	35	36.1	43.9	43.2	60.1	94.2	124.7	1738.660
184.9	139.6	106.1	35	36.1	44.2	43.4	60.3	92.8	124.8	1744.320
184.6	139.5	106.4	35	36.1	44	43	60.6	94.2	125	1749.980
187	139.5	106.8	35	36.1	44	43.4	60.5	93.2	124.9	1755.640
187.2	139.3	107.4	35	36.3	44	43.8	60.4	94.6	124.5	1761.347
187.3	139.2	106.8	35	36.3	43.8	43.2	60.6	95.3	124.6	1767.058
187.2	139.4	106.6	35	36.2	43.9	43.7	60.7	94.5	124.4	1772.769
187.7	139.4	105.8	35	36.4	43.9	43.5	61.2	93.7	124.6	1778.429
187.8	139	105	35.1	36.1	44.1	43.2	61	94.7	124.4	1784.089
185.7	139	105.3	35.1	36.4	44	43.7	60.5	93.5	124.5	1789.750
187.5	139	105.5	35.1	36.1	44.1	43.4	61.1	94.2	124.5	1795.507
186.5	139	105.2	35.1	36.2	43.8	43.4	60.8	93.8	124.5	1801.328

DEDICATION

TO MY

FATHER AND MOTHER SPIRIT

TO MY

FAMILY

With Respect and Love

CERTIFICATION

I certify that this thesis titled ***"Theoretical and Experimental Investigation of Conduction Heat Transfer in Porous Media"*** was prepared by **Mr. Hussein Mahmood Jassim** under my supervision at the University of Babylon as a partial fulfillment of requirements for the degree of **Master of Science in Mechanical Engineering (Power Mechanics).**

I recommend that this thesis be forwarded for examination in accordance with the regulation of the University of Babylon.

Signature
Dr.Adil.A.AL-Moosawy
Assistant Professor
(Supervisor)

ACKNOWLEDGMENT

*First of all, all praises are due to **ALLAH** who gave me the ability and desire to complete this work*

*I would like to express my deep thanks and gratitude to my supervisor **: Dr.Adil.A.AL-Moosawy** and for all staff of mechanical engineering and especially for the staff of power plant laboratory*

I record my deep thanks for my family especially for my wife and my friends for their help during this work

Hussein

/ / 2008

Introduction

1.1. General

A porous media is a solid contains a void space . There are essentially two types of porous solids ;those produced by packing or sintering solid particles or cylinders together and those by casting or foaming a material during solidification The final product consists of interspersed regions of solid and fluid or (void) . Figure(1-1) explains an approximate imagination of natural porous media construction, and figure (1-2) shows a sample of man made solid – fluid matrix to analogue porous media ,figure (1-3) shows a real porous media which is an aluminum foam .Alternatively, porous media can also consist of fibrous materials. Many examples of these types of media have both natural and man-made applications. In particular, when air is trapped in the void space of fibrous porous media, the overall thermal conductivity of the medium is very low.

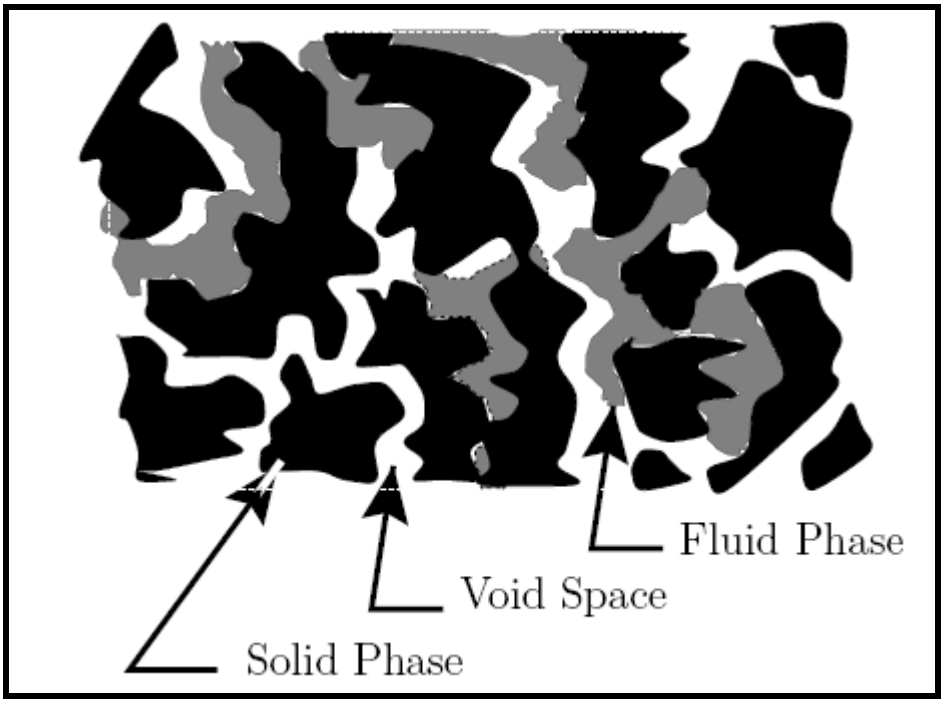

Fig(1-1) natural porous media structure .Ref. [1].

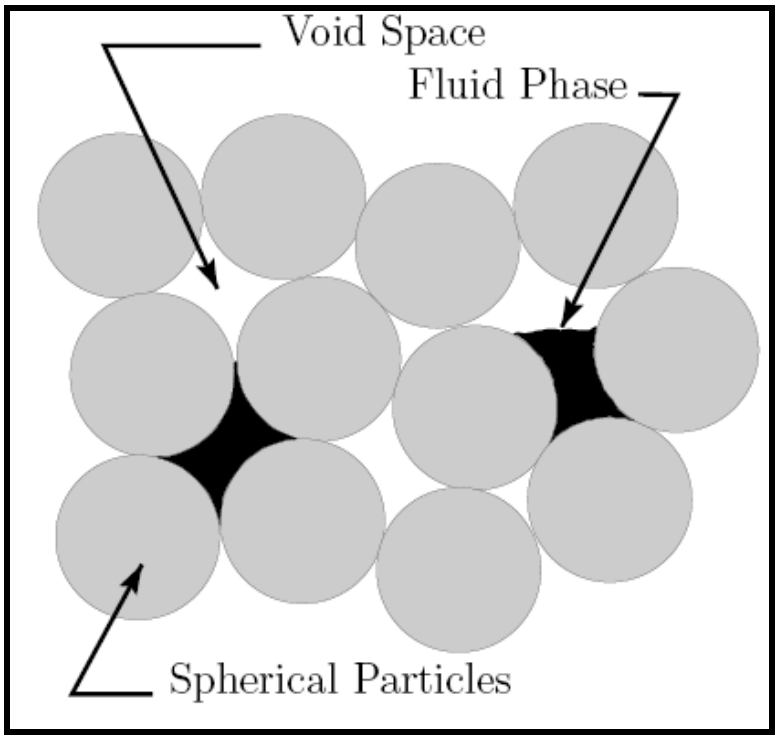

Figure (1-2) man made porous media structure Ref.[1]

Analysis of fluid flow and heat transfer in a porous medium has been a subject of continuous interest during the past decades because of the wide range of engineering applications. In addition to conventional applications such as solar receivers, building thermal insulation materials, packed bed heat exchangers, and energy storage units, investigators have found new applications in the engineering field of micro scale heat transfer [3]. For example, smaller flow passages and fins are needed for compact heat exchangers and electronics cooling. Table (1-1) shows some use of porous material in industry.

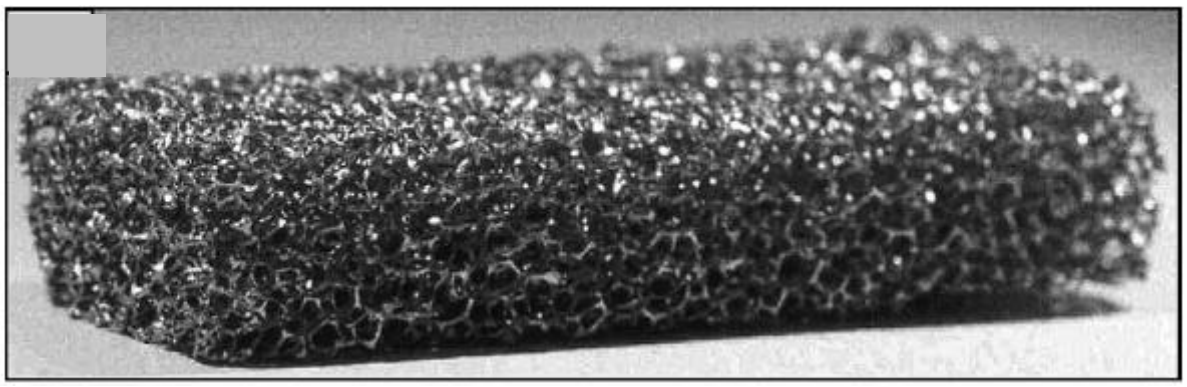

Figure (1-3) Open-cell aluminum foam (T-6106 alloy) in its as-manufactured state with a porosity of $\phi = 92\%$ and approximately 6 mm diameter pores ($k_s \approx 200 \mathrm{Wm^{-1}\,K^{-1}}$) .Ref.[2].

1.2. Heat Transfer in Porous Media

Heat transfer in porous media has been the subject of many investigations due to the increasing interest in chemical catalytic reactors, building thermal insulation, heat exchangers, petroleum reservoirs and geothermal operations.

Table (1-1) some uses of porous media .Ref. [4].

Material	Uses
(aluminum oxide) Al_2O_3	Spark-plug insulating bodies, substrates for microelectronic packaging
(magnesium oxide) MgO	electrical insulators, refractory brick
(Silicon dioxide) SiO_2	Cookware, optical fibers
(zirconium oxide) ZrO_2	cubic zirconia, oxygen sensors
(silicon carbide) SiC	kiln parts, heating elements, abrasives
(silicon nitride) Si_3N_4	turbocharger rotors, piston valves

Heat transfer occurs through a porous material depending on the interaction between the following mechanisms :-

(i) -heat conduction between solid and fluid

(ii)-thermal radiation between cavity surface

(iii)-convection of fluid in cavities

These ways are always coupled with each other therefore the heat transfer in porous media is very complicated .The relative importance of these three mechanisms depends on a number of parameters which are governed by properties and structure of the solid material. There are two ways of heat transport in solid

phase at high temperatures, the photonic and radiation mechanisms of thermal conductivity. The radiation component is significant at high temperatures only $T \geq 1000$ °C [5]

1.3. Thermal Properties of Porous Media

Thermal properties of porous media are the main factor affecting the heat transfer rate from or to it .Thus the study of these properties gives a good guide to understanding the mechanism of heat transfer in void ,solid and pure fluid regions. Variation of thermal properties affects directly in the calculation of heat transfer rate. Because of the composite structure of porous media , there are effective properties of it .These effective properties have been the topic of many researches branches in physics, engineering, and chemistry.

1.4. Effective Thermal Conductivity

Generally there are two ways to study heat transfer in porous media, first if the fluid flow through it is impact on heat transfer rate then the convection term must be taken in account .This type of porous media always have a very high porosity values such as metal foams and heat storage systems ,the Second when the fluid assumed stagnant such as electrical insulators .Their are many models have been developed to predict effective thermal conductivity .This models identify three dominating variables which is:

(i) The solid phase thermal conductivity (k_s)

(ii) The fluid phase thermal conductivity (k_f)

(iii) The microstructure of porous media

The first two variables are very important , but certainly not sufficient to completely describe conduction within the porous medium because the inter-facial dependence is completely neglected. Consequently, most of the effort expended toward modeling the effective thermal conductivity has focused upon geometric effects.

1.4. 1. The Stagnant Effective Thermal Conductivity

In the case when the fluid phase is stagnant, the effective thermal conductivity is determined by conduction through the porous medium described in reference [1] The influence of geometry on the effective thermal conductivity has primarily been investigated through the use of spatially-periodic models of porous media having simple geometries. It is interesting that the seemingly very simple geometric models are largely successful in capturing the microstructure dependence. For instance, if a porous medium is modeled as being composed of layers in a series or parallel arrangement, and the heat flux is assumed to be one-dimensional, then k_e can be predicted from an electrical circuit analog. The accuracy of the layer models, however, is acceptable only when the thermal conductivities of the solid and fluid phases are roughly equal, that is $k = \frac{k_s}{k_f} \approx 1$ as described in reference [1] Obviously, this is due to the fact that k_e is ultimately bounded by k_s and k_s. Consequently, when these bounds are very close, the influence of the microstructure is small and virtually any averaging procedure will yield a reasonable prediction for k_e.

When two-dimensional conduction is incorporated into a model through either a numerical solution or a lumped parameter analysis, the ability to accurately predict k_e is markedly increased. In fact, reasonably accurate predictions for k_e can be obtained up to $k \approx 10^3$. The accuracies of the models are related to how accurately the pore geometry is modeled. Nonetheless, crude two-dimensional models are significantly more accurate than the one-dimensional models.

When $k > 10^3$, virtually all of the heat transfer occurs through the particle-to-particle contact points. Currently, the effects of particle-to-particle contact are handled empirically. Recently, attempts have been made to use solid mechanics to predict the geometry of the particle-to-particle contact, and hence predict effective thermal conductivity for $k > 10^3$, on a purely theoretical basis[1].

1.5. Objective of the Present Work

(i) To measure temperature distribution in porous media during heating with constant heat flux, the transient heating phenomenon has been modeled using classical Fourier conduction theory with two methods for calculating effective thermal conductivity Computer program has been developed for numerical solution of equations by using finite difference method with explicit technique of numerical solution .This technique has been used to give more realistic three- dimensional description of temperature profile within the porous material. This has been dealt with chapter three.

(ii)In chapter four experimental work measures the temperature distribution for similar material analyzed in theoretical part and calculate the effective thermal conductivity for MgO by building an experimental rig in laboratory using advanced interface to measure temperature with thermocouples which can be directly connected to computer.

(iii) Results and discussion for the suggested mathematical model for temperature profiles ,and the experimental results for temperature distribution and thermal conductivity of porous media has been discussed in chapter five .

(iv) Conclusion and suggestions for further work are given in chapter six.

Literature Review

2.1. General

The interest in multi-phase composite materials has continued for over a century. This is essentially due to the wide application of composite materials in industry. The bulk features of the materials depend on factors such as composition, internal structure and external environment. It will be, however ,too complicated to consider all the factors in the study of heat transfer in porous medium .No report of universal models incorporating all the influencing factors has yet been found.

There are still many researchers working in this field in recent years hopes to make further progress. Their works mainly concentrated on two aspects. The first was to introduce more refined mathematical averaging methods to get an exact or approximate analytical solution. The second is to consider the effects of geometry factors such as shape, size, etc. on the effective thermal properties .Various parameters were introduced to modify the original equations in order to extend their application range or to improve the accuracy.

Deissler and **Eian [6]** proposed early recent models for heat transfer in porous medium such as the area-contact model, the phase-symmetry model, the single-scale lumped parameter model, and the multi scale lumped parameter model which were emphasized. Simple algebraic expressions for the effective stagnant thermal conductivity of a number of geometries based on these recent models were presented. These include two-dimensional geometries such as square, circular, and elliptic cylinders and composite materials consisting of fiber bundles, as well as three-dimensional geometries such as ellipsoids, cubes, and wire screens. The effects of existing analytical models for predicting the effective stagnant thermal conductivity of fluid-saturated spatially periodic media were summarized porosity, shape, and arrangement of the solid phases, as well as the solid-to-fluid thermal

conductivity ratio are illustrated. The effects of point and finite contacts between the solid phase on the effective thermal conductivity of the porous medium were discussed. Comparisons of the analytical expressions with numerical solutions and experimental data were made whenever possible.

There are two ways to analytic heat transfer in porous media . The first is the one-equation model is similar to the advection-diffusion equation for energy transfer in a homogeneous fluid. Heat capacity effects are significant in the fluid and the solid phases, but transport is that of the fluid alone. This simulation needs one equation to describe heat transfer in porous media .The second way is the two-equation model, in which additional equations were required for the individual temperatures of the fluid and the solid phases along with a relationship to represent inter phase heat transfer between them.

It is useful to introduce some effective homogeneous, in general, an isotropic media. The response of external heating was equal to that of the porous media under consideration. The thermal conductivity of this effective media will be identified with the effective thermal conductivity of the porous media.

2.2.The Stagnant Effective Thermal Conductivity

There was a large number of literature on determining effective material properties, including conductivity of porous and inhomogeneous materials. Classical theories proposed by **Maxwell J.C. [7]** , these models assumed an ‘‘effective’’ composition with particles of smooth or regular shape e.g circular inclusions.

Deissler and **Boegli[8]** investigated the effective thermal conductivity of two simple models two planar layers first the solid and fluid in parallel layers and second the layers in series. For parallel arrangement as shown in figure (2-1a) their expression of effective thermal conductivity was given by

$$k_e = \phi k_f + (1-\phi) k_s \qquad \ldots\ldots(2.1)$$

And the effective thermal conductivity occurs when the solid and fluid layers assume a series arrangement as shown in figure (2-1b) .The effective thermal conductivity is given by

$$\frac{1}{k_e} = \frac{\phi}{k_f} + \frac{1-\phi}{k_s} \qquad \text{..... (2.2)}$$

The two expressions predict effective conductivities with variations as high as 7% for k =2, and as high as 99% for k =1000 with (ϕ =0.4). This is due to the fact that when is high the solid material arrangement has a great influence on the effective conductivity. As such, for high k applications such as porous carbon foam, an accurate characterization of the internal geometry is necessary.

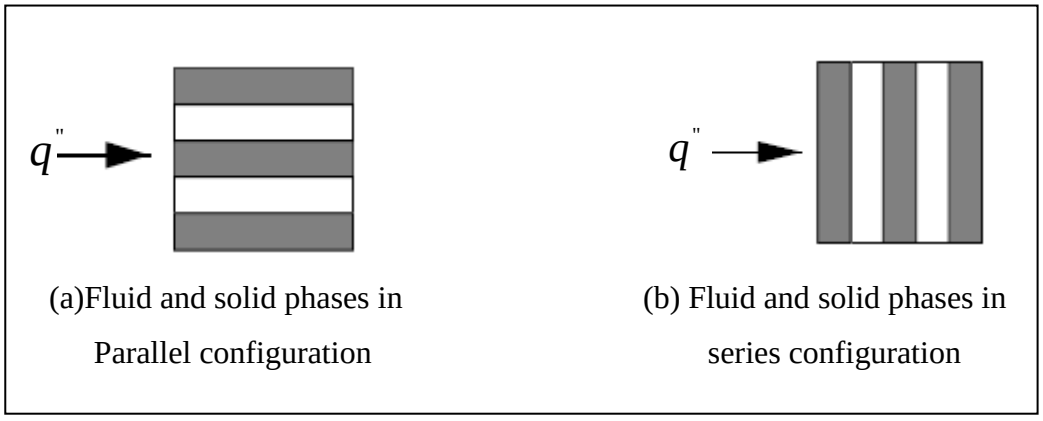

(a)Fluid and solid phases in Parallel configuration

(b) Fluid and solid phases in series configuration

Figure (2-1) One-dimensional composite models .Ref.[8].

The both models for several porosities was plotted ,they hypothesized that their data can be correlated in terms of $\frac{k_e}{k_f}$ and k as presented in figure (2-2).

kunii and Smith [9] presented a model for heat transfer in packed beds of unconsolidated materials by considering unidirectional heat flow through two contacting spherical particles illustrated in figure (2-3a). The following assumptions were considered for heat transfer modes: (1) heat transfer through the void space by conduction and radiation; (2)heat transfer through the solid phase by conduction; (3) heat transfer through the particle-to-particle contact surface; (4) conduction through

the fluid near the contact surface; (5) radiation between particle surfaces; and (6) heat transfer by conduction through the particle-to-particle contact surface. To analyze the

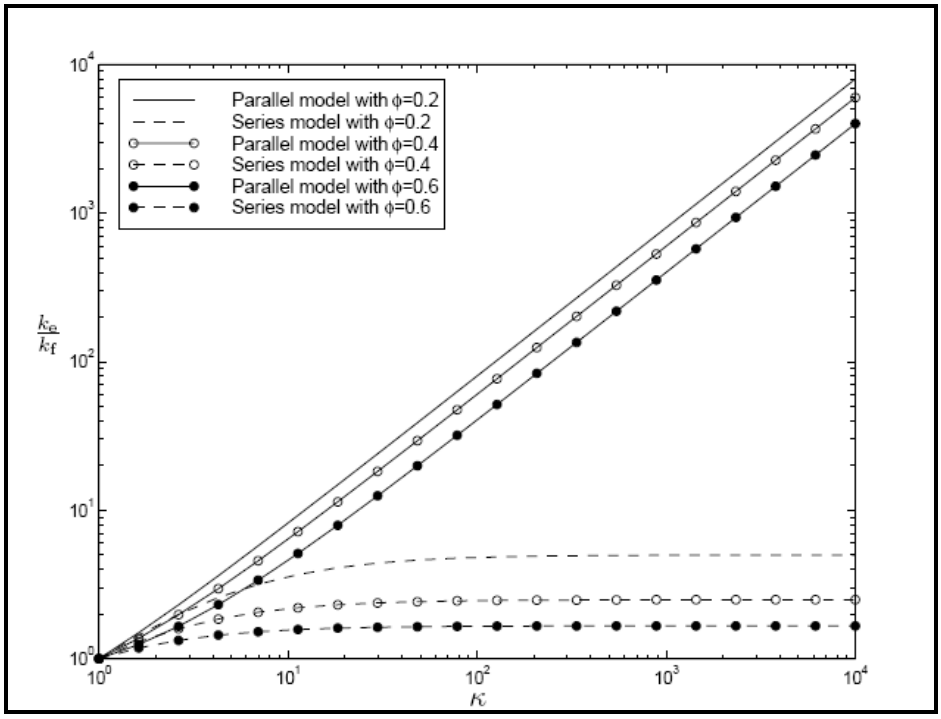

Figure (2-2) Unidirectional heat flow model bounds on k_e.Ref.[8].

system, the heat transfer through assumed the solid and fluid phases can be decomposed into separate modes acting in series and parallel. The system in figure (2.3a) was then approximated by a one-dimensional composite model depicted in figure (2.3b).Then the porous medium was assumed saturated with liquid, thus neglecting radiation in the void space. Therefore, heat transfer through the void space was by conduction alone, while heat transfer through the solid phase comprised of conduction through the particle, contact surface, and fluid in the vicinity of the particle-to-particle contact surface. The effective thermal conductivity of the composite system was then given by

$$\frac{k_e}{k_f} = \phi + \frac{\beta(1-\phi)}{\Psi + \frac{\gamma}{k}} \qquad \text{……..(2.3)}$$

Where β,ψ and γ were non-dimensional geometry parameters.

Krupiczka [10] developed four models of heat conduction in packed beds. First, two unidirectional models, one composed of a bundle of cylinders, and one composed of a lattice of spheres was considered . For these configurations, porosities of 0.215 and 0.476, respectively were assumed. He found that his one-dimensional model under predicted *k*e when it compared with the result of Deissler and Boegli[8] . He had anticipated this result because he assumed unidirectional heat conduction, the effects of transverse conduction were eliminated. Hence the effective thermal conductivity of the unit cell was diminished.

(a)

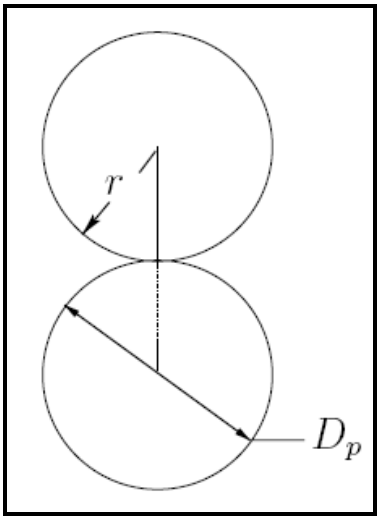

(b)

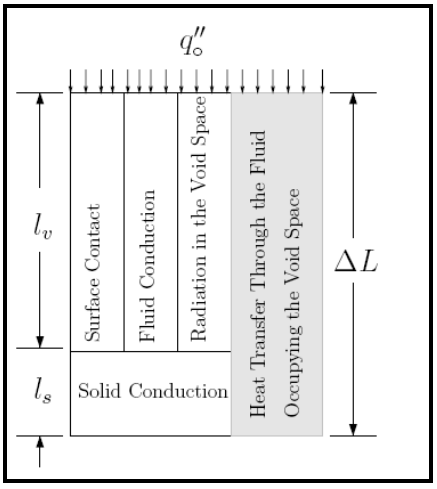

Figure (2-3) Kunii and Smith model for heat transfer near contact points of particles. Ref.[9]. (a) Actual configuration of spherical particles.(b) One-dimensional composite model used to estimate *k*e.

He also developed two three-dimensional models for heat conduction within a packed bed. The first three-dimensional model comprised of a bundle of semi-infinite cylinders was depicted in figure (2-4a).Due to the assumption of cylinders were assumed to be semi-infinite, the solution was two-dimensional. The conduction equation was then solved in the solid and fluid phases. The result is a non-orthogonal series The second three-dimensional model is a spherical lattice shown in figure (2-4b).Rather than solve the conduction equation in three-dimensional spherical coordinates, He introduced simplifications which enabled him to approximate the spherical geometry with a semi-infinite cylinder. He demonstrated that this approximation introduced minimal error. This solution also yields a non-orthogonal series. He found the solutions to both the cylinder and sphere models in terms of infinite non-orthogonal series are very difficult to evaluate. He developed functions which approximated the exact solution. After comparing his approximating functions with data from the literature .A general function of the form given by

$$\frac{k_e}{k_f} = (k)^{A^o + B^o \log_{10} k} \qquad \text{.....(2.4)}$$

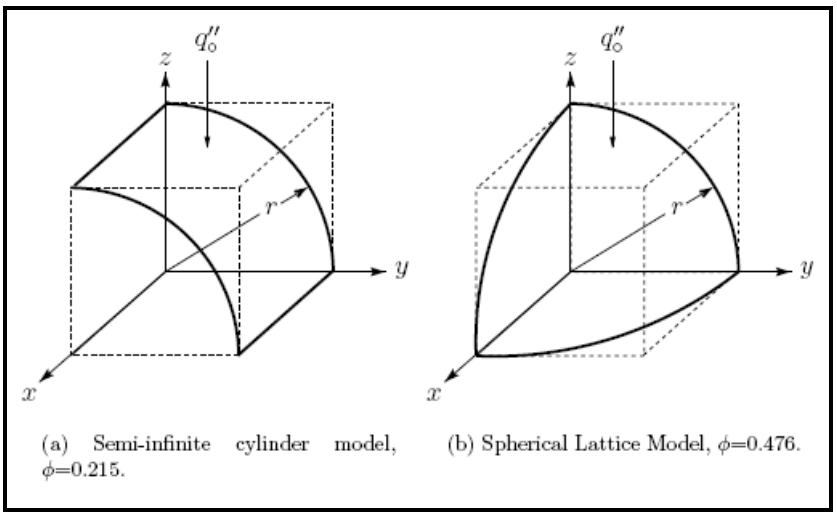

(a) Semi-infinite cylinder model, ϕ=0.215. (b) Spherical Lattice Model, ϕ=0.476.

Figure(2-4),Three dimensional spatially –periodic models considered by Krupiczka Ref.[10].

Where

$$A^O = 0.280 - 0.757 \log_{10} \phi \qquad \text{.....(2.5)}$$

and

$$B^O = -0.057$$

Zehner and **Schlunder [11]** developed a model for the effective thermal conductivity of packed beds by considering thermal conduction through a cylindrical cell comprised of a solid sphere and a fluid. The cell under consideration was illustrated in figure (2-5). The inner cylinder, $0 < r < 1$ contains one-eighth of a solid sphere, while the remaining volume was occupied by the fluid phase. The annular region $1 < r < R$ contains only fluid. They assumed that axial thermal conduction travels in parallel paths through the inner cylinder and outer annulus. The effective thermal conductivity of the cell was then given by

$$k_e = (1 - \frac{1}{R^2})k_f + \frac{1}{R^2} k_{sf} \qquad \text{.....(2.6)}$$

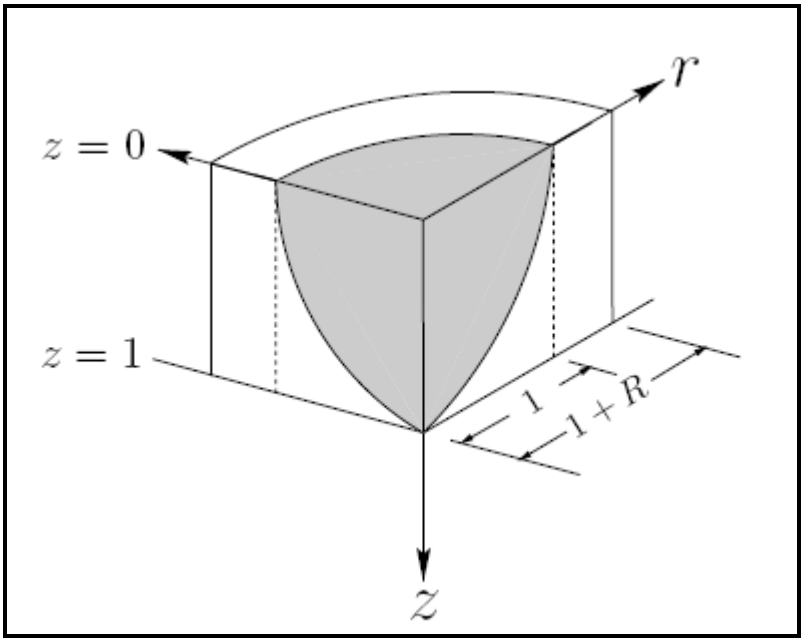

Figure (2-5) unit cell presented by Zehner and Schlunder [11].

where k_{sf} is the effective thermal conductivity of the inner cell consisting of both solid and fluid phases. Then they fond that effective thermal conductivity of the cell, is given by

$$\frac{k_e}{k_f} = \left[1 - \sqrt{1-\phi}\right] + \frac{2\sqrt{1-\phi}}{1-k^{-1}B} \times \left[\frac{(1-k^{-1})B}{(1-k^{-1}B)^2} \ln\left(\frac{1}{k^{-1}B}\right) - \frac{B+1}{2} - \frac{B-1}{1-k^{-1}B}\right] \quad \text{.....(2.7)}$$

If value of $B = 0$, which corresponds to the inner cylinder being completely occupied by the fluid, and $B \to \infty$ which corresponds to the inner cylinder being completely occupied by the solid. B is related to porosity as

$$\phi = \left(\frac{B(3 - 4B + B^2 + 2\ln B)}{(B-1)^3} \right)^2 \quad \text{.....(2.8)}$$

Batchelor and **O' Brien [12]** derived an analytical solution for effective thermal conductivity of a packed bed of spheres by solving an integral equation for the temperature distribution over the sphere surface. A thermal electrical approach was used . They considered three limiting cases for contact between spherical particles: point contact, no contact, and contact through a large circular area-presumably caused by particle deformation. They found that the thermal conductivity ratio had a relatively small effect on the effective thermal conductivity of the medium. They found that the number of particle-to-particle contact points was the dominant factor. The number of contact points was related to the porosity of the medium. Further, they found that for particles with large thermal conductivity, almost all of the heat flux through the particles occurs through flattened regions resulting from local particle deformations. Hence the particle-to-particle contact area significantly affected the effective thermal conductivity of the medium. From their analysis of spherical particles in point contact, They were able to derive a closed-

form model for k_e based upon the assumption of a random, isotropic spherical packing arrangement. This assumption was necessary because k_e was a function of the number of particle-to-particle contact points. Hence, they assumed 6.5 contact points per sphere. This yielded a theoretical porosity of ϕ = 0.63. Their result was given by the approximate a final formula which is

$$k_e = 4.0k_f \ln(\frac{k_s}{k_f}) - 11 \qquad \text{.....(2.9)}$$

Nozad, **et al [13]** used the volume averaging technique and judicious assumptions to reduce the general governing equations for conduction heat transfer in a two-phase porous medium to a single governing equation for the spatially averaged temperature. While considerably simpler than the initial governing equations. The one-equation model contained spatial temperature fluctuations which necessitated the derivation of a closure model to relate fluctuations to mean quantities before it can be solved. After deriving the closure model. He solved the closure equations for two representative cases of spatially periodic porous media. The numerical solutions to the closure equations were then used to compute the effective thermal conductivity tensor for each spatially periodic unit cell. The representative cell types were continuous and discontinuous fluid phases. The continuous fluid phase model approximated a porous medium in which the solid particles either do not make contact, or make point contact. This cell corresponds to the situation analyzed by Batchelor and Brien [12] . The discontinuous fluid phase model, on the other hand, incorporated the effects of particle-to-particle contact through an empirical parameter.

Hadley [14] conducted experiments to measure the effective thermal conductivity of two and three-phase porous media composed of packed metal powders saturated with air and water. He then used volume averaging to develop a semi-empirical mixture correlation to predict the effective thermal conductivity in two and three-phase porous media. He conducted experiments to measure the effective thermal conductivity of two and three-phase porous media composed of

packed metal powders saturated with air and water. He then used volume averaging to develop a semi-empirical mixture correlation to predict the effective thermal conductivity in two and three-phase porous media .He assumed one-dimensional heat conduction in the sample and a steady-state temperature gradient to measure the thermal conductivity of a sample. He next considered the model for the effective thermal conductivity of a dilute suspension of spherical particles which was derived by Maxwell [7] which is given by

$$\frac{k_e}{k_f} = \frac{2k^2(1-\phi)+(1-2\phi)}{(2+\phi)k+1-\phi} \qquad \text{…….. (2.10)}$$

Next, to model the effective thermal conductivity for consolidated media, he assumed that the effective thermal conductivity can be expressed as a combination of the non-touching effective thermal conductivity and a correction term to account for the effects of particle-to-particle contact. His correlation was then given by

$$\frac{k_e}{k_f} = (1-\alpha_p)\frac{\phi f_o + k(1-\phi f_o)}{1-\phi(1-f_o)+k\phi(1-f_o)} + \alpha_p \frac{2k^2(1-\phi)+(1+2\phi)k}{(2+\phi)k+1-\phi} \qquad \text{……. (2.11)}$$

where α_p is a parameter introduced to account for particle-to-particle contact. Both f_o and α_p are determined empirically.

Prasad et al [15] found that the correlation given by reference [11] and the models developed by reference [12] and reference [10] were adequate as long as the solid thermal conductivity was larger than the fluid thermal conductivity. None of the models and correlation's considered were recommended for use when $k \le 1$. Also, the parallel model, given by equation (2.1) was found to predict k_e only when $k \approx 1$

Nield [16] noted that some of the effective thermal conductivities presented by Prasad et al[15] were not within the bounds for effective thermal conductivities given

by the series and parallel models. A model for k_e based upon the geometric mean of k_f and k_s, and weighted by the porosity was presented. This model is given by

$$k_e = k_f^{\phi} k_s^{(1-\phi)} \qquad \text{……..(2.12)}$$

and was plotted in figure (2-6).This model for use when $k \approx 1$ and offered it as a prototype for correlations as the functional form was very similar to the correlation presented by Krupiczka [10]

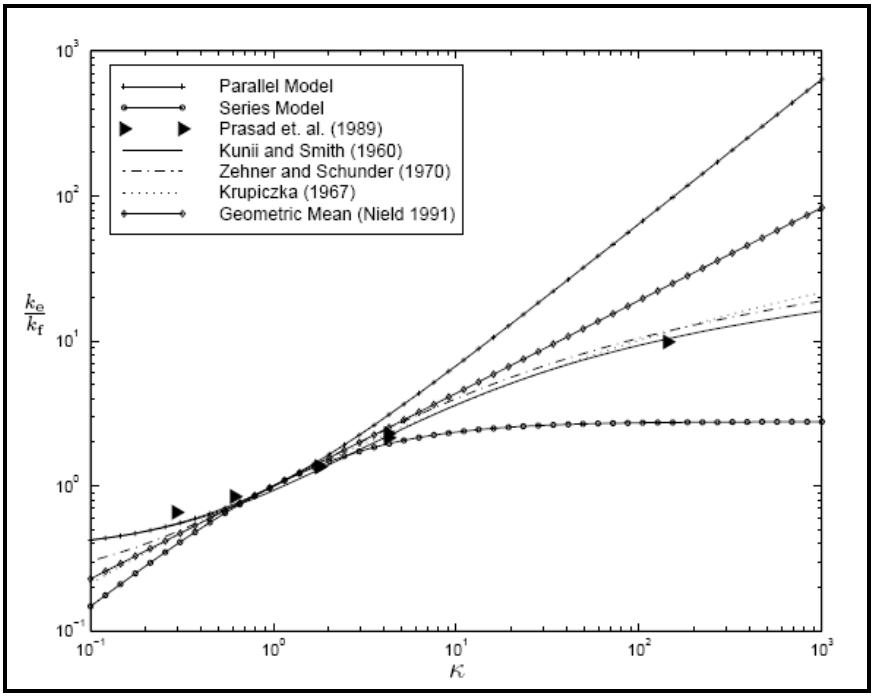

Figure (2-6) Comparison of experimental data from Pasad et al [16]and various models for k_e with $\phi = .36$

Hsu <u>et</u> <u>al</u> [17] noted that the model of reference [12]assumed point contact between particles so that they postulated that this model which could be improved by incorporating the effects of particle-to-particle contact through an infinite-area contact point. They modified to the model of by the introduction of a flat region on the surface of the sphere occupying the unit cell, as illustrated in figure (2-7). They introduced that the effective thermal conductivity of the unit cell is then given by

$$\frac{k_e}{k_f}=\left[1-\sqrt{1-\phi}\right]+\frac{\sqrt{1-\phi}}{k^{-1}}\left(1-\frac{1}{(1+\alpha_o B)^2}\right)+\frac{2\sqrt{1-\phi}}{\left[1-k^{-1}B+(1-k^{-1})\alpha_o B\right]}$$
$$\left(\frac{(1-k^{-1})(1+\alpha_o)B}{\left[1-k^{-1}B+(1-k^{-1})\alpha_o B\right]^2}\times\ln\frac{1+\alpha_o B}{(1+\alpha_O)Bk^{-1}}-\frac{B+1+2\alpha_o B}{2(1+\alpha_O B)^2}-\right. \qquad \text{.....(2.13)}$$
$$\left.\frac{(B-1)}{\left[1-k^{-1}B+(1-k^{-1})\alpha_o B\right](1+\alpha_o B)}\right)$$

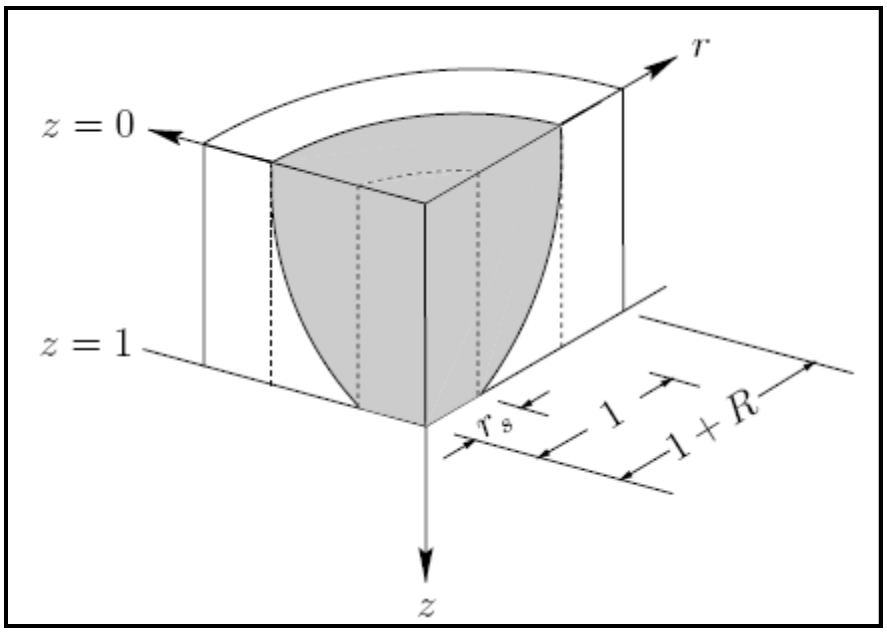

Figure (2-7) Zehner and Schlunder as modified by .Ref. [17]

In addition, the introduction of the contact parameter caused the geometric parameter *B*, in equation (2.13) to become a function of α_o. Consequently for a given porosity and contact parameter, *B* is determined from:

$$\phi=\frac{B^2}{(1-B)^6(1+\alpha_o B)^2}\{(B^2-4B+3)+2(1+\alpha_0)$$
$$(1+\alpha_o)\ln\frac{(1+\alpha_o)B}{1+\alpha_o B}+\alpha_o(B-1)(B^2-2B-1)\}^2 \qquad \text{.....(2.14)}$$

Hsu <u>et</u> <u>al</u> [18]also developed lumped parameter models for the effective thermal conductivity of porous media composed of spatially periodic unit cells. They considered a two-dimensional unit cell comprised of contacting square cylinders. Using the discontinuous fluid phase model of Nozad <u>et</u> <u>al</u> [13] illustrated in figure

(2-8a) as a guide, they used symmetry arguments to reduce Nozad et al.'s model to a single quadrant depicted in figure (2-8b). They modeled the unit cell as a composite material comprising three layers, and the three layers as thermal resistance's in parallel. They found that the effective thermal conductivity of the unit cell then becomes

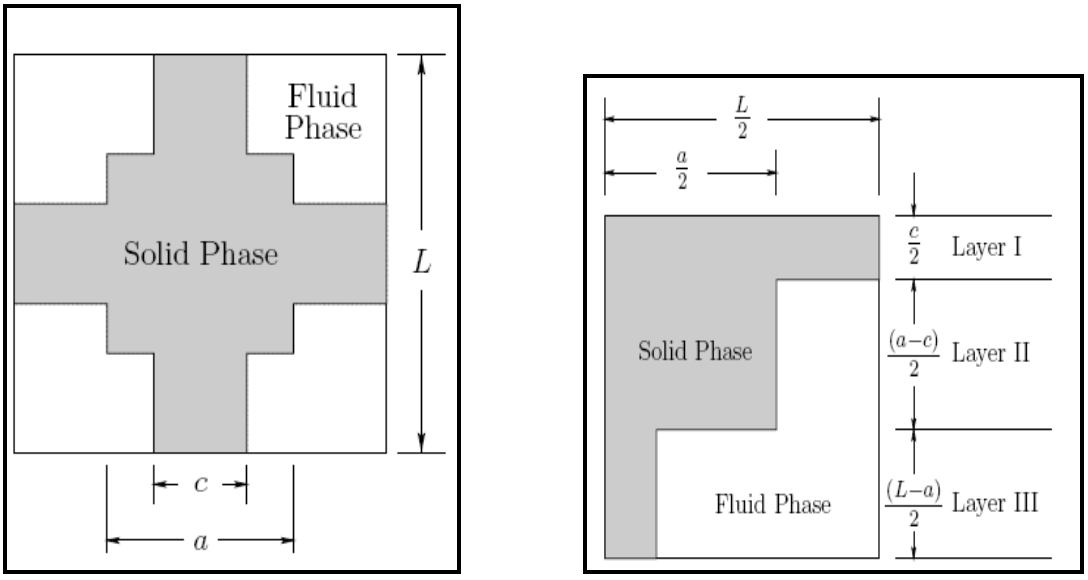

(a) Both phases continues , contacting solid particles

(b) Touching square model

Figure (2-8) ,models proposed by .Ref. [13] and modified by. Ref. [18].

$$\frac{k_e}{k_f} = \frac{\gamma_a \gamma_c}{k^{-1}} + \frac{\gamma_a (1-\gamma_c)}{1+(k^{-1}-1)\gamma_a} + \frac{(1-\gamma_a)}{1+(k^{-1}-1)\gamma_a \gamma_c} \qquad \text{.....(2.15)}$$

The geometric parameter γ_a was related to the porosity and the adjustable parameter γ_c through

$$1-\phi = \gamma_a^2 + 2\gamma_c \gamma_a (1-\gamma_a) \qquad \text{.....(2.16)}$$

Kuznetsov [19] had analytically investigated the effect of thermal non-equilibrium between the solid and fluid phases in packed beds and semi-infinite porous media. The temperature difference between fluid and solid phases formed a thermal wave localized in space. Phase difference was suggested to occur between

the propagating waves in fluid and solid phases due to the effects of thermal non-equilibrium.

M. Kaviany [20] presented that the assumption of local thermal equilibrium was valid when the temperature difference between the solid phase and the fluid phase in a representative elementary volume (REV) enclosing both the fluid was much smaller than that occurring over the system dimension .

$$\Delta T_L >> \Delta T_l$$

where ΔT_L was the temperature difference occurring over the dimension of the system and ΔT_l was the temperature difference between the solid phase and fluid phase in an REV as shown in figure (2-9)

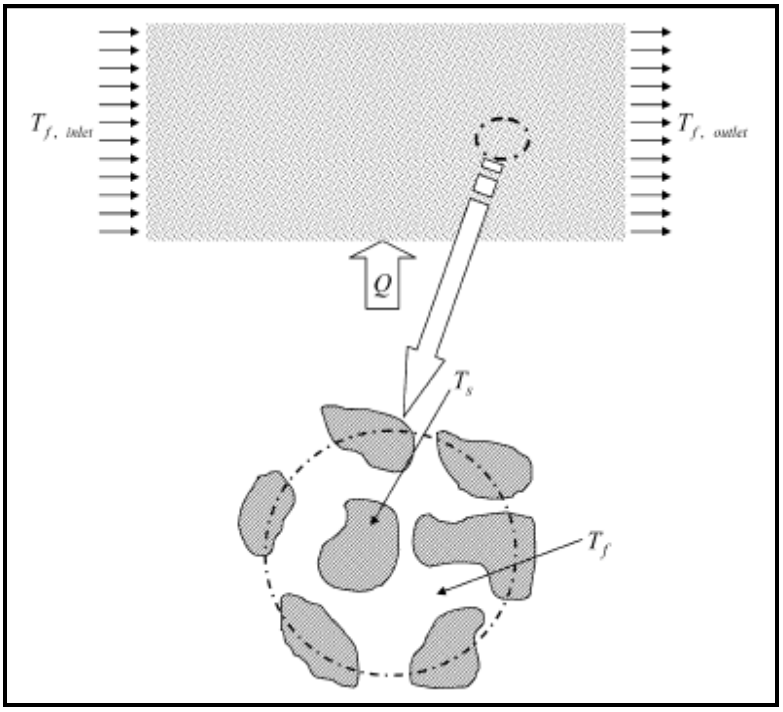

Figure(2-9) Schematic diagram of a system and a representative elementary volume .Ref. [20].

Fu et al [21] developed an analytical model to determine the effective thermal conductivity of cellular ceramics. Two unit cells were developed to predict the effective thermal conductivity of porous materials using the electrical-circuit analogy. The first unit cell was a cubic-shaped box. The second unit cell was a cube with a

pore in the center, the effective thermal conductivity of the second model expressed as

$$\frac{k_e}{k_f}=\left[\frac{2t}{(1-2t)^2k+\left[1-(1-2t)^2\right]}+\frac{(1-2t)}{4t^2k+(1-4t^2)}\right]^{-1} \qquad \text{.....(2.17)}$$

Where the parameter t related to the porosity as:

$$(1-2t)^3+6(1-2t)^2t=\frac{\phi}{100} \qquad \text{.....(2.18)}$$

Liang and W.Qu [22]studied effective thermal conductivity of gas solid composite materials The temperature difference effect at high temperature was founded .The affect of the temperature difference over the bulk material on the effective thermal conductivity was discussed and proposed a local equivalent thermal conductivity. They applied it to derive the effective thermal conductivity for the bulk material .They gave an analytical expressions for cavities with cylindrical and spherical shapes , then they compared the experimental data of the spherical case There calculations showed that the local equivalent thermal conductivity over the bulk material more different .They found that the temperature difference was not significant if the diameter of the cavity is below 4 mm and the porosity was smaller than 78%.When the porosity was higher than 78% and the cavity diameter was greater than 4 mm a strong temperature difference effect was expected at a high temperature and the temperature difference effect should be considered

.

Hans T. Aichlmayr [1] presented many results by figure (2-10) for an experimental investigations to determine the accuracy of several models for the stagnant effective thermal conductivity of saturated porous media. Experiments were conducted for four solid-to-fluid combinations: glass-water, glass-air, steel-water, and steel-air. These solid-fluid combinations yield solid-to-fluid thermal conductivity ratios of 2, 48, 102, and 2,400 respectively. He obtained porosities of 0.365 and 0.403

with glass and steel spheres respectively. A thorough uncertainty analysis was performed and found that uncertainties in the stagnant effective thermal conductivity range from 14% to 32%. The effective thermal conductivities obtained in his experiments were generally lower than those found in the literature possible .

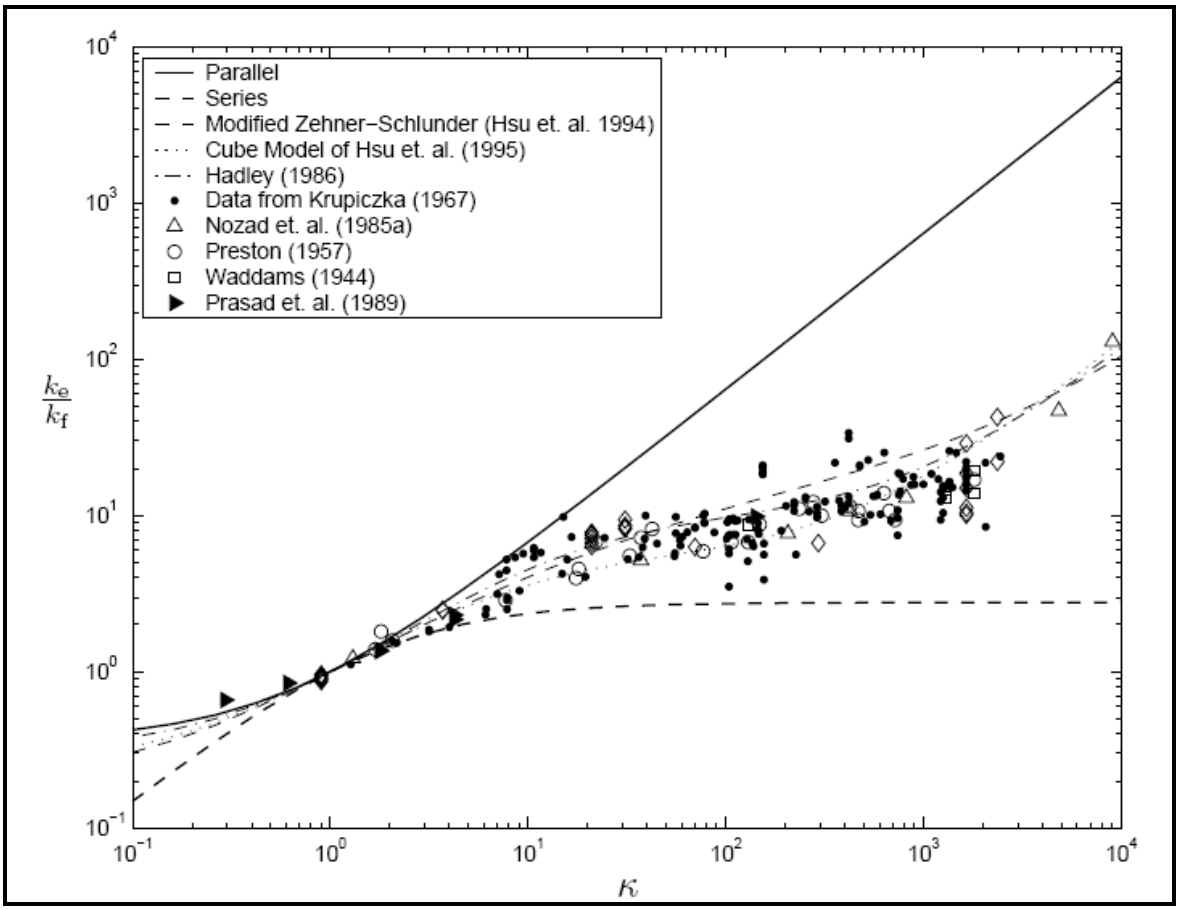

Figure (2-10)Comparison of models for the effective thermal conductivity and experimental data .Ref.[1].

Muralidhar and **Suzuki [23]** analyzed the oscillatory flow and heat transfer in a regenerator using the thermal non equilibrium model. A pulsating flow of gas was used with metallic mesh screens over a wide range of Reynolds number and frequencies. Quantities such as the friction factor and regenerator effectiveness had been calculated.

Ramvir Singh [24] gave an empirical correlation for easy estimation of effective thermal conductivity (ETC) of highly porous two-phase systems based on

experimental data available. He tried to develop empirical relation for quick estimation of effective thermal conductivity of highly porous systems. In order to incorporate varying individual geometries and non-linear flow of heat flux lines generated by the difference in thermal conductivities of constituent phases, he introduced a correlation term (F), the expression for correlation term (F) has been obtained by simulating experimental data reported in the literature. He found that his empirical correlation is for highly porous foam like materials, but it was equally valid for the calculation of ETC for other types of materials. It had a single correlation factor, which was valid for all types of systems. It has potential for further refinements to predict ETC values of consolidated and reinforced composites.

Singh et al [25] gave a comparison of the one-equation and the two-equation models by a comparison for two different porous domains consisting of glass-water and air-metal. They found that for glass-water porous medium, the one-equation model predicts a faster temperature front as compared to the two-equation model at low Reynolds number. With an increase in Reynolds number, the difference went on decreasing .For air-metal porous medium, the temperature front predicted by the two-equation model is faster than the one-equation model up to a Reynolds number of 1000. At higher Reynolds number, the two-equation model was slower than the one-equation model and the heat loss taking place through the transverse boundaries in glass-water porous medium did not change the thermal front significantly. In case of air metal porous medium, the heat loss had significant effect on the thermal front and was seen to become immobile and the domain size is equivalent to long time scales.; During this time interval, the initial length of the porous medium attains thermal equilibrium and the overall difference between the one- and the two-equation models is diminished.

Zhao et al [26] studied the dependence of the effective thermal conductivity on the temperature in metal foams. In their work, the effective thermal conductivity of five FeCrAlY foam samples with different pore sizes and relative densities were measured using a guarded-hot-plate apparatus under both vacuum and atmospheric

conditions. The results showed that the effective thermal conductivity increased rapidly as the temperature increased, particularly in the higher temperature range (500-800 K) where the thermal radiation dominated the transport. The results showed that the contribution of the heat transfer by natural convection was also significant. The effective thermal conductivity increased as the pore size or relative density increased. In addition, relative density had a great effect on the natural convection in the metal foam**.**

Wang et al[27] proposed to use the microscopy image of porous structure to calculate its thermal conductivity. His model included the image analysis, which was necessary to develop the model structure comprising the pores, cracks, and voids of different sizes. This model structure had been used then for the direct calculation of thermal conductivity with the finite element method. The approach allowed one to obtain a detailed map of the temperature field and the heat flux distribution. However, consideration of a large structure containing too many pores and cracks of different sizes seemed to be difficult because of computational complexity.

2.5. Summary

According to what researches reported ,their main study concentrate on simulating thermal conductivity only by assuming different empirical equations and measuring this experimentally .Therefore, modern technique was needed to give reliable solution of the transient heating phenomenon .Using this technique in numerical solutions to solve these equations which calculated the spatial and temporal temperature distribution of porous media .

Also advance instruments were used in experimental work to give more reliable and accurate results .

Theoretical Work

3.1. Introduction

Heat transfer within a porous medium occurs due to temperature gradients in the fluid and solid phases. Desmond [28] presented that when the Grashof number based on the spacing inside medium as characteristic length is less than 1700,a pure conduction is the only mode of heat transfer. Conduction within the solid and fluid phases is made evident by volume averaging, but the determination of the conductivity coefficients requires numerical experiments and is unique to the geometry and conductivity's of the two phases. Qijun Yu et al [29] proposed a unit-cube geometry model to characterize the internal structure of porous carbon foam. This model is based on interconnected sphere-centered cubes, where the interconnected spheres represent the fluid or void phase. They used the unit-cube model to derive all of the geometric parameters required to calculate the heat transfer and flow through the porous foam. Their expression for the effective thermal conductivity is derived based on the unit-cube geometry. Validations show that the conductivity model gives excellent predictions of the effective conductivity as a function of porosity. Torquato et al [30] presented an optimization method to design three-dimensional composite microstructures with multifunctional characteristics to illustrate the fascinating types of microstructures that can arise in multifunctional optimization. John Hernlund et al [31] present a numerical model for calculating the temperature distribution inside resistance-heated high-pressure solid-medium axi-symmetric cell assemblies that incorporates both composition and temperature dependent thermal conductivity.

In the present work a local thermal equilibrium is assumed between solid and fluid phases and there is no fluid flow through porous media ,so that the problem under investigation is related to transient heat conduction in three dimension

Cartesian domain .The model is subjected to uniform heat flux from below and it bounded by convection boundary conditions in other surfaces. This way allows to study the models of thermal conductivity in three direction heat flow.

The purpose of the present work is to study the temperature distribution in porous media as a function of its properties by predictive unsteady state three dimensional model. The advantage of this part of the study that the manner modification to the computer model could be used to predict the results as similar of experimenters without having to run costly experiments .

The basic of any computer simulation is the specification of the model equations and utilizing adequate mathematical and computational procedures to simulate the process .Finite difference time domain methods (FDTD) will be used to solve the heat transfer equations .

3.2. Mathematical Analysis

When a macroscopic description was used to model conduction heat transfer in porous medium, the effective thermal conductivity is defined by Fourier's law,

$$q''(t) = -k_e \nabla T \qquad \text{.....(3.1)}$$

Typically ,the effective thermal conductivity was assumed isotropic with equation (3.1) ; heat conduction within the porous medium can be described by Holman [32]as :

$$(\rho c_p)_e \frac{\partial T}{\partial t} = k_e \frac{\partial^2 T}{\partial x^2} + k_e \frac{\partial^2 T}{\partial y^2} + k_e \frac{\partial^2 T}{\partial z^2} \qquad \text{.....(3.2)}$$

Where $(\rho c_p)_e$ is the volumetric heat capacity of the porous medium ,and is defined to be void fraction .weighted average of the fluid and solid volumetric heat capacities given by [12]

$$(\rho c_p)_e = \phi(\rho c_p)_f + (1-\phi)(\rho c_p)_s \qquad \text{.....(3.3)}$$

Where ϕ is the porosity , which is defined as the fraction of the void space volume to the total volume , If the porosity is zero, the element represents a volume

containing solid material, whereas a porosity value of 1.0 means the element that is completely filled with fluid. A value between 0.0 and 1.0 indicates that the volume contains both fluid and solid material.

Temperature, on the other hand ,is an intensive macroscopic property .Through equation (3.1) , k_e is also an intensive macroscopic property .Therefore, in addition to being a function of the fluid and solid phase thermal conductivities, k_e is also a function of the microstructure of the porous medium .In the case when the fluid phase is stagnant ,the effective thermal conductivity is determined by conduction through the porous medium .If the solid and fluid phases are assumed to be in local thermal equilibrium ,then both phases can be represented by single volume-averaged continuum. Using two models to calculate effective thermal conductivity from past studies emphasizing on that the thermal conductivity is varied with temperature.

The first model that was presented by Zehner and Schlunder [11] ,that is

$$\frac{k_e}{k_f} = \left[1-\sqrt{1-\phi}\right] + \frac{2\sqrt{1-\phi}}{1-k^{-1}B} \times \left[\frac{(1-k^{-1})B}{(1-k^{-1}B)^2}\ln\left(\frac{1}{k^{-1}B}\right) - \frac{B+1}{2} - \frac{B-1}{1-k^{-1}B}\right] \qquad \text{.....(3.4)}$$

where they also give a new relation of B to porosity in addition to equation (2.7) , where

$$B = C\left(\frac{1-\phi}{\phi}\right)^m \qquad \text{...}\text{.....(3.5)}$$

The parameter C and m values are taken from Hsu et al [18] that is

C=1.346

m=1.055

The second model used that was presented by Hadley [14],which is

$$\frac{k_e}{k_f} = \frac{2k^2(1-\phi)+(1-2\phi)}{(2+\phi)k+1-\phi} \qquad \text{.....(3.6)}$$

Correlation values of k_s and k_f are done to give more accurate calculations in equations (3.4) and (3.6) that was detailed in appendix (A) ,The values of thermal conductivity were taken as a function of temperature for MgO-air system and Chrome steel -air matrix.

From the theoretical development of Nozad et al [13],then a three – dimensional equation of transient heat conduction in a porous medium :

$$\frac{1}{\alpha_e}\frac{\partial T}{\partial t} = \frac{\partial^2 T}{\partial x^2} + \frac{\partial^2 T}{\partial y^2} + \frac{\partial^2 T}{\partial z^2} \qquad \text{..... (3.7)}$$

Where α_e is the effective thermal diffusivity of porous medium which is :

$$\alpha_e = \frac{k_e}{(\rho c_p)_e} \qquad \text{.....(3.8)}$$

The term $(\rho c_p)_e$ was defined in equation (3.3)

Consider a cube filled with porous medium subjected to uniform heat flux $q''(t)$ from above ,as illustrated in figure (3-1).When the medium is in the configuration shown in figure (3-1) ,then the fluid can be assumed quiescent .Hence, heat transfer within the porous medium will be conduction only, and therefore equation (3.7) is applicable .

These assumptions yield the following initial and boundary conditions ,the initial condition is : $T(x, y, z, 0) = T_0$

Subjected to the boundary conditions :

The interior nodes at center of material when $z > 0$,the heat effected is conduction only ,then heat equations represented on these sides are illustrated in equation (3.7).While when $z = 0$,the heat flux was effected ,then the boundary condition is:

$$q''(t) = -k_e \left.\frac{\partial T}{\partial z}\right|_{z=0} \qquad \text{……(3.9)}$$

The heat transfer effected on surface (2) and surface (3) is conduction and convection ,then the boundary conditions on these sides are :

$$-k_e A \frac{dT}{dx} = hPdz(T - T_\infty) \qquad \text{at} \quad z > 0 \qquad \text{..……..(3.10)}$$

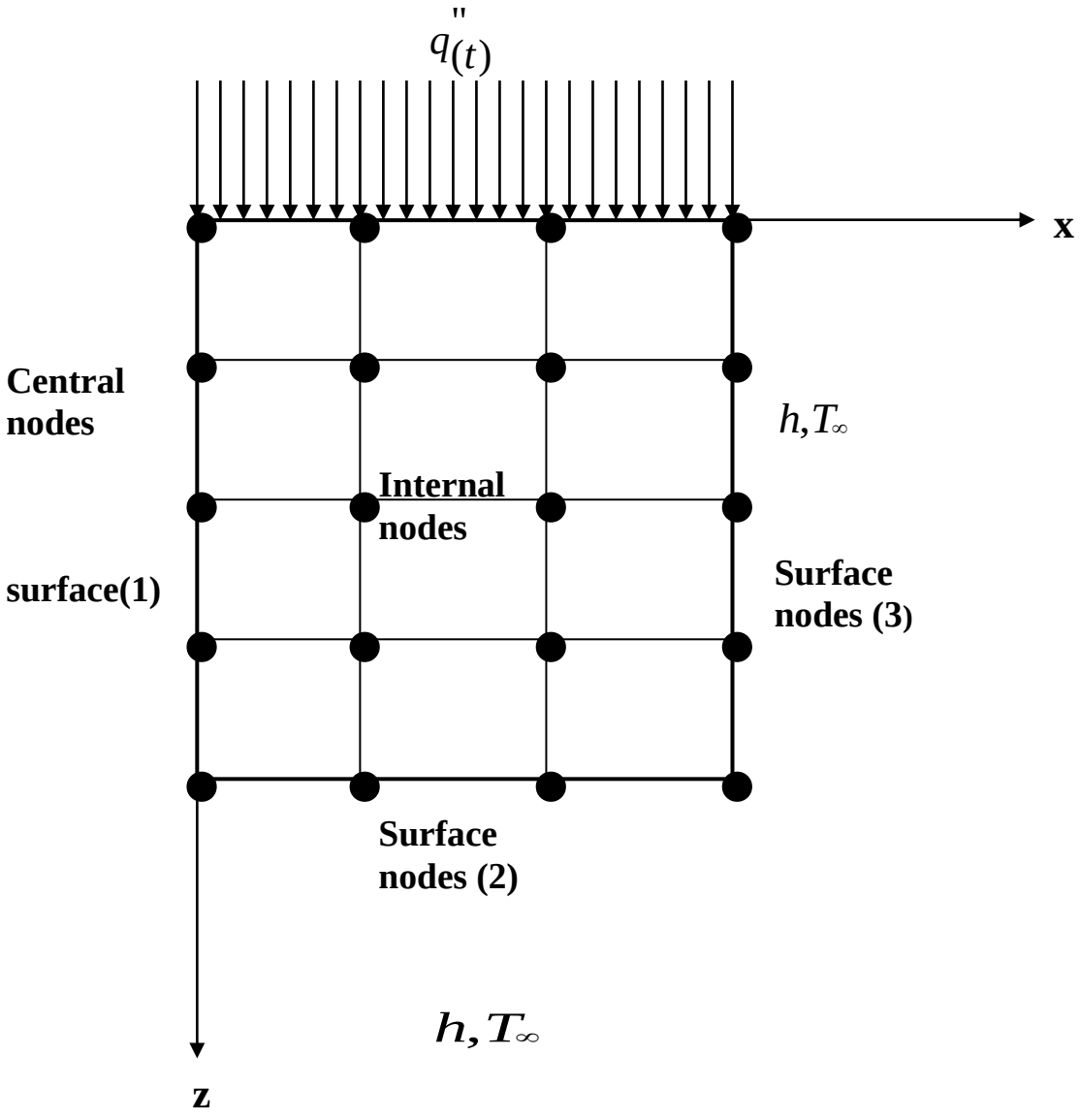

Figure (3-1) boundary conditions for material is assumed to be cube

Where

T_∞ is the ambient temperature

h is the convection heat transfer coefficient ,the value of h was calculated as shown in appendix [A.]

A is the convection area = P dz

P is the perimeter

dz is the thickness

Then the governing equation of the heat transfer is represented as

$$\frac{1}{\alpha_e}\frac{\partial T}{\partial t}+\frac{hp}{Ak_e}(T-T_\infty)=\frac{\partial^2 T}{\partial x^2}+\frac{\partial^2 T}{\partial y^2}+\frac{\partial^2 T}{\partial z^2} \qquad \text{.....(3.11)}$$

Partial differential equations (PDEs) can be solved by using finite difference approximation , so that the problem can be solved by using computer. It has been considered the approximation is in the region over which have an orthogonal grid with an equal spacing (the distance between neighboring points).The indices i,j and k will be used for indicating points in x, y and z directions respectively .The index n will be used for indicating the points over the time layers . Approximation of the first order accuracy shall be used for time and second order for the space. The distances between points in the established grid are Δx ,Δy ,Δz and Δt. The grid is represented in figure (3-2).Notice that temperature values in the time layer n are known and we search for temperature values of the time layer n+1.The partial derivative with respect to time is approximated by forward –difference scheme :

$$\frac{\partial T}{\partial t}=\frac{T^{n+1}_{(i,j,k)}-T^{n}_{(i,j,k)}}{\Delta t}+0(\Delta t) \qquad \text{.....(3.12)}$$

The centered –difference scheme will be used to approximate the derivatives of temperature in space ,while the values involved in the approximation will be taken from the time layer n :

$$\frac{\partial^2 T}{\partial x^2} = \frac{T^n_{(i+1,j,k)} - 2T^n_{(i,j,k)} + T^n_{(i-1,j,k)}}{(\Delta x)^2} + 0(\Delta x)^2 \qquad \text{…….(3.13)}$$

and

$$\frac{\partial^2 T}{\partial y^2} = \frac{T^n_{(i,j+1,k)} - T^n_{(i,j,k)} + T^n_{(i,j-1,k)}}{(\Delta y)^2} + 0(\Delta y)^2 \qquad \text{…….(3.14)}$$

and

$$\frac{\partial^2 T}{\partial z^2} = \frac{T^n_{(i,j,k+1)} - T^n_{(i,j,k)} + T^n_{(i,j,k-1)}}{(\Delta z)^2} + 0(\Delta z)^2 \qquad \text{……(3.15)}$$

and at z=0 ;

$$\frac{q^{"}_{(t)}}{k_e} = -(\frac{T^n_{(i,j,k+1)} - T^n_{(i,j,k-1)}}{2\Delta z}) \qquad \text{…….(3.16)}$$

The finite difference form of governing equation (3.7) can be written as :

$$\frac{1}{\alpha_e}(\frac{T^{n+1}_{(i,j,k)} - T^n_{(i,j,k)}}{\Delta t}) = \frac{1}{(\Delta x)^2}(T^n_{(i+1,j,k)} - 2T^n_{(i,j,k)} + T^n_{(i-1,j,k)}) + \frac{1}{(\Delta y)^2}$$
$$(T^n_{(i,j+1,k)} - 2T^n_{(i,j,k)} + T^n_{(i,j-1,k)}) + \frac{1}{(\Delta z)^2}(T^n_{(i,j,k+1)} - 2T^n_{(i,j,k)} + T^n_{(i,j,k-1)})$$

… ……....(3.17)

and for equation (3.11) ;

$$\frac{1}{\alpha_e}(\frac{T^n_{(i,j,k)} - T^n_{(i,j,k)}}{\Delta t}) + \frac{hP}{Ak_e}(T^n_{(i,j,k)} - T_\infty) = \frac{1}{(\Delta x)^2}(T^n_{(i+1,j,k)} - 2T^n_{(i,j,k)} + T^n_{(i-1,j,k)})$$
$$+ \frac{1}{(\Delta y)^2}(T^n_{(i,j+1,k)} - 2T^n_{(i,j,k)} + T^n_{(i,j-1,k)}) + \frac{1}{(\Delta z)^2}(T^n_{(i,j,k+1)} - 2T^n_{(i,j,k)} + T^n_{(i,j,k-1)})$$

……..(3.18)

Equations (3.17) and (3.18) are called explicit formulation of equations (3.7) and (3.11).In the explicit formulation , there is only point at the n+1 layer ,and the temperature at that point can be easily calculated from the values of the previous time .

Finite difference method is devoted to basic techniques for solving parabolic PDEs. Typical explicit approximation has been explained .The computer program gives more reliability to calculate temperature profile against x ,y and z coordinates depending upon the boundary conditions .This gives different form of equation in explicit finite difference technique .Principles of stability analysis with numerical schemes were discussed by Anderson et al [33], where $\lambda = \dfrac{\alpha_e \Delta t}{(\Delta x)^2}$ is convergence factor , assuming that $\Delta x = \Delta y = \Delta z$ and

At point o as shown in figure (3-2) $x = 0$, $y = 0$ and $z = 0$,

when :

$$q^{"}(t) = -k_e \left.\frac{\partial T}{\partial z}\right|_{z=0}$$

then

$$\frac{q^{"}_{(t)}}{k_e} = -\left(\frac{T^n_{(i,j,k+1)} - T^n_{(i,j,k-1)}}{2\Delta z}\right) \qquad \text{……..(3.19)}$$

$$T_{(i,j,k-1)} = T_{(i,j,k+1)} + \frac{2q^{"}_{(t)}\Delta z}{k_e} \qquad \text{……..(3.20)}$$

Upon the boundary conditions were assumed .Then $T^n_{(i+1,j,k)} = T^n_{(i-1,j,k)}$ and $T^n_{(i,j+1,k)} = T^n_{(i,j-1,k)}$ symmetrical about this point .Therefore , $\dfrac{\partial^2 T}{\partial x^2} = \dfrac{\partial^2 T}{\partial y^2}$,

Equation (3.17) becomes

$$T^{n+1}_{(i,j,k)} = 4\lambda T^n_{(i+1,j,k)} + (1-6\lambda)T^n_{(i,j,k)} + 2\lambda T^n_{(i,j,k+1)} + \frac{2q^{"}_{(t)}\Delta z \alpha_e \Delta t}{k_e} \qquad \text{….(3.21)}$$

As for a computational grid of three dimensional model (see figure (3-2)) .At points where i= 2 to L-1 , the value of y=0 and z=0 ,then subjected heat flux ,The temperature profile through x- axis is presented as :

$$T_{(i,j,k)}^{n+1} = \lambda T_{(i+1,j,k)}^{n} + (1-6\lambda)T_{(i,j,k)}^{n} + \lambda T_{(i-1,j,k)}^{n} + 2\lambda T_{(i,j+1,k)}^{n} + 2\lambda T_{(i,j,k+1)}^{n} + \frac{2q_{(t)}^{"}\Delta z\alpha_e\Delta t}{k_e} \quad \text{……..……(3.22)}$$

When $x=0, z=0$ then subjected to heat flux .The grid increment of y-axis is presented as j= 2 to M-1 .Thus the new form of equation (3.17) becomes

$$T_{(i,j,k)}^{n+1} = 2\lambda T_{(i+1,j,k)}^{n} + (1-6\lambda)T_{(i,j,k)}^{n} + \lambda T_{(i,j+1,k)}^{n} + \lambda T_{(i,j-1,k)}^{n} + 2\lambda T_{(i,j,k+1)}^{n} + \frac{2q_{(t)}^{"}\Delta z\alpha_e\Delta t}{k_e} \quad \text{…….……(3.23)}$$

This equation is calculated the temperature profile through y- axis.

Another assumption at x=y=0 allows to calculate the temperature profile against depth at k= 2 to N-1 ,the form of equation (3.17) becomes:

$$T_{(i,j,k)}^{n+1} = 4\lambda T_{(i+1,j,k)}^{n} + (1-6\lambda)T_{(i,j,k)}^{n} + \lambda T_{(i,j,k+1)}^{n} + \lambda T_{(i,j,k-1)}^{n} \quad \text{.....(3.24)}$$

At points when i= L to L , y=2 to M-1 and k= 2 to N-1 ,surface (3). subjected boundary condition (3.10) in equation (3.13)

$$-k_e\frac{\partial T}{\partial x} = h(T-T_\infty) \quad \text{……(3.25)}$$

$$\frac{T_{(i+1,j,k)}^{n} - T_{(i,j,k)}^{n}}{\Delta x} = -\frac{h}{k_e}(T_{(i,j,k)}^{n} - T_\infty) \quad \text{…….(3.26)}$$

$$T_{(i+1,j,k)}^{n} = -\frac{h\Delta x}{k_e}\times T_{(i,j,k)}^{n} + \frac{h\Delta x}{k_e}\times T_\infty + T_{(i,j,k)}^{n} \quad \text{……..(3.27)}$$

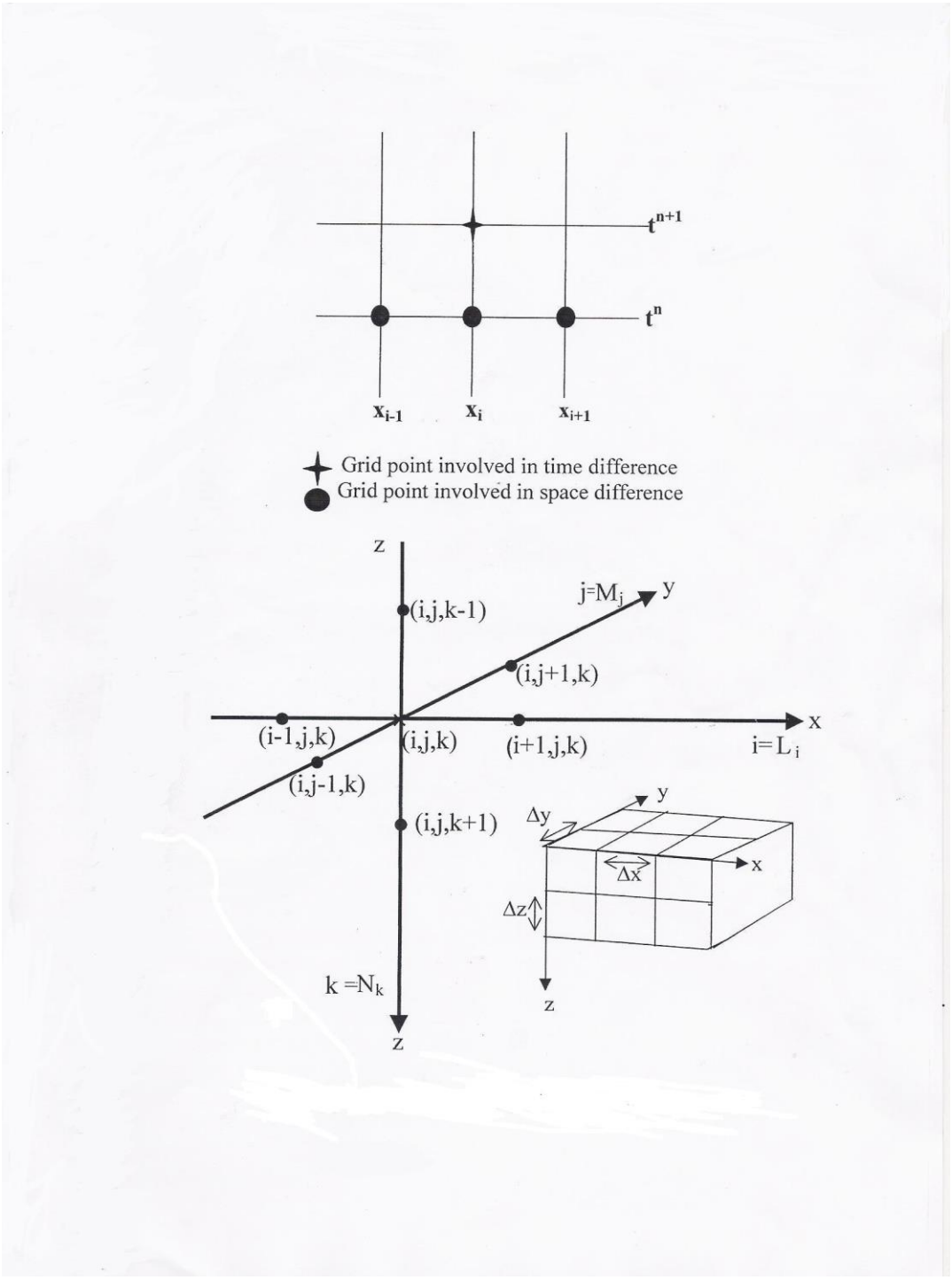

Figure (3-2) computational grid for Cartesian model

Then equation (3.18) becomes

$$T_{(i,j,k)}^{n+1} = (1 - \frac{hp}{k_e A}\alpha\Delta t - \frac{\lambda h\Delta x}{k_e} - 5\lambda) \times T_{(i,j,k)}^{n}$$
$$+ (\frac{\lambda h\Delta x}{k_e} + \frac{hp}{k_e A}\alpha\Delta t)T_{\infty} + \lambda T_{(i-1,j,k)}^{n} \quad \text{……....(3.28)}$$
$$+ 2\lambda T_{(i,j+1,k)}^{n} + \lambda T_{(i,j,k+1)}^{n} + \lambda T_{(i,j,k-1)}^{n}$$

and the same for surface (2) when i= 2 to L-1, y= 2 to M-1 and k= N to N subjected to boundary condition (3.10) ,equation (3.18) becomes :

$$T_{(i,j,k)}^{n+1} = \lambda T_{(i+1,j,k)}^{n} + \lambda T_{(i-1,j,k)}^{n} + (1 - \frac{hp}{k_e A}\alpha\Delta t - 5\lambda)T_{(i,j,k)}^{n}$$
$$+ (\frac{\lambda h\Delta x}{k_e} + \frac{hp}{k_e A}\alpha\Delta t)T_{\infty} + +2\lambda T_{(i,j+1,k)}^{n} + T_{(i,j,k-1)}^{n} \quad \text{……..…(3.29)}$$

and the for surface when i =2 to L -1 , y= 0 to and k= 2 to N-1 equation (3.17) becomes :

$$T_{(i,j,k)}^{n+1} = \lambda T_{(i+1,j,k)}^{n} + (1 - 6\lambda)T_{(i,j,k)}^{n} + \lambda T_{(i-1,j,k)}^{n}$$
$$+ 2\lambda T_{(i,j+1,k)}^{n} + \lambda T_{(i,j,k+1)}^{n} + \lambda T_{(i,j,k-1)}^{n} \quad \text{……(3.30)}$$

Also the computer program which was written by quick Basic language gives reliability for calculation of the temperature profile of all nodes in x- z plane as grid increment standard from i=2 to L-1 ,k= 2toN-1 at y=0 and for y- z plan it is started from j= 2 to M-1 ,k= 2 to N-1 at x=0 as shown figure (3-3) .The advantage of calculation of temperature profile through x-z and y- z planes is shown in the isothermal contours in these coordinates versus temperature .

Flowchart of the computer program calculated three – dimensional model is presented in figure (3-4) .

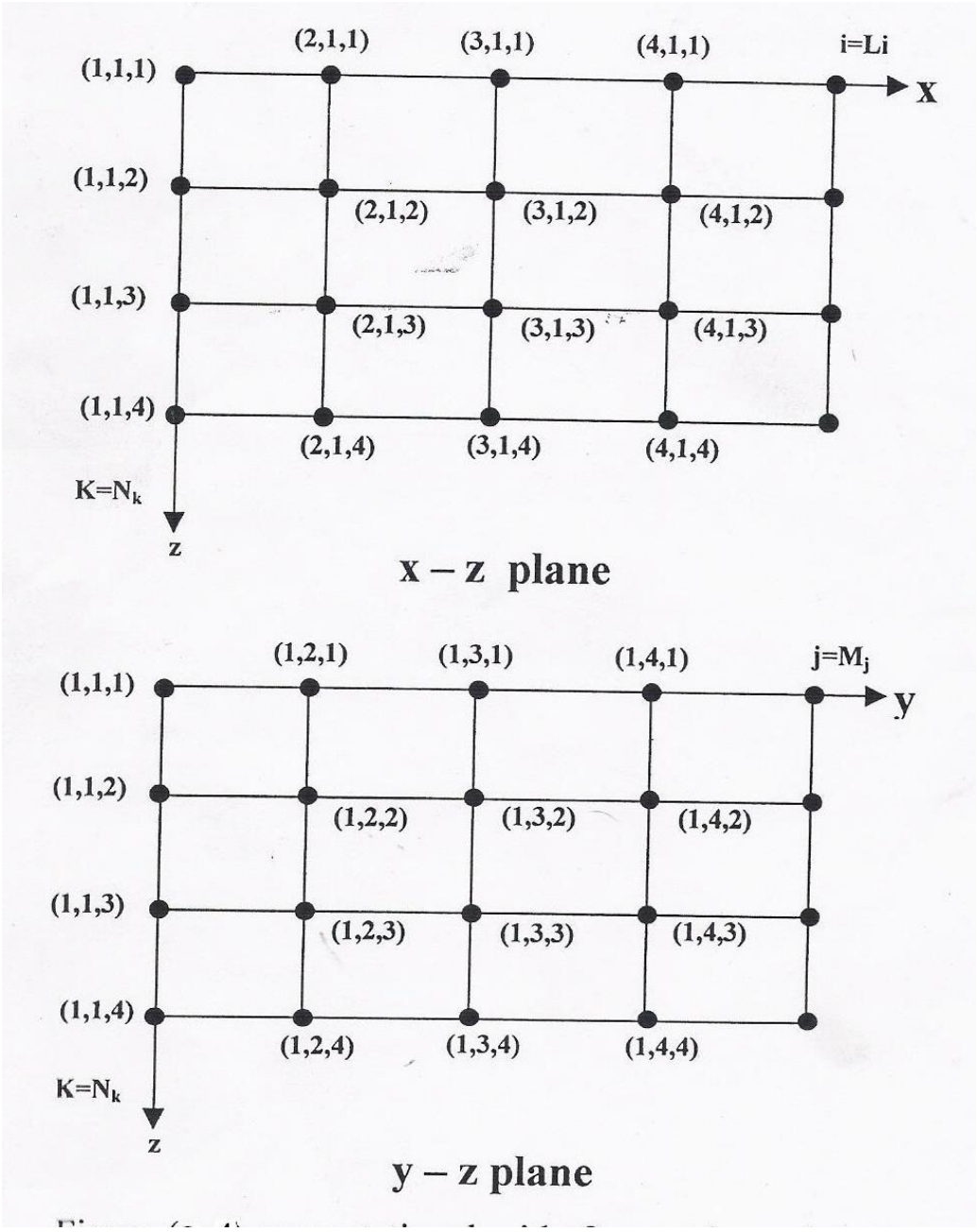

Figure (3-3) computational grid of X-Z and Y-Z planes

3.2.1. Convergence and stability :

Convergence means that Δx, Δy, Δz and Δt approach zero ,and result finite difference technique approaches true solution .Stability means that errors at any stage of the computation are not amplified but they are attenuated as computation progresses. It can be shown that the explicit method is both convergence and stable if $\lambda = 1/6$.Another way to formulate this criterion is

$$\Delta t = \frac{1}{2}\frac{\Delta x^2}{\alpha}$$

In addition ,it should be noted that setting $\lambda = \frac{1}{2}$ could result in solution in which errors do not grow but oscillate .Setting $\lambda = \frac{1}{4}$ ensures that the solution will not oscillate It is also known that setting $\lambda = \frac{1}{6}$ tends to minimize truncation error.

The flowcharts used to show the basic procedure of solution approach is given in figure (3-4).This figure shows two subroutine that's due to the two different effective thermal conductivity model used in this study. The procedure used for calculating the two effective thermal conductivity model was shown flowchart in figure (3-5).

Experimental Work

4.1. Introduction :

The purpose of this part of study is to find the temperature distribution in porous media experimentally and to calculate thermal conductivity for different samples of porous media . First one must determine the allowed boundaries that can be taken to give a close accurate accepted results ,Second the main difficultly in studying porous media experimentally is the insulation of it because of all the insulators are infect is porous media .To avoid this problem as far as possible the boundary conditions are taken similar to that one assumed in theoretical work .So the test sample will be subject to uniform heat flux from below and the other surfaces free to lose heat by convection .These two points are taken as a main guide to build a test rig .This rig must be allowed to test different samples .

4.2.Test Equipment :

4.2.1.Heater :

In order to supply a uniform heat flux which is required in this study, a plate heater was used to heat a test sample .This heater gives nearly (1000) watt at full load .This value allowed to make several tests at range (200 to 700) watt .These values are enough to give a good range of temperature in theoretical part of this study and it would to be exams experimentally. The heater resistance is 37.2 Ω. The heat flux required for the present work must be directed upward just ; this is not possible completely .Using enough quantity of glass wool in wire net container as shown in figure (4-1) gives an accepted heater insulation from below .This process is examined by fixing a three thermocouples on different distance of the external wall of heater container .

Figure (4-1) heater insulation

These thermocouples locations are chosen by dividing the height of container to three equal distance and take the first three locations as shown in figure (4-2).During the test process, a very small variation and sometimes constant temperature reading of the external wall of heater container .This temperature can already be compared with air temperature which is measured and tabled in order to check the insulation of heater.

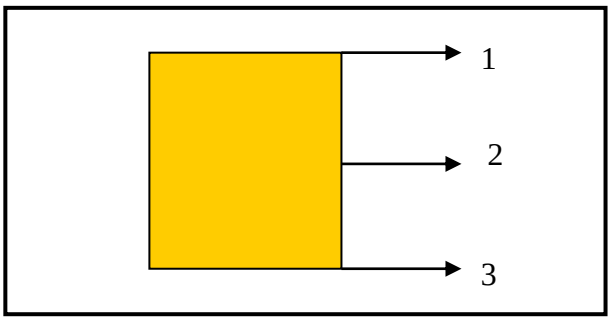

Figure (4-2) thermocouple location on heater insulation

4.2.2. Voltage variation device :

To control the value of heat flux, a variable voltage device was used .This device can supply different values of voltage with range of (0 -240) volt . This variation is controlled by changing of internal resistance until reaches the required value of voltage .

4.2.3.Voltage and Current measurement devices :

The values of this heat flux were determined by using a single digital voltmeter to measure voltage and single digital ammeter to measure the current of the heater in order to calculate the electrical power supply .Where

$$\text{Power (watt)} = \text{Voltage (volt)} \times \text{Current (amp.)}$$

$$\text{Power} = V \times I \times 0.83 \qquad \text{.....(4.1)}$$

4.2.4.Temperature Measurements :

The measurement of temperature is crucial importance in monitoring the performance of the process involved .The choice of the suitable instrument is very important to take optimum measurements advantage results.

In this work thermocouples were used to measure the temperature on a lot off positions over porous material .Some of these values were used to find temperature distribution in porous media while the others were used to measure the effective thermal conductivity of porous media .

4.2.4.1 . Thermocouples

Copper-constantan thermocouples type (*T*) were extensively used for temperature measurements in range -200°C to +300°C.Omega [34] gave information of thermocouple types as shown in table (4-1).In this research eleven thermocouples were used to measure the temperature at difference positions inside porous media. The thermocouples were calibrated using results produced by Alwan [35] who used correction temperature equations depend on the number of thermocouples .A program code (NOEDREG 164) was used to compare the resistance thermometer temperature with thermocouple temperature to obtain the true temperature for every

thermocouple, hence the constants a_0, a_1, a_2 and a_3 were determined. .The general equation is :

$$T_{true} = a_0 + a_1 T + a_2 T^2 + a_3 T^3 \quad \text{.....(4.2)}$$

Where

a_0, a_1, a_2 and a_3 are constants .

T : is the temperature of thermocouple recorded by (CMTO1). The thermocouple equations are :

Thermocouple number one :

$$T_{true1} = -0.572389449 + 1.0971406 T_1 - 1.03240643 \times 10^{-4} T_1^2 + 2.29859156 \times 10^{-7} T_1^3 \quad \text{.....(4.3)}$$

Thermocouple number two:

$$T_{true2} = -0.236971516 + 1.00482355 T_2 + 4.42338038 \times 10^{-5} T_2^2 - 2.27122518 \times 10^{-7} T_2^3 \quad \text{.....(4.4)}$$

Thermocouple number three:

$$T_{true3} = -0.359331102 + 1.01127635 T_3 - 7.6876892 \times 10^{-7} T_3^2 + 1.5107187 \times 10^{-7} T_3^3 \quad \text{.....(4.5)}$$

Thermocouple number four

$$T_{true4} = -0.341961683 + 1.00638 T_4 + 2.83107834 \times 10^{-5} T_4^2 - 1.77804587 \times 10^{-7} T_4^3 \quad \text{.....(4.6)}$$

Thermocouple number five

$$T_{true5} = -0.57648419 + 1.01902833 T_5 - 1.0705613 \times 10^{-4} T_5^2 + 2.455437732 \times 10^{-7} T_5^3 \quad \text{.....(4.7)}$$

Thermocouple number six

$$T_{true6} = -.0209019145 + 0.9995666297 T_6 + 9.60522688 \times 10^{-5} T_6^2 - 3.86482898 \times 10^{-7} T_6^3 \quad \text{.....(4.8)}$$

Thermocouple number seven

$$T_{true7} = -.507282043 + 1.01463498 T_7 - 5.865787 \times 10^{-5} T_7^2 + 8.11705617 \times 10^{-8} T_7^3 \quad \text{.....(4.9)}$$

Thermocouple number eight

$$T_{true8} = -0.2954495052 + 1.00483713 T_8 + 4.331822963 \times 10^{-5} T_8^2 - 2.39681065 \times 10^{-7} T_8^3 \quad \text{.....(4.10)}$$

Thermocouple number nine

$$T_{true9} = -0.488828026 + 1.01317177 T_9 - 4.000442 \times 10^{-5} T_9^2 + 2.16269615 \times 10^{-8} T_9^3 \quad \text{.....(4.11)}$$

Thermocouple number ten

$$T_{true10} = -0.24644188 + 1.00400299 T_{10} + 5.5128341 \times 10^{-5} T_{10}^2 - 2.8323866 \times 10^{-7} T_{10}^3 \quad \text{.....(4.12)}$$

These equations are used with computer program to correct temperature readings.

Table (4-1) thermocouples information .Ref. [34].

Thermocouple Type	**Name of Materials**	**Useful Application Range (°C)**
B	Platinum 30% Rhodium(+) Platinum 6% Rhodium (-)	**1370 – 1700**
C	Tungsten 5% Rhenium (+) Tungsten 26% Rhenium(-)	**1650 – 2315**
E	Chromium (+) Constantan (-)	**-200 – 900**
J	Iron (+) Constantan (-)	**0 – 750**
K	Chromium (+) Aluminum (-)	**-200 –1250**
N	Nicrosil (+) Nisil (-)	**650 – 1260**
R	Platinum 13% Rhodium(+) Platinum (-)	**870 – 1450**
S	Platinum 10% Rhodium(+) Platinum (-)	**980 – 1450**
T	Copper (+) Constantan (-)	**-250 – 350**

4.2.4.2. Temperature Recording Device

A computerized temperature meter (CTMO1) was used to record the temperature readings at different position on the samples. There is an interface cart logically used to change the measured data (temperature) from test sample to PC. This device can transform (15) thermocouple reading to digital readings at the same time as shown in figure (4-3). The temperature rang achieved by this device is (0 to 500) ^{o}C. The time recorded represented a true time between time steps because it is programmed to calculate the real time required .

This device was calibrated by using a thermometer reading air temperature at the same time of (CTMO1) readings in different time intervals .Thermometer and CTMO1 readings were recorded in table (4-2) and figure (4-4) represented this calibration. This process was done in order to know the best time, which the CTMO1 response the true reading. Experiments show that the reading must be started after 18 second from the switching on of (CTMO1) in order to give more stability for readings . The important calibration through this experimental work was the thermocouples reading which were calibrated depending upon the equations (4.3) to (4.12) .These equations give more reliable results for temperature measurement through test samples.

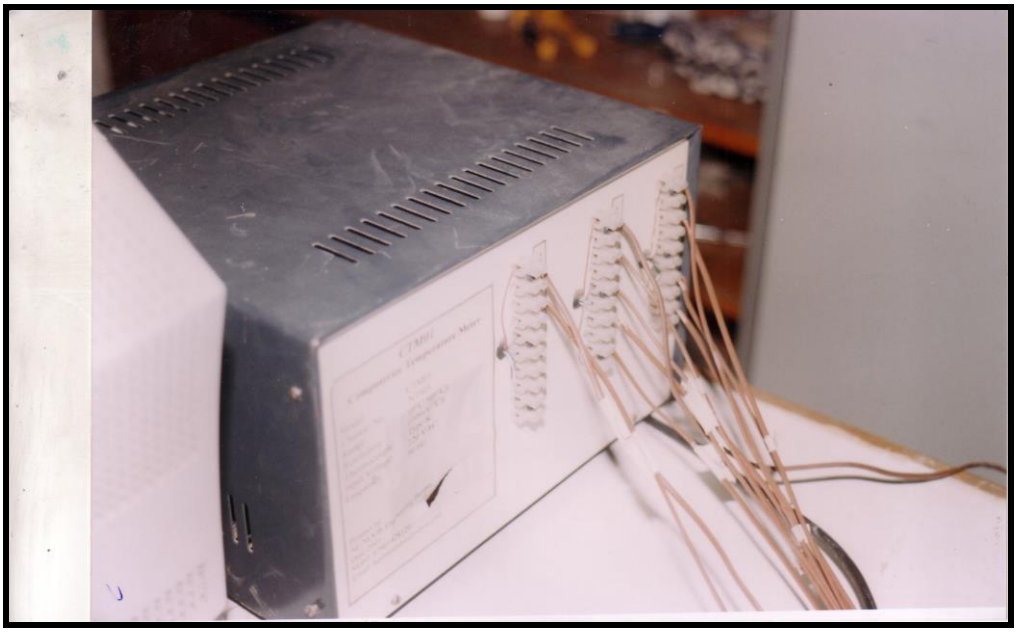

Figure (4-3) CMTO1 thermocouples connection.

Table (4-2) thermometer and CMTO1 device air temperature readings

Time (second)	Thermometer readings (℃)	CTMO1 device readings (℃)
5	27.8	25.4
10	27.6	28.9
15	27.7	28.12
20	27.7	27.67
25	27.6	27.7
30	27.6	27.53
35	27.6	27.72
40	27.8	27.7
45	27.7	27.65
50	27.6	27.72
55	27.7	27.7
60	27.7	27.67
65	27.6	27.71
70	27.7	27.73
75	27.6	27.8
80	27.7	27.72
85	27.6	27.68
90	27.8	27.76
95	27.7	27.8
100	27.5	27.63
105	27.6	27.71
110	27.7	27.68
115	27.7	27.73
120	27.6	27.63

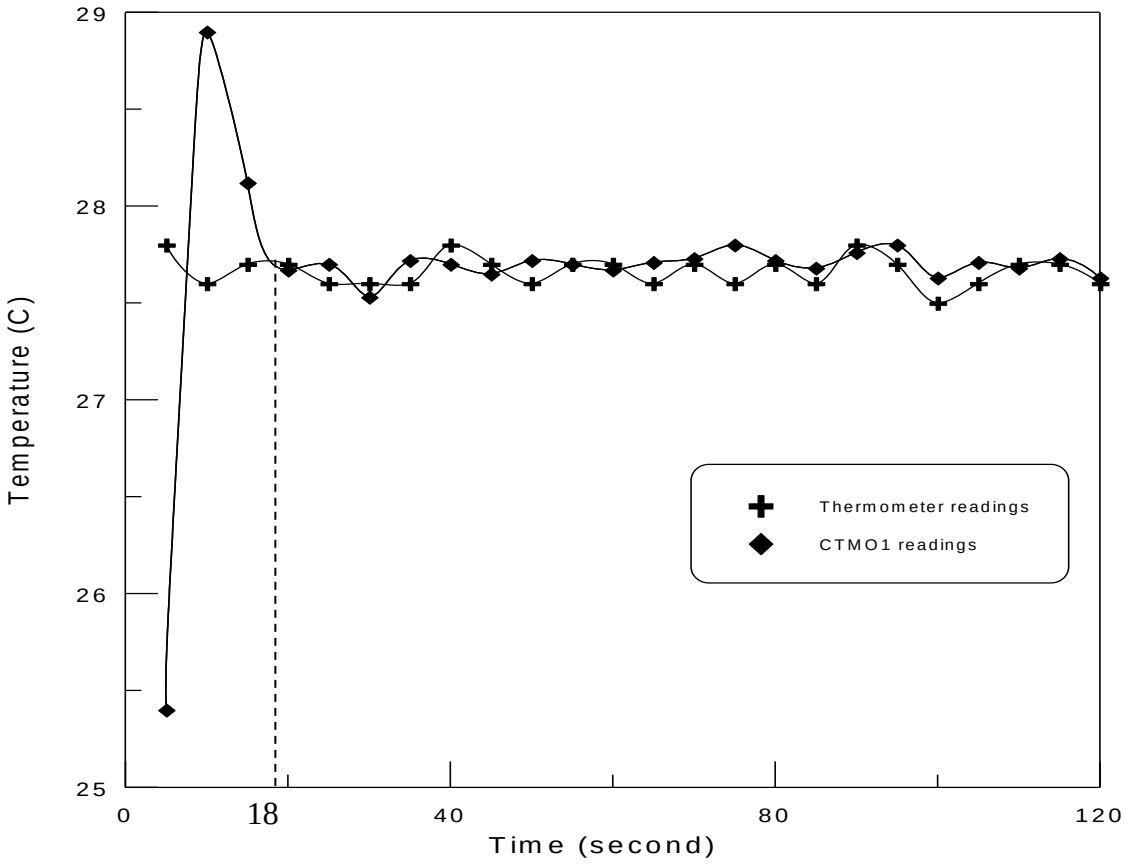

Figure (4- 4)CMTO1 calibration curve

4.3. **Sample Preparation.**

A three cubes samples of porous media are used in this study .These samples are made from two types of porous media .One is a real porous media which is the MgO as shown in figure (4-5) ,While the others are made from a chrome steel balls arrangement together in order to make a matrix analogs a porous media as shown in figure(4-6).These balls are (6)mm and (4.8)mm in diameter.

Fig (4-5) MgO test sample with heater

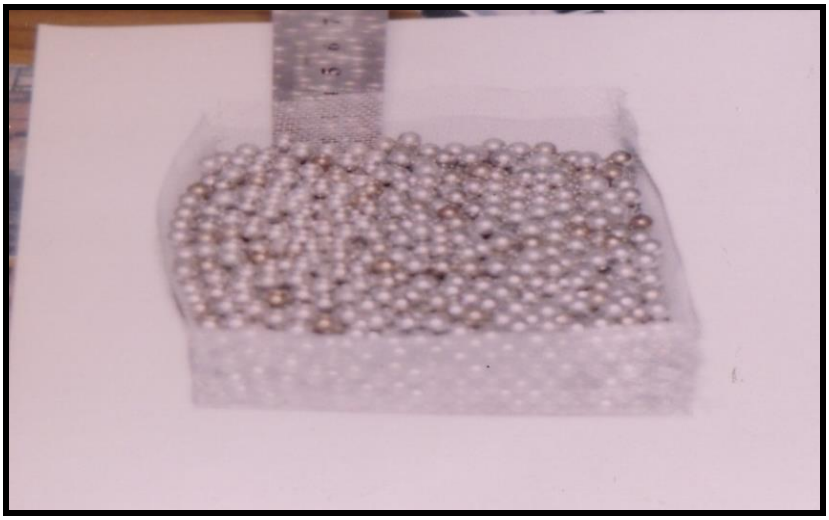

Fig (4-6) chrome-steel balls matrix

. The MgO test sample dimensions are (10×10×6) cm with porosity of (0.378) , and it is fulfilled with air .The steel balls matrix is (10×10×3)cm and it is fulfilled with air too .The area of surface subjected to uniform heat flux is(100) cm^2 in all test samples .That's mean the heat generated in heater divided by this area to give the value of heat flux which caused the temperate increasing in sample

4.4.Equipment Assembly :

After the heater has been fully insulated from below and all the sides. The rig elements are assembled together . Figure (4-7) shows a schematic diagram of equipment

4.5. Experimental Procedure:

First , thermocouples were fixed on the test sample .The location distribution of thermocouples was chosen to cover a maximum area of the samples , similarity of test samples helps to reach this purpose.

After preparing the computer and a CMTO1 device a power was supplied to the rig without test sample .Reading and recording to the outer wire net container in addition to environment air temperature .When this reading is approximately constant with time ,test sample was added to rig and the computer starting record and save the results in files as shown in figure (4-8).Values of temperatures were tabled with time for each test sample as shown in tables in appendix (B) .For MgO the temperature recorded for z-axis . For Chrome steel –air matrixes the temperature for x-axis were recorded .For both type of test sample the temperature of center point of the surface subjected to heat flux are recorded with time .All of these readings were repeated for two values of heat flux which were 40000 and 70000 W/m^2 respectively . The experimental work was made with environment temperature of 27°C and atmospheric pressure .All temperatures reading were calibrated by using the calibration equations (4.3) to (4.12) in order to get accurate results for the measurement of temperature distribution through the porous media.

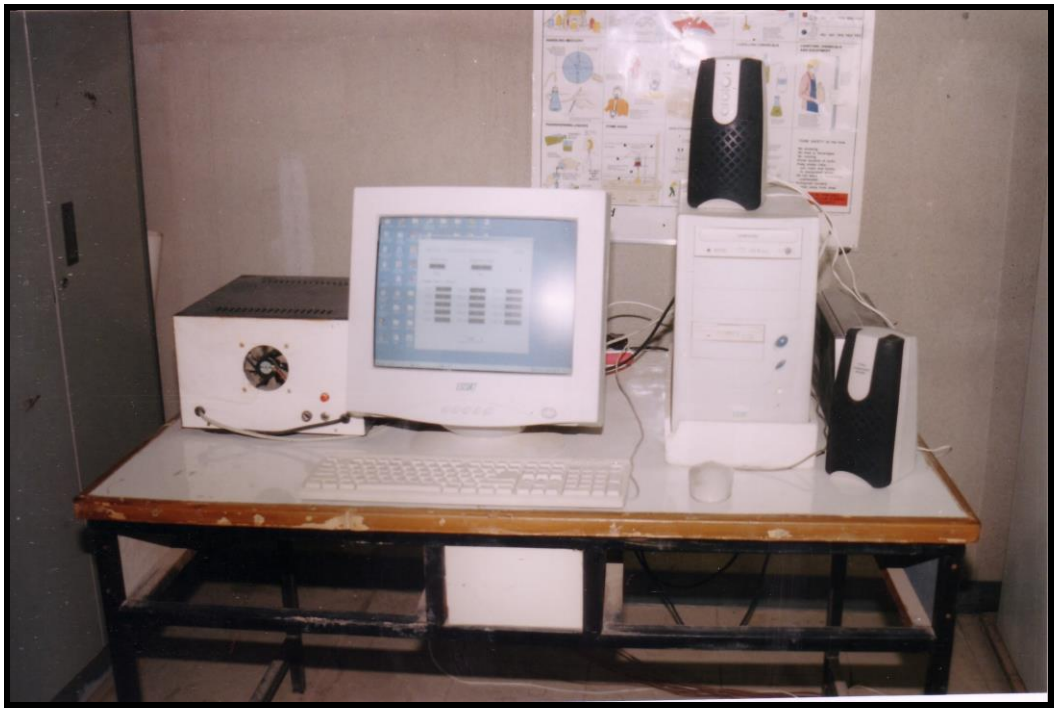

Figure (4-8) CMTO1 device recording temperature with computer

4.6. Measurement of Porosity :

Porosity was measured for Chrome steel balls matrix .The values of porosity were used as feeding parameters when effective thermal conductivity calculated in theoretical part of this study . The porosity measured by filling the test chamber with a known volume of water as shown in figure (4-9) ,then steel balls were added to create the porous medium. While the steel balls added ,the displaced water was measured .Hence the porosity was calculated from :

$$\phi = 1 - \frac{V_d}{V_i} \qquad \text{.....(4.13)}$$

where

V_i = Initial volume

V_d = Displaced volume.

This operation repeated for two type of steel matrix .

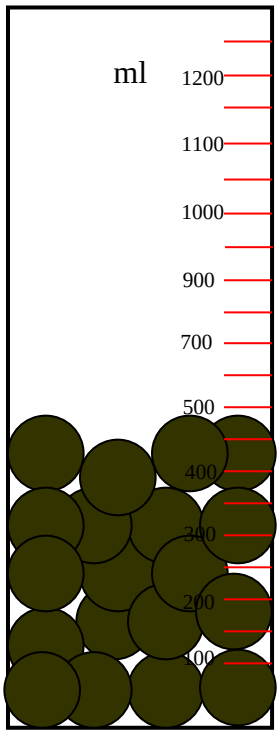

Figure (4-9) equipment used to measure porosity of chrome steel matrix

4.7. Measurement of Thermal Conductivity

4.7.1. Readings:

It should be measured the temperature distribution over the MgO-air system in order to calculate the effective thermal conductivity . In the present work some points were chosen over MgO-air system in order to calculate the effective thermal conductivity .These readings were shown in tables (4-3) to (4-8).In MgO sample ,a (2)mm diameter holes with different depths were done to fix thermocouples as shown in figure (4-10).

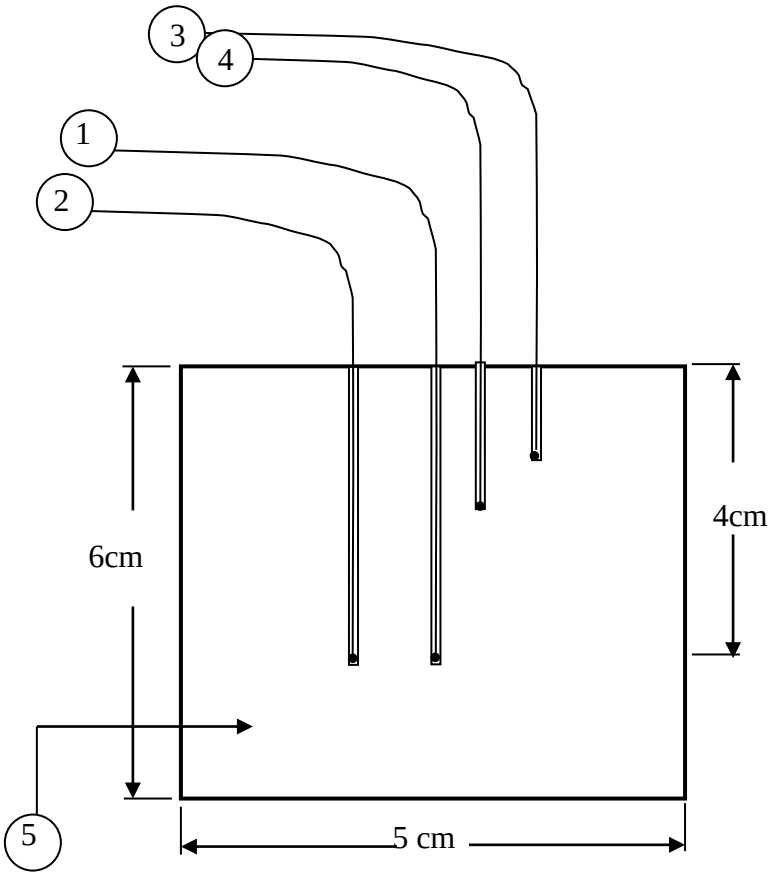

1 and 2	X-direction thermocouples positions
3 and 4	Y-direction thermocouples positions
5	MgO test sample

Figure (4-10) thermocouples location in MgO test sample

These readings were also calibrated by using the same method used in section (4.2.4.1) and calculating the temperature of these measurements .Experimental work was done with three time intervals .The values of heat flux subjected was 40000 and 70000 W/m^2 .Tables (4-3) to (4-8) shows the calibrated temperature values of the selected points of test sample at three time intervals and for two values of uniform heat flux.

Table (4-3)temperature distribution along x-axis and heat flux =40000 W/m^2

Time(sec)	X= .01 m	X= .02 m	X =.03 m
600 660	38.55 °C 38.96 °C	38.11°C 39.79°C	36.43°C 36.81°C
1200 1260	48.26°C 50.12°C	46.51°C 48.76°C	44.98°C 45.79°C
1800 1860	57.32°C 58.32°C	53.33°C 54.72°C	48.39°C 48.84°C

Table (4-4)temperature distribution along y-axis and heat flux =40000 W/m^2

Time (sec)	Y= .01 m	Y= .02 m	Y =.03 m
600	39.23°C	38.11°C	35.77°C
1200	49.21°C	46.51°C	43.65°C
1800	56.11°C	53.33°C	50.57°C

Table (4-5) temperature distribution along z-axis and heat flux =40000 W/m^2

Time (sec)	Z= .01 m	Z= .02 m	Z =.03 m
600	49.87°C	38.11°C	36.64°C
1200	62.7°C	46.51°C	41.11°C
1800	68.47°C	53.33°C	44.23°C

Table (4-6) temperature distribution along x-axis and heat flux =70000 W/m^2

Time(sec)	X= .01 m	X= .02 m	X =.03 m
600 660	44.11°C 46.73°C	43.91°C 44.72°C	42.71°C 44.11°C
1200 1260	62.08°C 63.93°C	59.77°C 61.11°C	57.23°C 57.99°C
1800 1860	73.35°C 74.05°C	66.43°C 68.17°C	62.12°C 63.13°C

Table (4-7)temperature distribution along y-axis and heat flux =70000 W/m^2

Time(sec)	Y= .01 m	Y= .02 m	Y =.03 m
600	43.87°C	43.31°C	41.22°C
1200	61.48°C	58.83°C	56.51°C
1800	72.85°C	67.09°C	62.88°C

Table (4-8)temperature distribution along z- axis and heat flux =70000 W/m^2

Time(sec)	Z= .01 m	Z= .02 m	Z =.03 m
600	64.41°C	56.22°C	53.15°C
1200	88.32°C	70.11°C	58.91°C
1800	96.37°C	78.37°C	62.94°C

4.7.2. Calculation of Effective Thermal Conductivity

In case of steady state ,one dimensional conduction heat flow Fourier's law can be applied

$$q''_{(t)} = -k\frac{dT}{dx} \qquad \text{.....(4.14)}$$

Where $q''_{(t)} = \frac{q}{A}$ is the heat flux subjected

A is the perpendicular area of heat flow direction

$\frac{dT}{dx}$ is the temperature gradient by distance

In this study the heat transfer was in three direction because of the test sample did not insulated in all surfaces except the one subjected to heat flux .In this case there was a heat lost by convection due to temperature difference with the environment. So the heat flux subjected is in fact :

$$q''_{(t)} = q''_x + q''_y + q''_z \qquad \text{.....(4.15)}$$

For modeling heat conduction in a material, the energy conservation law(the first law of thermodynamics) was applied. At a time t, the energy conservation law for a control volume was expressed as

$$\frac{\partial}{\partial x}\left(k_x\frac{\partial T}{\partial x}\right)+\frac{\partial}{\partial x}\left(k_y\frac{\partial T}{\partial y}\right)+\frac{\partial}{\partial x}\left(k_z\frac{\partial T}{\partial z}\right)=(\rho c_p)_e\frac{\partial T}{\partial t} \qquad \text{.....(4.16)}$$

Assuming that there is no change in thermal conductivity in space (dx, dy and dz) and time interval (Δt),

$$k_x = k_y = k_z = k_e$$

equation (4.16) becomes as

$$(\rho c_p)_e\frac{\partial T}{\partial t} = k_e\frac{\partial^2 T}{\partial x^2}+k_e\frac{\partial^2 T}{\partial y^2}+k_e\frac{\partial^2 T}{\partial z^2} \qquad \text{.....(4.17)}$$

Equation (4.17) could be written as

$$(\rho c_p)_e \frac{\partial T}{\partial t} = k_e(\frac{\partial^2 T}{\partial x^2} + \frac{\partial^2 T}{\partial y^2} + \frac{\partial^2 T}{\partial z^2}) \quad \text{.....(4.18)}$$

This equation used to calculate k_e at any point after analyzing it in finite difference time domain form with explicit technique as

$$(\rho c_p)_e(\frac{T^{n+1}_{(i,j,k)} - T^n_{(i,j,k)}}{\Delta t}) = k_e(\frac{T^n_{(i+1,j,k)} - 2T^n_{(i,j,k)} + T^n_{(i-1,j,k)}}{\Delta x^2} + \frac{T^n_{(i,j+1,k)} - 2T^n_{(i,j,k)} + T^n_{(i,j-1,k)}}{\Delta y^2} + \frac{T^n_{(i,j,k+1)} - 2T^n_{(i,j,k)} + T^n_{(i,j,k-1)}}{\Delta z^2}) \quad \text{.....(4-19)}$$

The point of coordinate of (2,2,2)cm from the center point was chosen to calculate the effective thermal conductivity at cretin time .The above equation can be applied after recording eight temperature values . Six of these temperature values were $(T_{i+1}, T_{i-1}, T_{j+1}, T_{j-1}, T_{k+1} and T_{k-1})$,all these temperatures values at old time. The temperature $(T_{i,j,k})$ recorded in both old and new time to complete equation (4.19) in addition the value of (ρc_p) and (Δt).

The value of (ρc_p) calculated according to reference [7] as

$$(\rho c_p)_e = \phi(\rho c_p)_f + (1-\phi)(\rho c_p)_s \quad \text{.....(4.20)}$$

Ziman [36] presented *Cp* of MgO equal (940) (J/kg. K) and Barry et al [37] presented value of $\rho = 3.58 g/cm^3$ .These values are used with equation (4.19) to determine k_e with the experimental readings .

Calculating the effective thermal conductivity from equation (4-19) can be used to determine thermal conductivity of solid phase k_s (MgO) with the assuming a constant value of thermal conductivity of fluid phase (k_f) .Figure (4-11) which was presented by [1] used to calculate the thermal conductivity's ratio depending on the results of effective thermal conductivity from equation (4.19) .These results were divided by fluid thermal conductivity to find k_e / k_f and this value used to find

K .The values of K were calculated for two studied models of effective thermal conductivity used in theoretical part of this study .

In this part of study effective thermal conductivity was measured for MgO due to it was a real porous media with a fixed particles .This procedure couldn't be used Chrome steel –air matrix because the ability of steel balls to slip as the thermocouples fixed in selected points and this gave an error in measuring temperature readings and then in calculations .

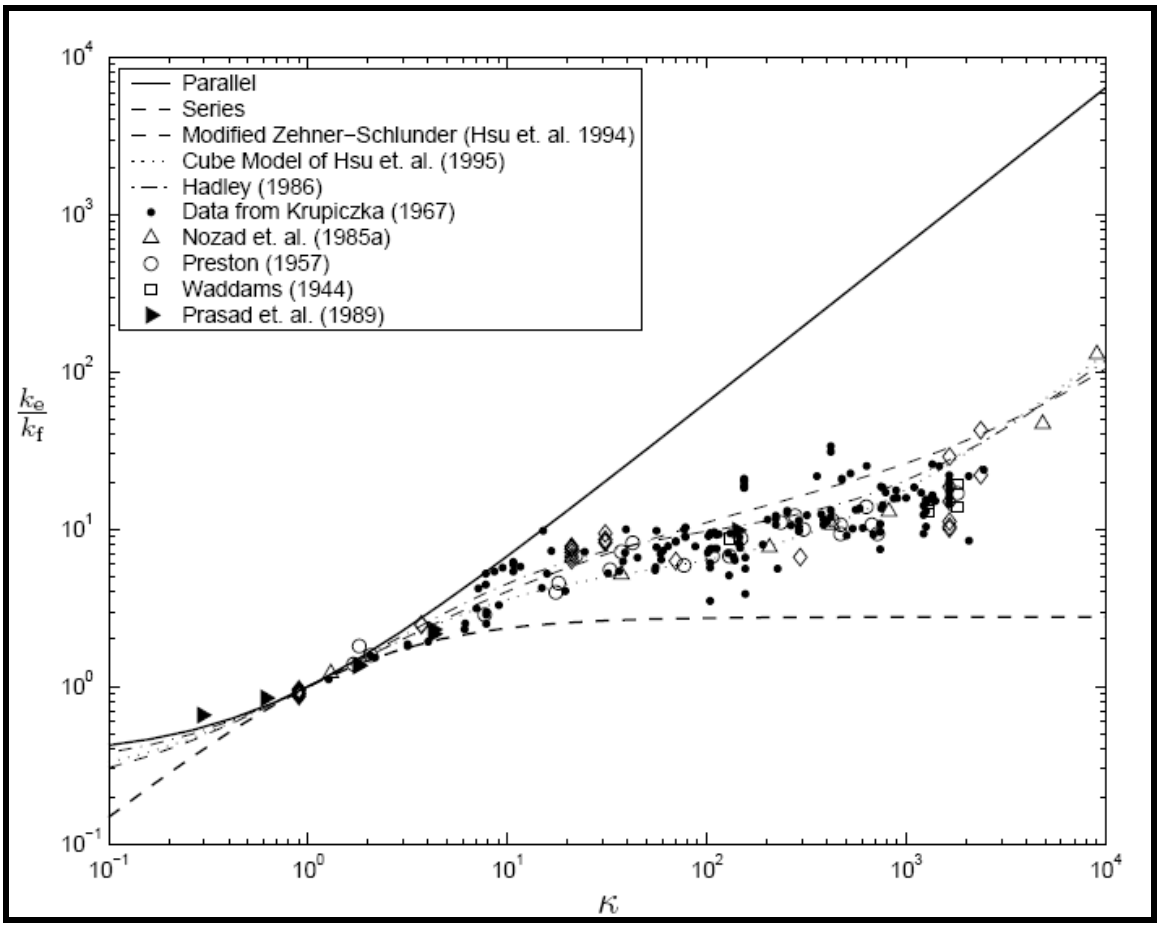

Figure (4-11)Comparison of models for the effective thermal conductivity and experimental data .Ref.[1].

4.8. Calculation of Dense Thermal Conductivity of MgO (k_{dense})

The results of effective thermal conductivity according equation (4-19) and figure (4-11) were tabled in (4-9) and (4-10) .Depending on the equations presented by Klumens [38] and Maxwell- Garnett [7],thermal conductivity of pure dense MgO was calculated and compared with that one used in theoretical part of this study .The equation presented by [39] is

$$\frac{k_{porous}}{k_{dense}} = 1 - \frac{4}{3}\phi \qquad \text{.....(4-21)}$$

And the equation presented by Maxwell- Garnett [7] which is

$$\frac{k_{porous}}{k_{dense}} = 1 - \frac{3}{2}\phi \qquad \text{.....(4-22)}$$

Where k_{porous} is thermal conductivity of porous MgO

k_{dense} is thermal conductivity of pure dense MgO

The results of calculations were presented in tables (4-11) and (4-12) where, k_z and k_h thermal conductivity ratio according to method number one and two for calculating effective thermal conductivity respectively .

Table (4-9) results of thermal conductivity ratio from figure (4-11) when heat flux 40000 W/m^2

Heat flux kW/m^2	Time (second)	Temperature °C	$k_e (w/m.c^o)$	$\frac{k_e}{k_f}$	k_h from Fig.(4-11)	k_z from Fig.(4-11)
40	600	38.11	.456	18.8	900	460
40	1200	46.51	.488	20.16	1000	580
40	1800	53.33	.463	19.132	950	490

Table (4-10) results of thermal conductivity ratio from figure (4-11) when heat flux 70000 W/m^2

Heat flux kW/m^2	Time (second)	Temperature °C	$k_e (w/m.c^o)$	$\frac{k_e}{k_f}$	k_h from Fig.(4-11)	k_z from Fig.(4-11)
70	600	43.91	.344	14.21	575	230
70	1200	59.77	.4025	16.63	880	400
70	1800	66.45	.372	15.37	620	250

Table (4-11) results of pure dens material according to eqs (4.21) and (4-22) when heat flux 40000 W/m^2

Heat flux kW/m^2	Time (second)	Temperature °C	k_{densh} from eq .(4.21)	k_{densh} from eq .(4.22)	k_{densz} from eq .(4.21)	k_{densz} from eq .(4.22)
40	600	38.11	43.9	50.31	21.95	25.15
40	1200	46.51	48.79	55.89	28.29	32.415
40	1800	53.33	46.36	53.09	23.9	27.38

Table (4-12) results of pure dens material according eqs (4-20) and (4-21) when heat flux 70000 W/m^2

Heat flux kW/m^2	Time (second)	Temperature °C	k_{densh} from eq .(4.21)	k_{densh} from eq .(4.22)	k_{densz} from eq .(4.21)	k_{densz} from eq .(4.22)
70	600	43.91	28.05	32.13	11.22	12.85
70	1200	59.77	38.35	43.93	19.516	22.38
70	1800	66.45	30.25	34.65	12.197	13.97

Results and Discussion

The theoretical model gave suitable results to explain temperature distribution inside porous media test samples .These results were carried out for two values of heat flux of 40000 W/m^2 and 70000 W/m^2 .These results were showed in figures for temperature distribution through x-axis, z-axis and y-z plane. The experimental work gave a results for temperature distribution in MgO sample system and in the two Chrome steel-air matrixes .Also this work allowed to calculate thermal conductivity for MgO. All experiments are carried out in this study with room temperature of $\approx$ 27°C. The steady state condition did not reached in this work because the ability of porous media received and stored the heat for a long time . Also the influence of thermal properties variation affected only with unsteady state case.

5.1. Temperature distribution

Part (I) Theoretical work

Figures (5-1) to (5-6) show the prediction results of temperature variation with time at center point of surface at two values of heat flux and porosity for two materials .These results indicate that the temperature variation increase with increasing time and also with increasing the values of heat flux. In these analyses two empirical equations (equation (3.4) and (3.6) were used to calculate the effective of thermal conductivity through the prediction model which was built in this work.

Figures (5-1) and (5-2) represent the temporal variation of temperature in MgO-air system at heat flux values of 40000 W/m^2 and 70000 W/m^2. These figures indicated that the effective thermal conductivity which was calculated by using two methods, gave a close results in both heat flux values.

Figures (5-3) to (5-6) illustrate the variation of temperature with time of steel – air systems at two values of heat flux and porosity .The values of measured porosity were 0.416 and 0.313 .It can be noticed that these is a difference of temperature prediction calculation when using two methods of calculation effective thermal conductivity .This difference appeared in figure (5-3) and (5-4) and it was to be 10°C.These figures represent two samples of Chrome steel- air system at different values of porosity.

Figures (5-7) to (5-14) represent temperature distribution for of MgO-air system and steel-air system through x and z directions at different values of heat flux.

Figures (5-7) to (5-10) show the spatial temperature of MgO –air system in x-axis at different time intervals of 600 second. Figure(5-7) represents spatial temperature distribution of MgO by calculation effective thermal conductivity by method number one, and figure (5-8) at method number two and value of heat flux 40000 W/m^2 .It was shown that temperature gradient was increased with distance.The maximum values of temperature at the center of the sample. It was shown that the temperature increasing with time interval and with heat flux.

Figure (5-11) and (5-12) show the temperature distribution through z- axis in MgO –air system at different times interval , with heat flux of 40000 W/m^2 depending upon the two methods of calculating the effective thermal conductivity. While, figures (5-13) and (5-14) represent the temperature distribution of MgO through z-axis at different times interval with heat flux of 70000 W/m^2 . These figures show a high degree of negative gradient in temperature through z-axis .This is due to heat flux concentrated on the upper surface of metal ,and temperature should be higher at the top and decreased gradually in depth .

Figures (5-15a),(5-15b) and (5-15c) show an isothermal contour maps for (y-z) plane of MgO-air system at heat flux of 40000 W/m^2 with different times interval depending upon the method number one of effective thermal conductivity .

Figures (5-16a),(5-16b) and (5-16c) give an isothermal contour maps for (y-z) plane in MgO-air system at heat flux of 40000 W/m^2 with different times interval

depending upon method number two of calculating the effective thermal conductivity. It was shown that the temperature decrease far away from the center point .That was depended upon the heat flux and time interval of heating.

Figures (5-17a) to (5-18c) show an isothermal contour maps for (y-z) plane of MgO-air system at heat flux of 70000 W/m^2 with different times intervals depending upon two methods for calculating the effective thermal conductivity .

In figure (5-17) and (5-18) the difference in results is not clear at starting time interval due to the solid and fluid phase thermal conductivities was effected grater than the geometrical parameter (porosity).The accumulation of impedance to heat flow in all direction leads to different results shown in figures between (5-17b)and(5-18b) and between (5-17c) and (5-18c).That was due to the inside of porous material the fluid phase was indicated.

Figures (5-19) to (5-22) present temperature distribution trough x- axis of Chrome steel-air matrix of porosity (0.416) with time interval of 600 seconds depending also on the two methods of calculating the effective thermal conductivity at two values of heat flux .

Figure (5-19) and (5-20) predict a small negative gradients of temperature distribution through x-axis in Chrome steel-air system at heat flux 40000 W/m^2 according to method number one and two of calculating effective thermal conductivity .

Figures (5-21)and (5-22)show a higher negative gradients of temperature distribution through x-axis in Chrome steel -air system when heat flux is 70000 W/m^2 depending on two methods for calculating effective thermal conductivity. The degree of gradients in both figures show that the temperature difference is sensible between the two models due to the effective thermal conductivity equations parameters .These graphs also indicated that temperature distributed increased with increasing the time interval and heat flux value .

Figures (5-23) to (5-26) presented temperature distribution through z- axis for Chrome steel($\phi = .416$)-air system at time interval of 600 seconds depending also

on the two methods to calculate the effective thermal conductivity for two value of heat flux.

Figures (5-23) and (5-24) show the temperature distribution through z- axis in Chrome steel($\phi = .416$)–air system at different times interval , with heat flux of 40000 W/m^2 according to method number one and two of calculating the effective thermal conductivity . These figures show a more negative gradient of temperature distribution than figures (5-25) and (5-26) .This due to the value of thermal conductivity ration (k) was decreased with increasing heat flux .The difference between these figures indicates that both methods gave the same effect of temperature distribution as the heat flux increased.

Figures(5-27a) to (5-28c) illustrate an isothermal contour maps for (y-z) plane in Chrome steel($\phi = .416$)–-air system with heat flux of 40000 W/m^2 at different times intervals depending upon the two methods for calculating the effective thermal conductivity .The above figures show that the temperature increased in both directions with time and with increasing the heat flux value .

Figure (5-29a) to (5-30c) show an isothermal contour maps for (y-z) plane for chrome steel($\phi = .416$)–air system with heat flux of 70000 W/m^2 at different time intervals depending upon the two methods for calculating the effective thermal conductivity .These two figures indicted the influence of geometrical parameter (porosity) is decrease as heat flux increase.

Figures (5-31) to (5-34) present temperature distribution of Chrome steel-air matrix through x-axis at different value of porosity($\phi = 0.313$) with different times interval ,also depending upon the two methods of calculating the effective thermal conductivity for two value of heat flux .These figures show a negative gradient of temperature distribution and show that the gradient increased with time due to heat flux subjected. Figures(5-33) and (5-34) indicated that the heat transfer in porous media was influenced by geometry at the starting of heating process . The thermal

conductivity ratio (k) is the main factor effects on temperature distribution as heating process increased .

Figures (5-35) to (5-38) describe the temperatures distribution of Chrome steel($\phi = .313$) -air system trough z- axis at time interval of 600 seconds depending upon the two methods of calculating the effective thermal conductivity for two value of heat flux ..The difference between these two figures is small because of the heat flux direction and the small porosity influence on heat transfer within porous media with high thermal conductivity ratio and low porosity .Figure (5-37) and (5-38) show higher temperature gradient than figures (5-25) and (5-26) that's ensured the fact of high thermal conductivity ratio ,low porosity porous media can be treated as solid material in heat transfer simulation taking in account the effective properties.

Figures(5-39a) to (5-40a) point an isothermal contour maps for (y-z) plane of Chrome steel($\phi = .313$)–air system with heat flux of 40000 W/m^2 at three time intervals of 600 second depending upon the two methods of calculating the effective thermal conductivity .These figures indicate that the temperature decreases far away from center point of sample .These figures show a difference in temperature distribution between two models and this difference stated as heating process start.

Figures (5-41a) to (5-42c) explain an isothermal contour maps for (y-z) plane of chrome steel($\phi = .313$)–air system with heat flux of 70000 W/m^2 at three time interval of 600 seconds depending also upon the two methods for calculating the effective thermal conductivity .These figures indicated that temperature increased as the heat flux and time increased and it decreased far away from center point.

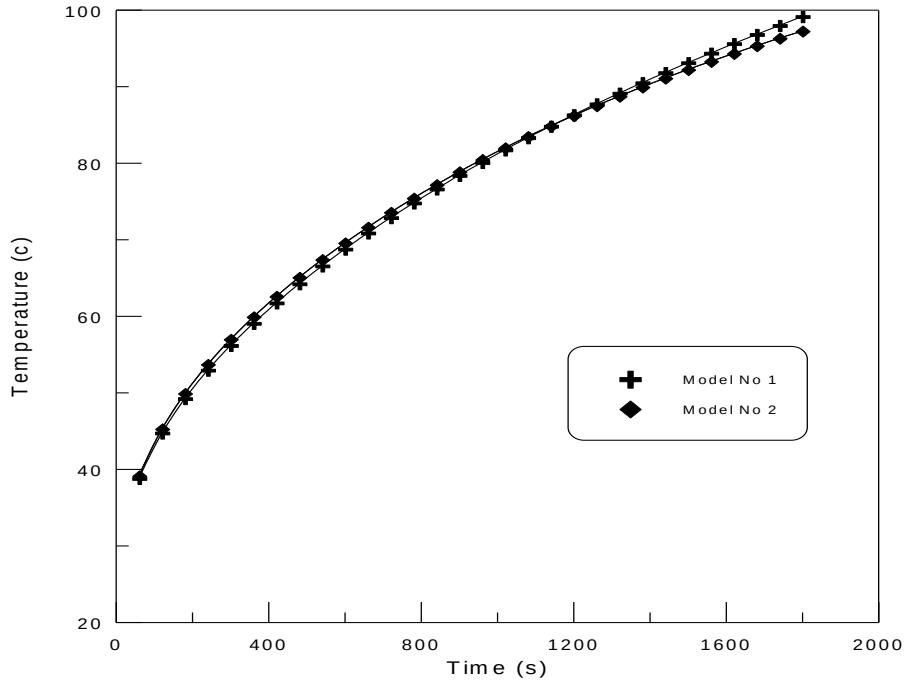

Figure (5-1) temperature variation with time at center point for MgO-air system when heat flux=40000W/m^2 according to method No1and No2 of calculating k_e

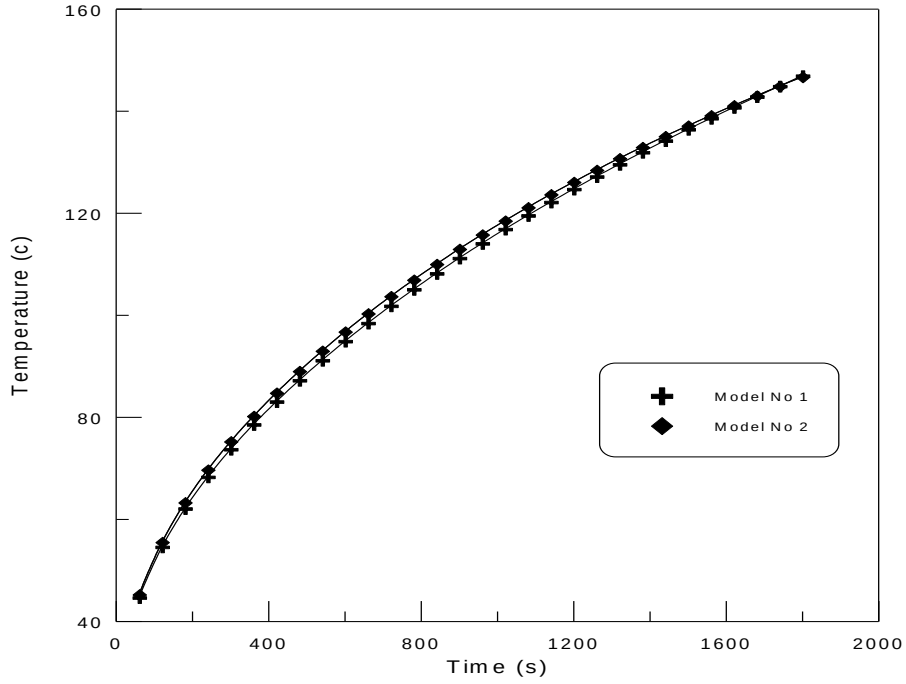

Figure (5-2) temperature variation with time at center point for MgO-air system when heat flux=70000W/m^2 .according to method No1and No2 of calculating k_e

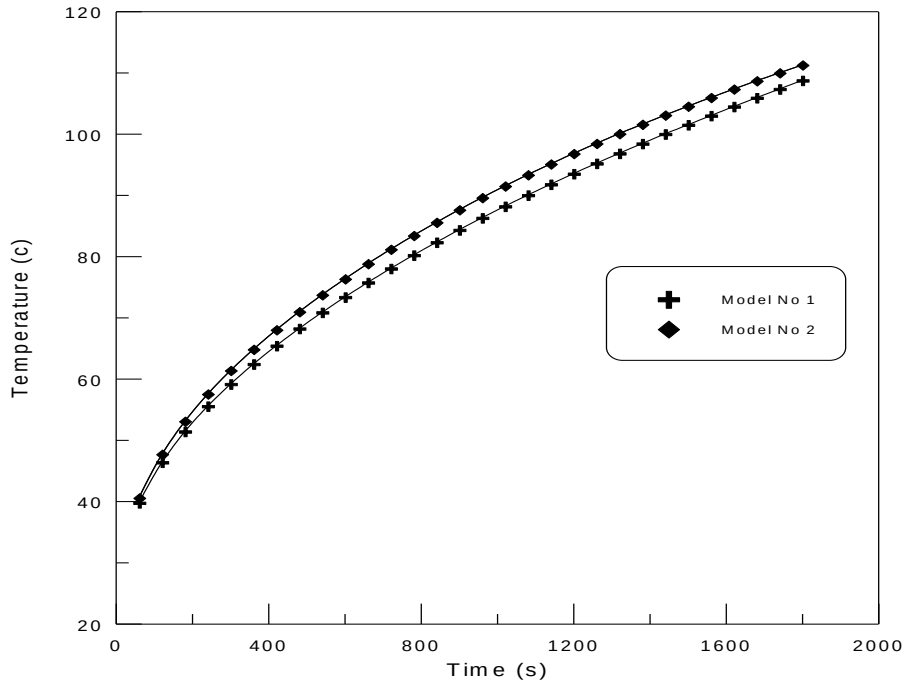

Figure (5-3) temperature variation with time at center point for steel-air ($\phi = .416$)system when heat flux=40000W/m^2 according to method No1and No2 of calculating k_e

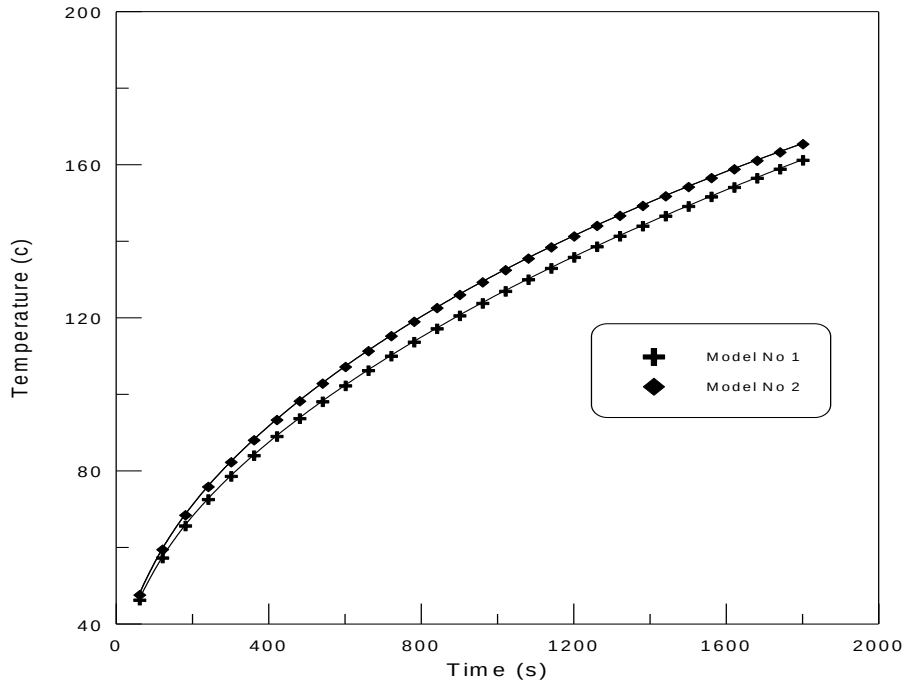

Figure (5-4) temperature variation with time at center point for steel-air ($\phi = .416$)system when heat flux=70000W/m^2 according to method No1and No2 of calculating k_e

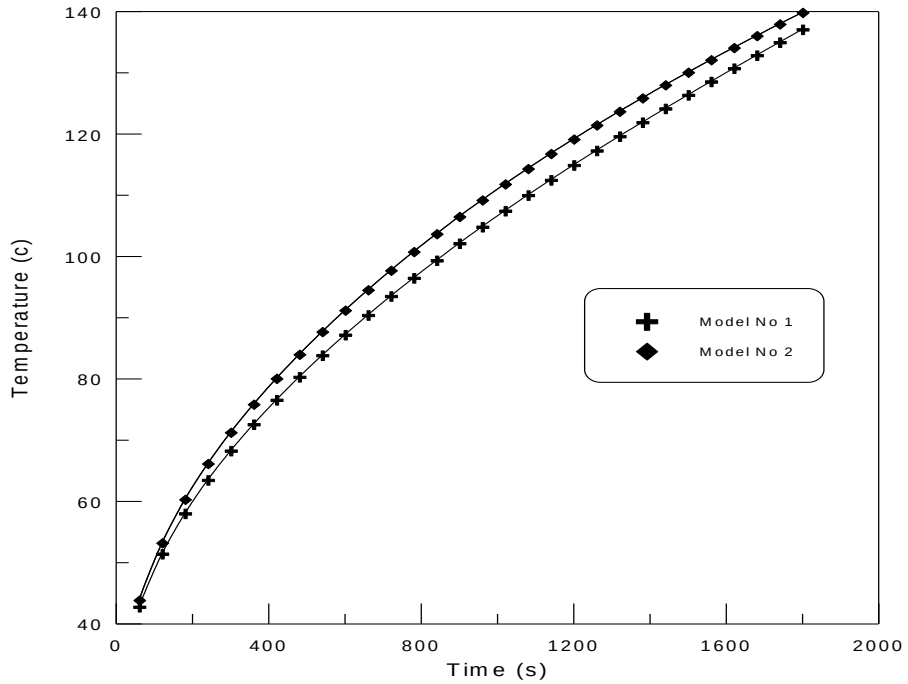

Figure (5-5) temperature variation with time at center point for steel-air ($\phi = .313$)system when heat flux=40000W /m^2 according to method No1and No2 of calculating k_e

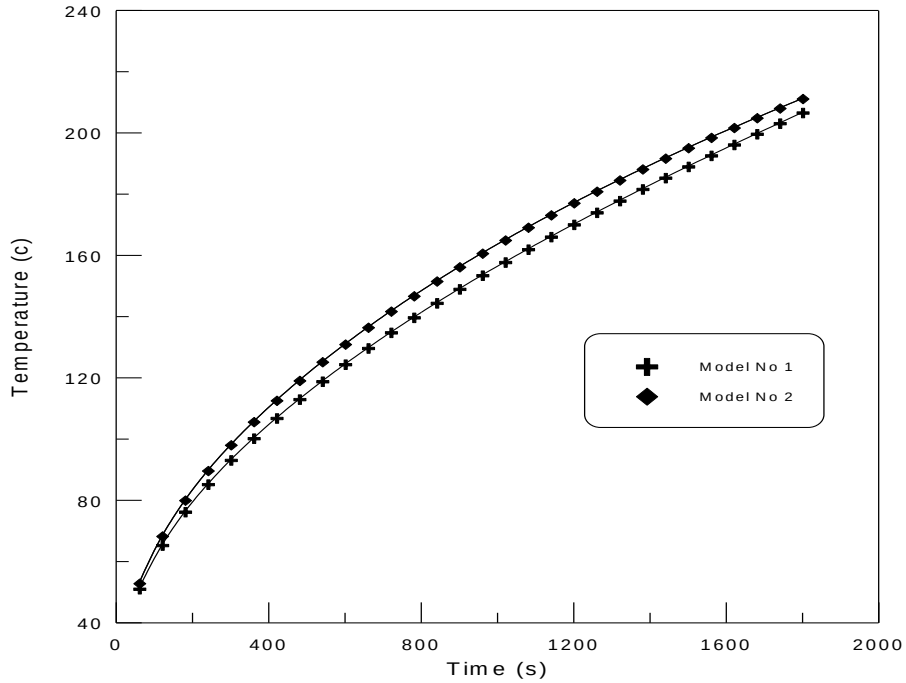

Figure (5-6) temperature variation with time at center point for steel-air ($\phi = .313$)system when heat flux=70000 W/m^2 according to method No1and No2 of calculating k_e

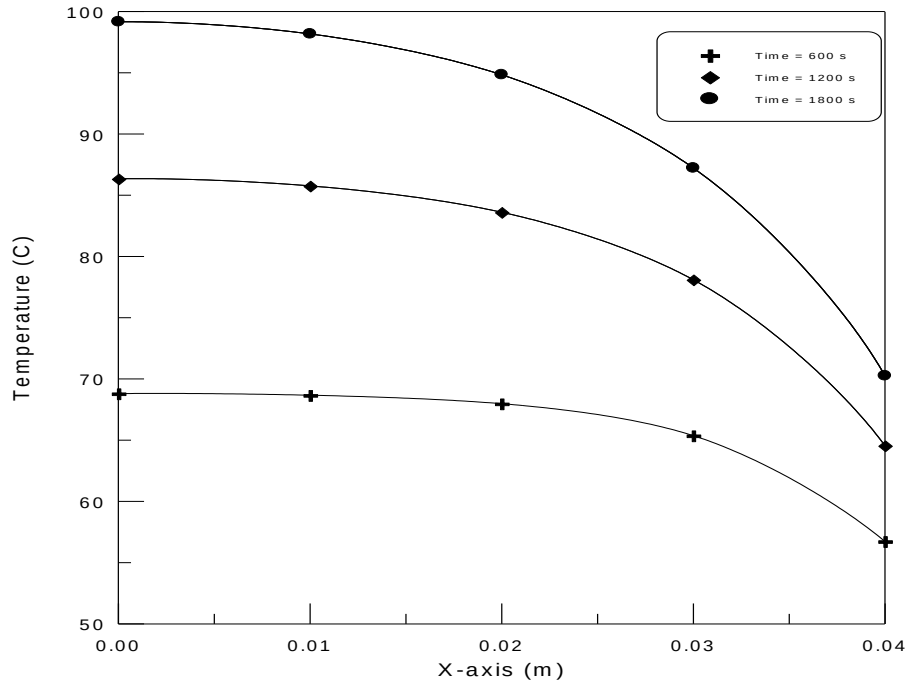

Figure (5-7) temperature distribution through x- axis in MgO –air system at different times, with heat flux of 40000 W/m^2 according to method No1 of calculating k_e

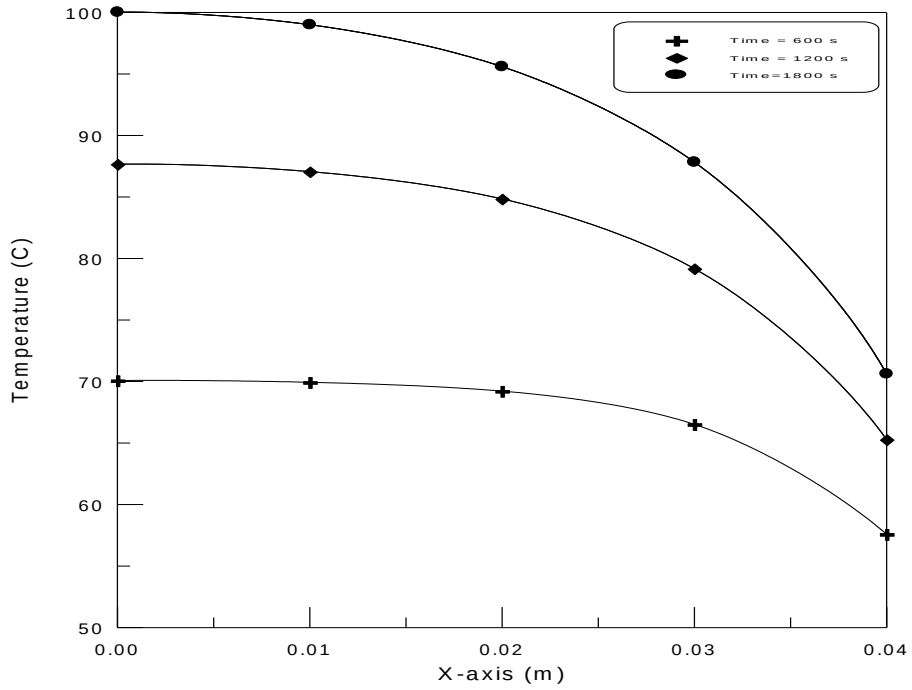

Figure (5-8) temperature distribution through x- axis in MgO –air system at different times, with heat flux of 40000 W/m^2 according to method No2 of calculating k_e

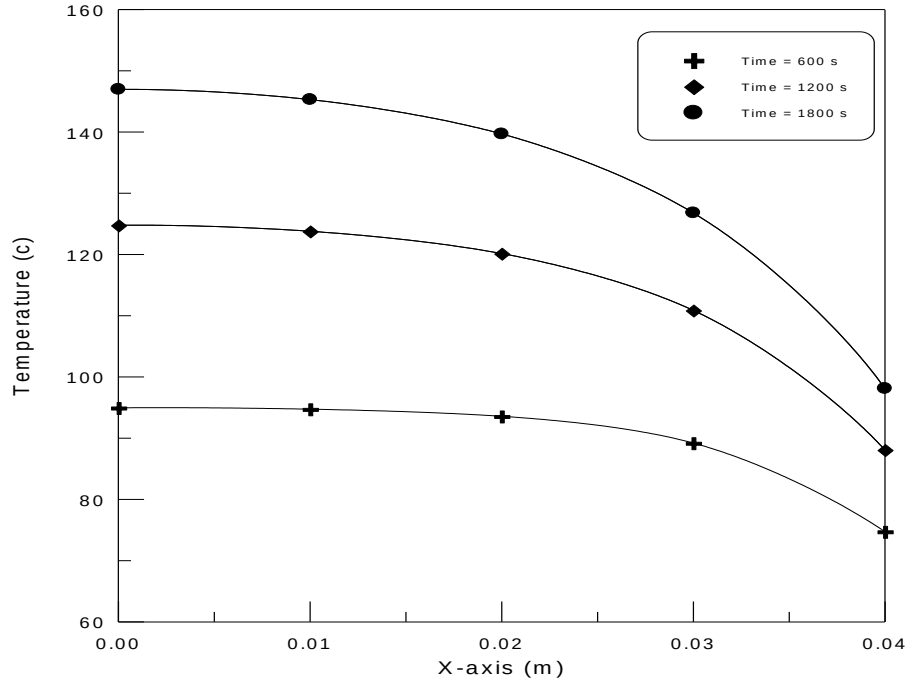

Figure (5-9)temperature distribution through x- axis in MgO –air system at different times, with heat flux of 70000 W/m^2 according to method No1 of calculating k_e

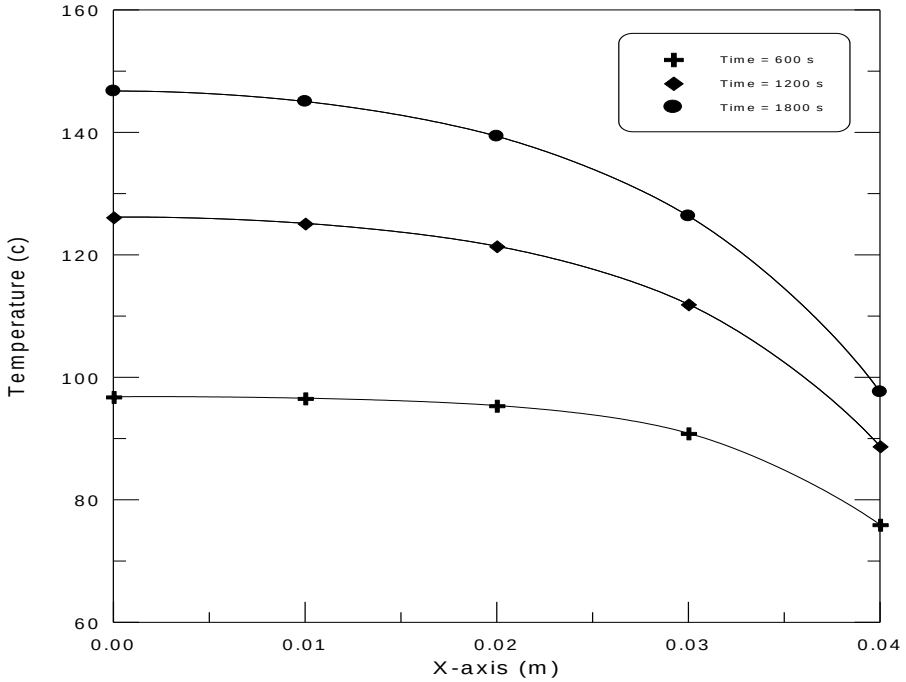

Figure (5-10)temperature distribution through x- axis in MgO –air system at different times, with heat flux of 70000 W/m^2 according to method No2 of calculating k_e

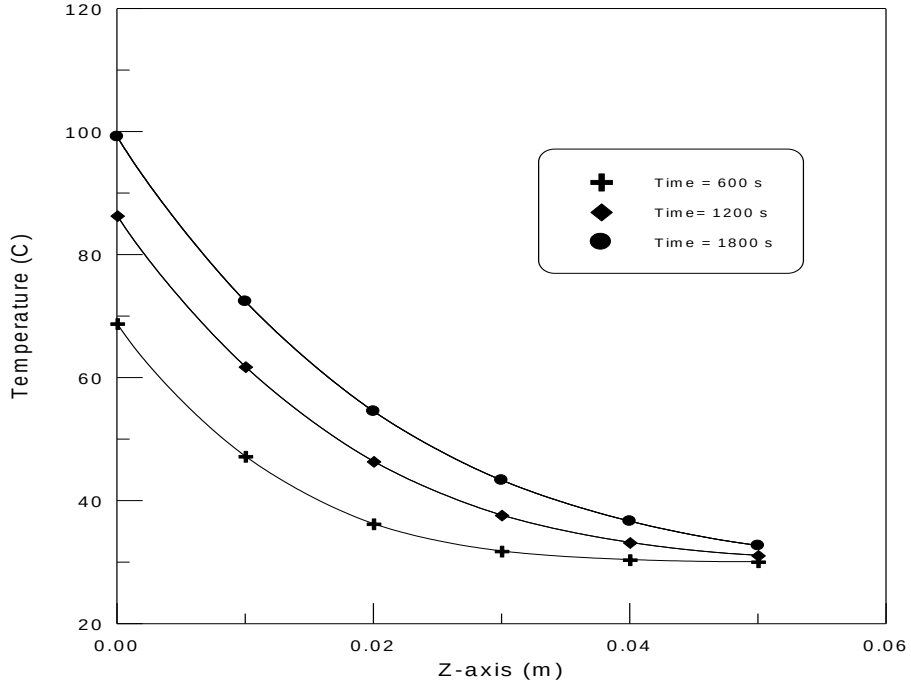

Figure (5-11)temperature distribution through z- axis in MgO –air system at different times, with heat flux of 40000 W/m^2 according to method No1 of calculating k_e

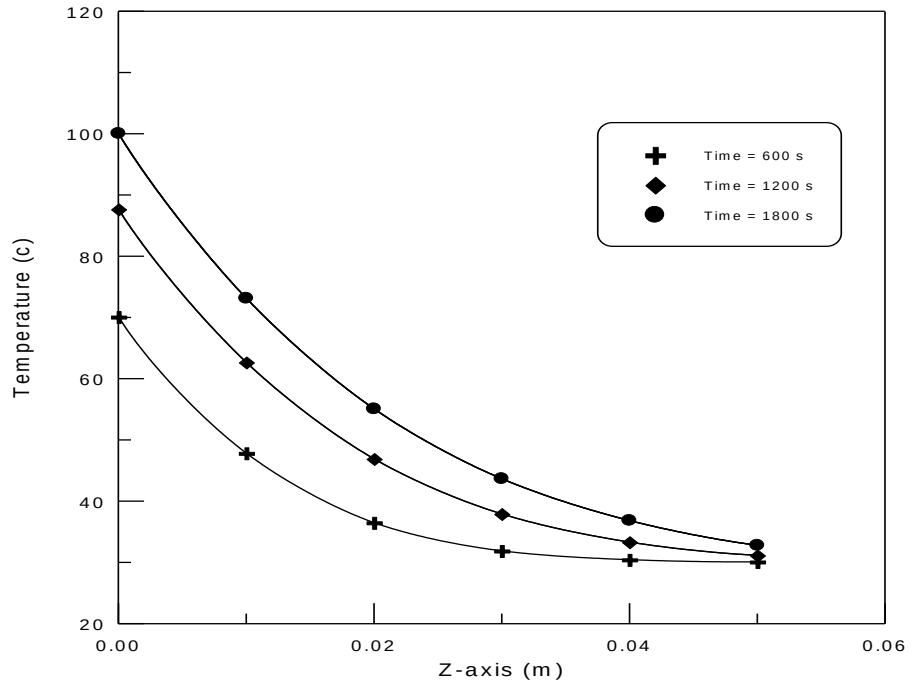

Figure (5-12) temperature distribution through z- axis in MgO –air system at different times, with heat flux of 40000 W/m^2 according to method No2 of calculating k_e

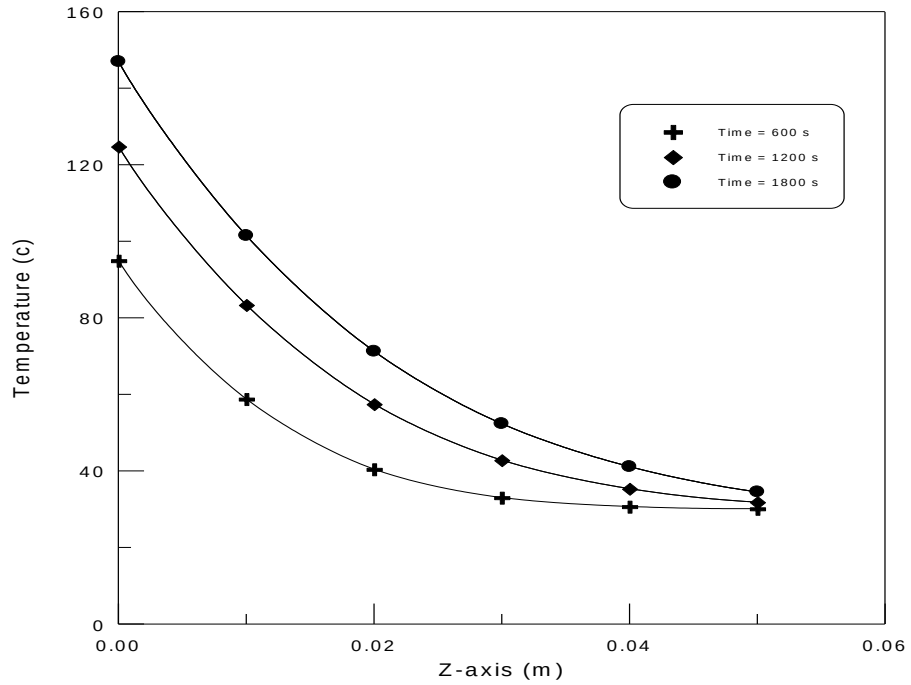

Figure (5-13) temperature distribution through z- axis in MgO –air system at different times, with heat flux of 70000 W/m^2 according to method No1 of calculating k_e

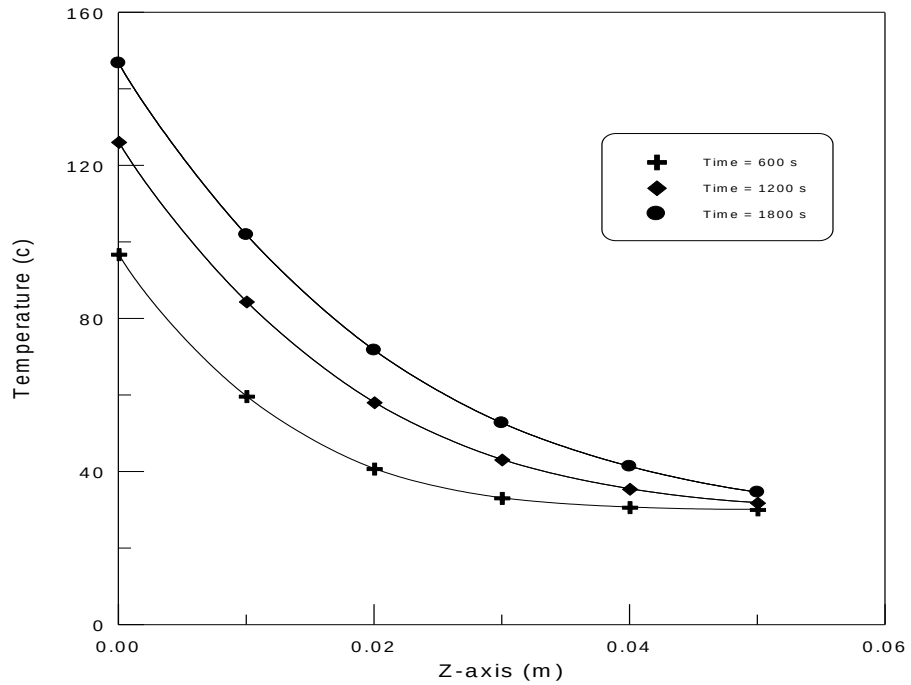

Figure (5-14) temperature distribution through z- axis in MgO –air system at different times, with heat flux of 70000 W/m^2 according to method No2 of calculating k_e

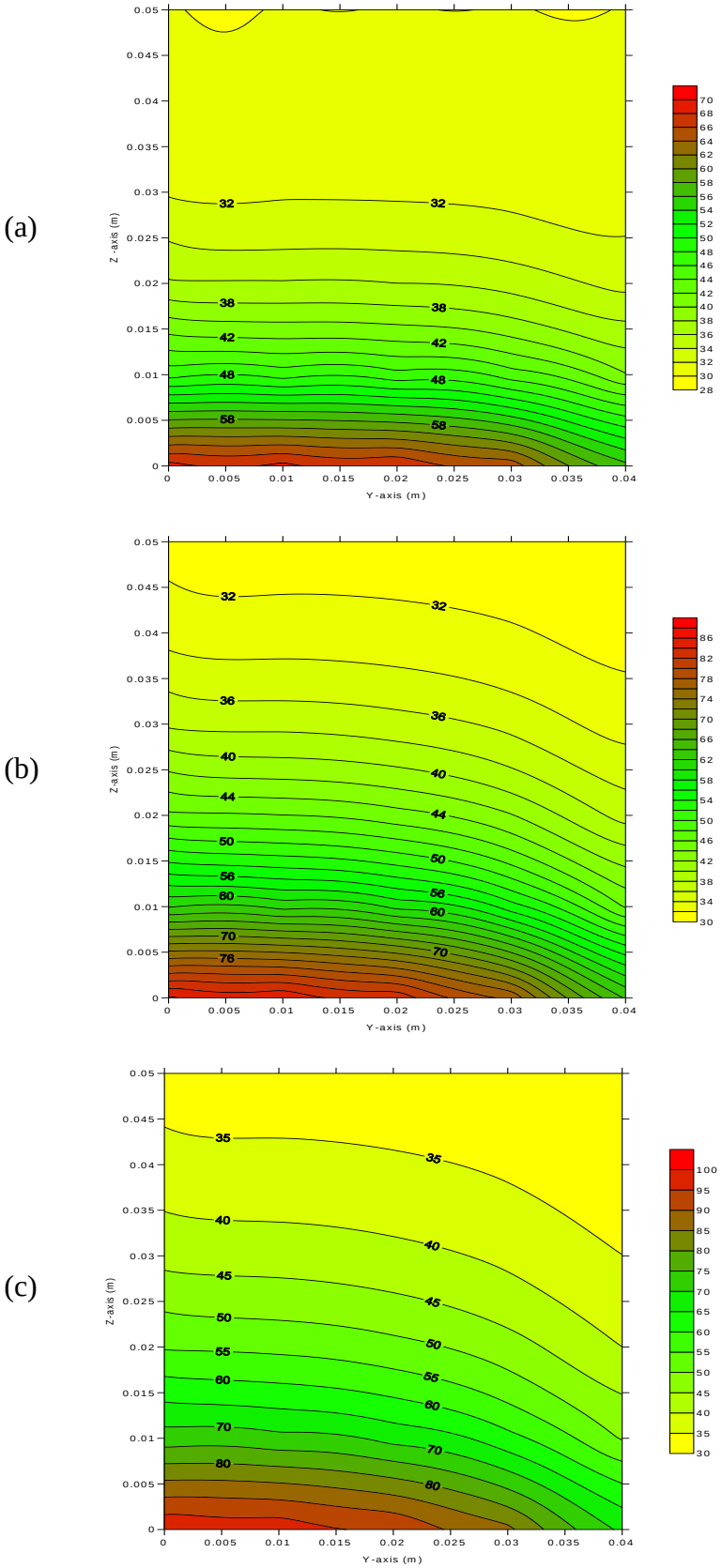

Figure (5-15)isothermal contour map for (y-z) plane in MgO-air system with $\phi = .378$ and heat flux of 40000 W/m^2 at different times (a-time =600s ,b-time=1200 s and c- time=1800) according method No 1 of calculating k_e

(a)

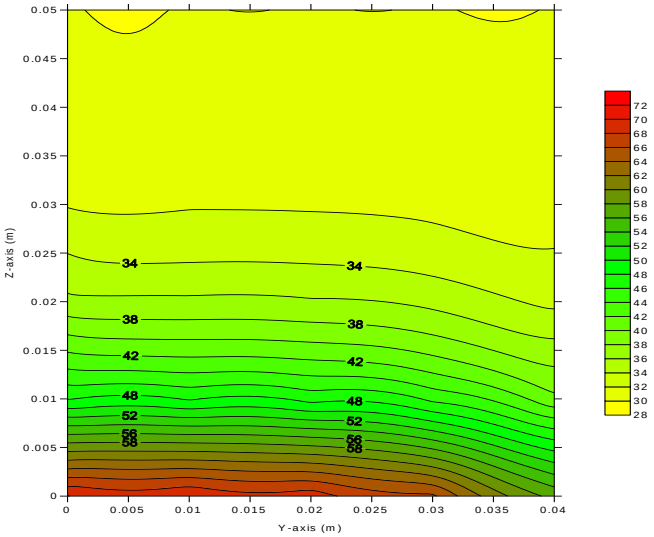
Z-axis (m)
Y-axis (m)
0 0.005 0.01 0.015 0.02 0.025 0.03 0.035 0.04 0.045 0.05
34 38 42 48 52 56 58
72 70 68 66 64 62 60 58 56 54 52 50 48 46 44 42 40 38 36 34 32 30 28

(b)

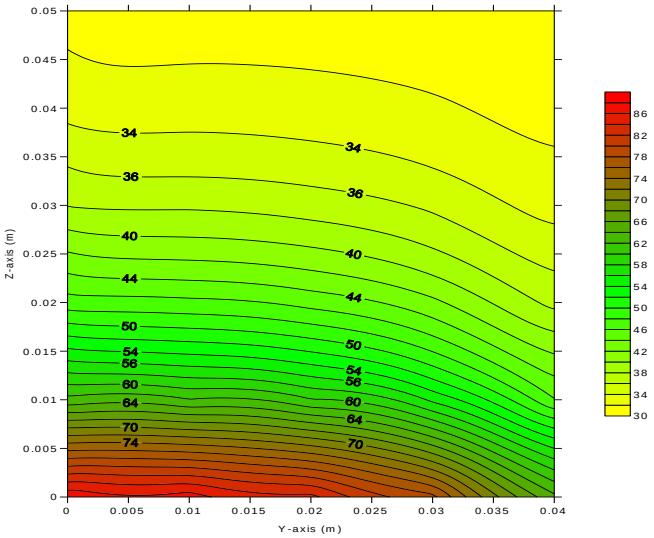
Z-axis (m)
Y-axis (m)
0 0.005 0.01 0.015 0.02 0.025 0.03 0.035 0.04 0.045 0.05
34 36 40 44 50 54 56 60 64 70 74
86 82 78 74 70 66 62 58 54 50 46 42 38 34 30

(c)

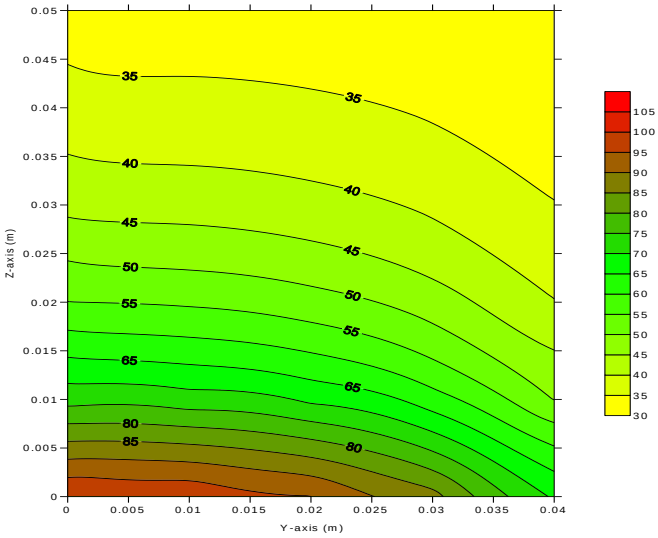
Z-axis (m)
Y-axis (m)
0 0.005 0.01 0.015 0.02 0.025 0.03 0.035 0.04 0.045 0.05
35 40 45 50 55 65 80 85
105 100 95 90 85 80 75 70 65 60 55 50 45 40 35 30

Figure (5-16)isothermal contour map for (y-z) plane in MgO-air system with $\phi = .378$ and heat flux of 40000 W/m^2 at different times (a-time =600s ,b-time=1200 s and c- time=1800)according method No2 of calculating k_e

(a)

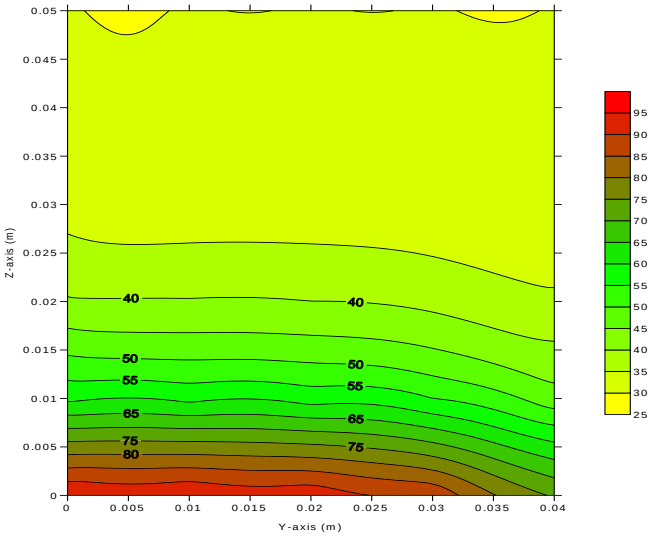

(b)

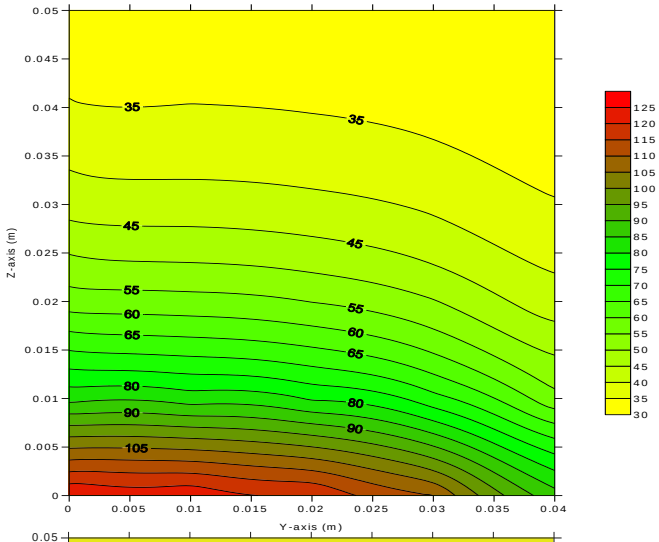

(c)

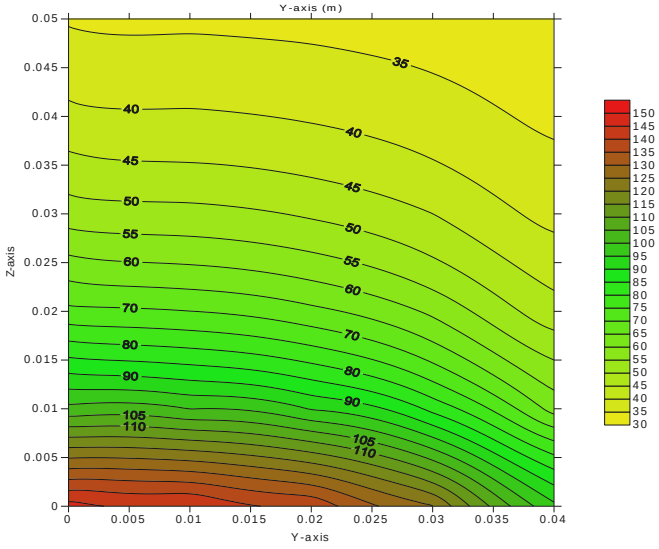

Figure (5-17)isothermal contour map for (y-z) plane in MgO-air system with $\phi = .378$ and heat flux of 70000 W/m^2 at different times (a-time =600s ,b-time=1200 s and c- time=1800) according method No1 of calculating k_e

(a)

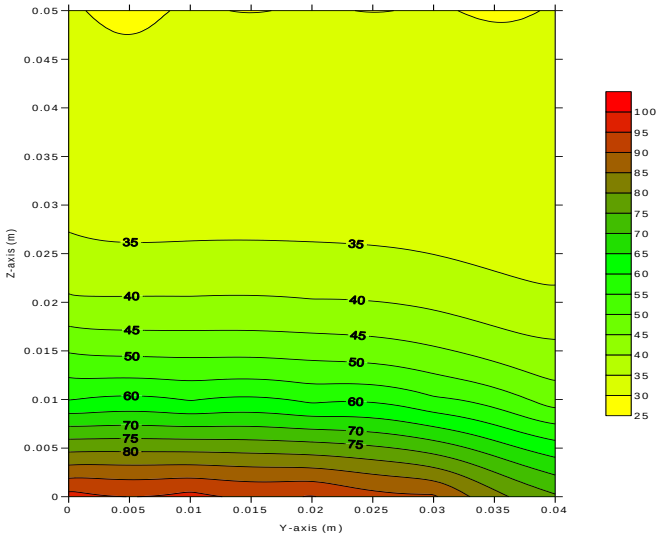

(b)

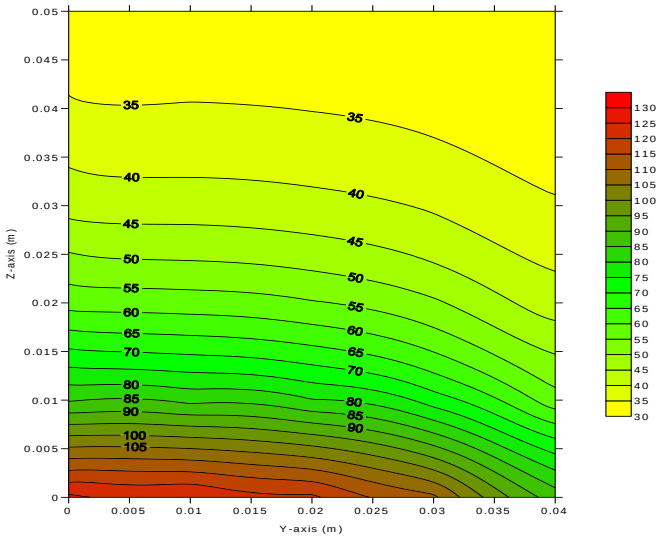

(c)

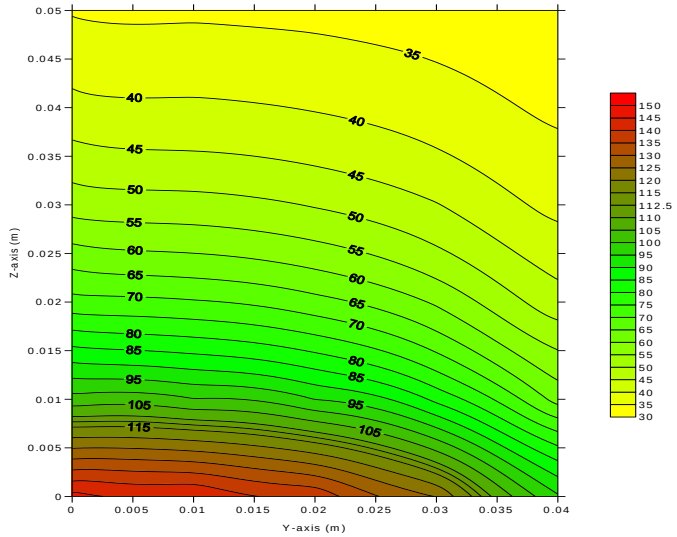

Figure (5-18)isothermal contour map for (y-z) plane in MgO-air system with $\phi = .378$ and heat flux of 70000 W/m^2 at different times (a-time =600s ,b-time=1200 s and c- time=1800) accordi method No2 of calculating k_e

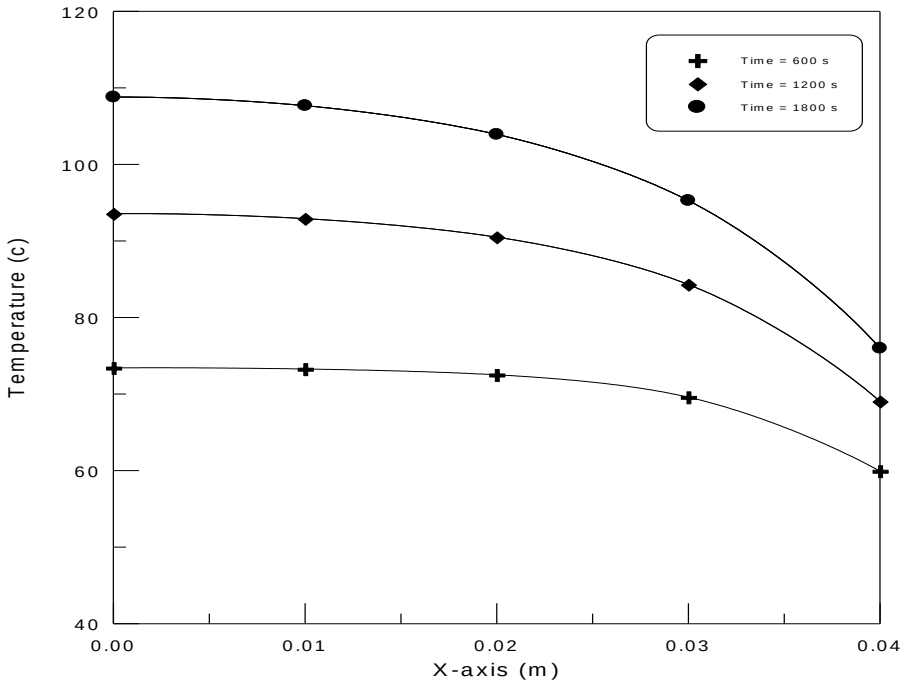

Figure (5-19) temperature distribution through x- axis in steel-air $(\phi = .416)$ system with heat flux of 40000 W/m^2 at different times, according to method No1 of calculating k_e

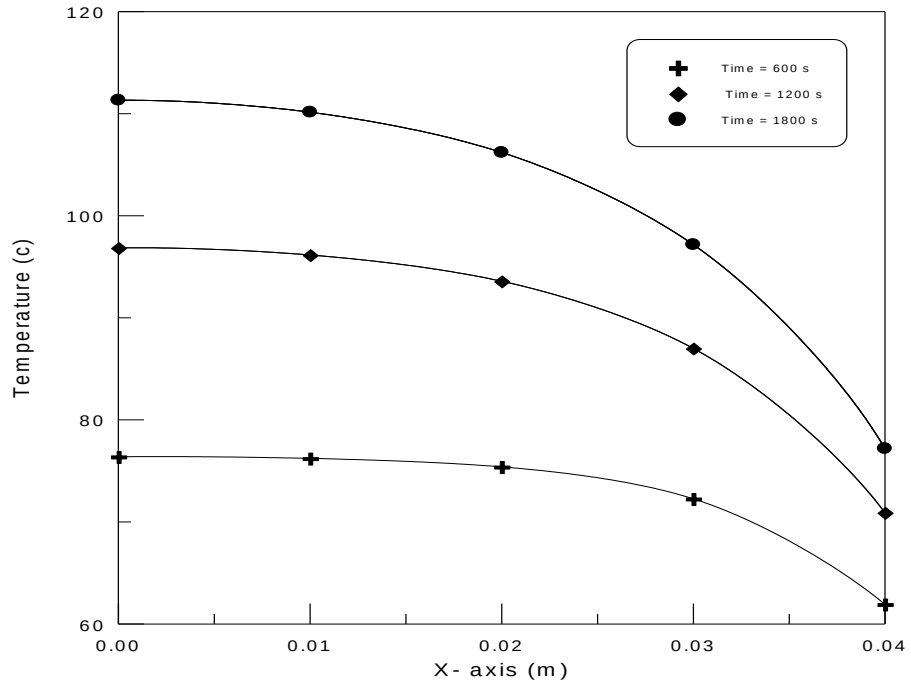

Figure (5-20) temperature distribution through x- axis in steel-air ($\phi = .416$) system with heat flux of 40000 W/m^2 at different times, according to method No2 of calculating k_e

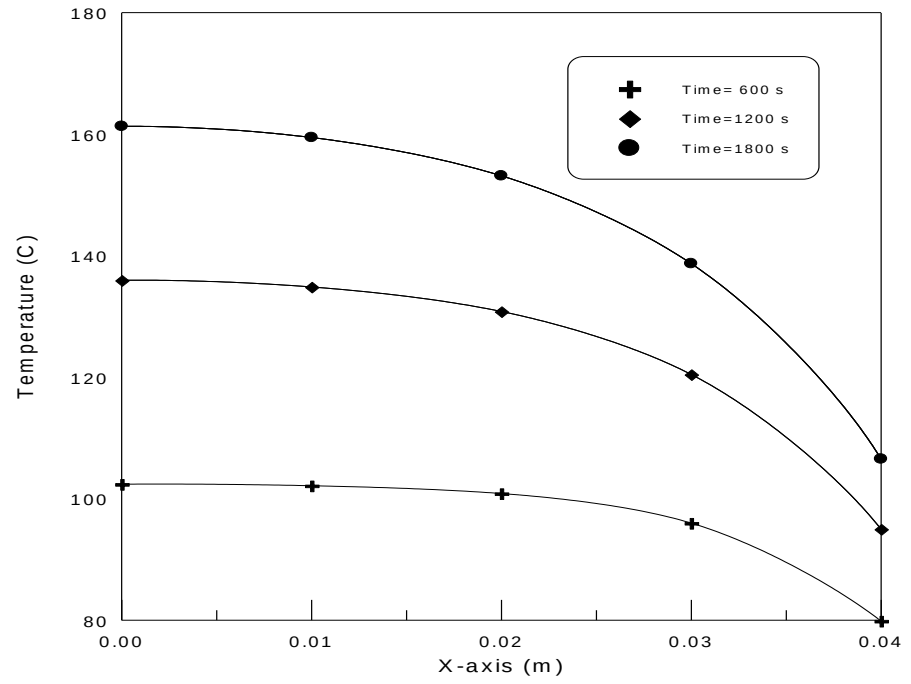

Figure (5-21) temperature distribution through x- axis in steel-air ($\phi = .416$) system with heat flux of 70000 W/m^2 at different times, according to method No1 of calculating k_e

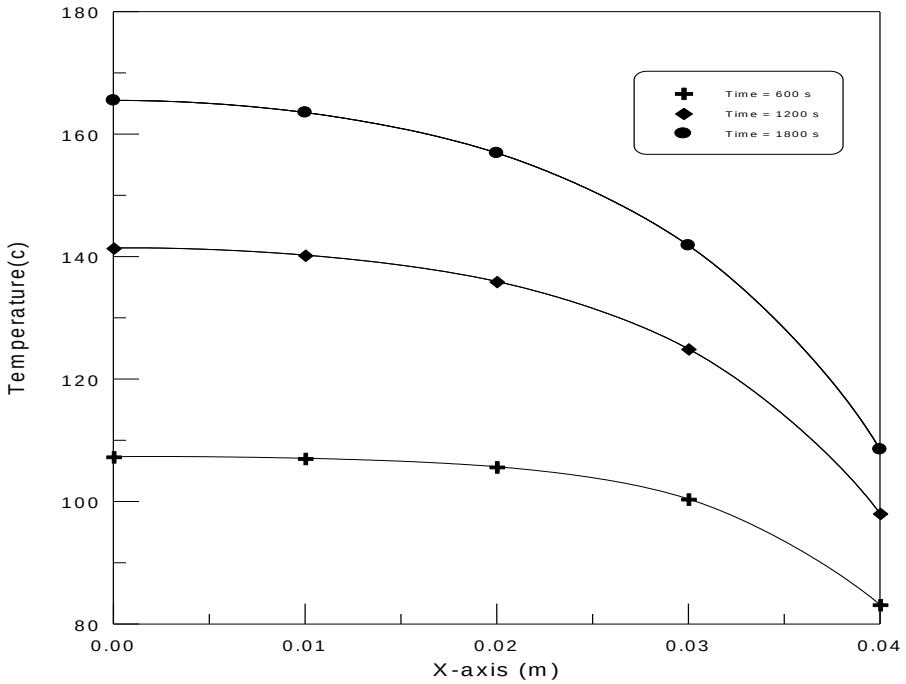

Figure (5-22)temperature distribution through x- axis in steel-air ($\phi = .416$) system with heat flux of 70000 W/m^2 at different times, according to method No2 of calculating k_e

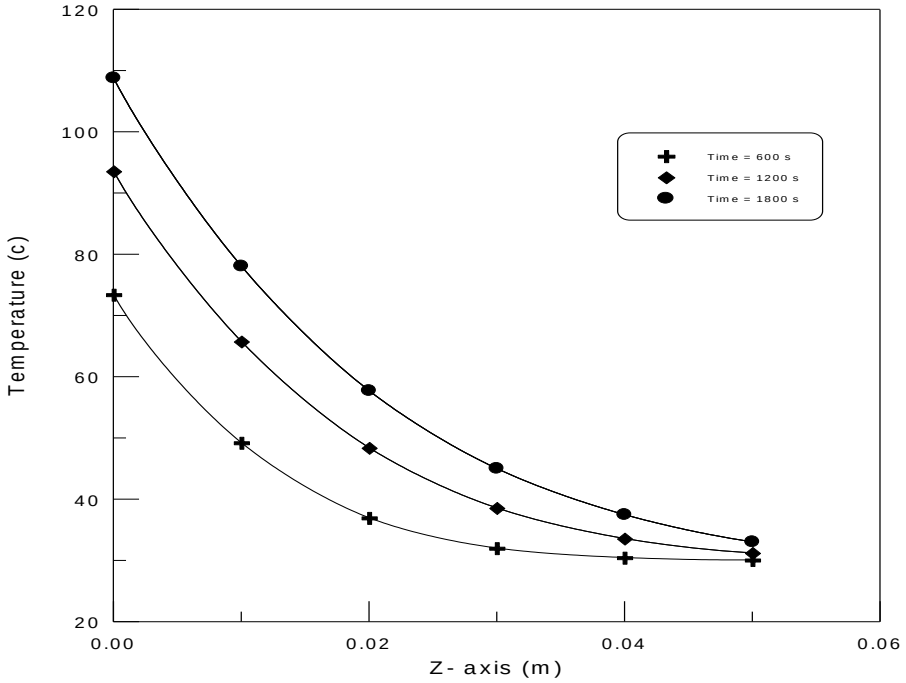

Figure (5-23) temperature distribution through z- axis in steel-air ($\phi = .416$) system with heat flux of 40000 W/m^2 at different times, according to method No1 of calculating k_e

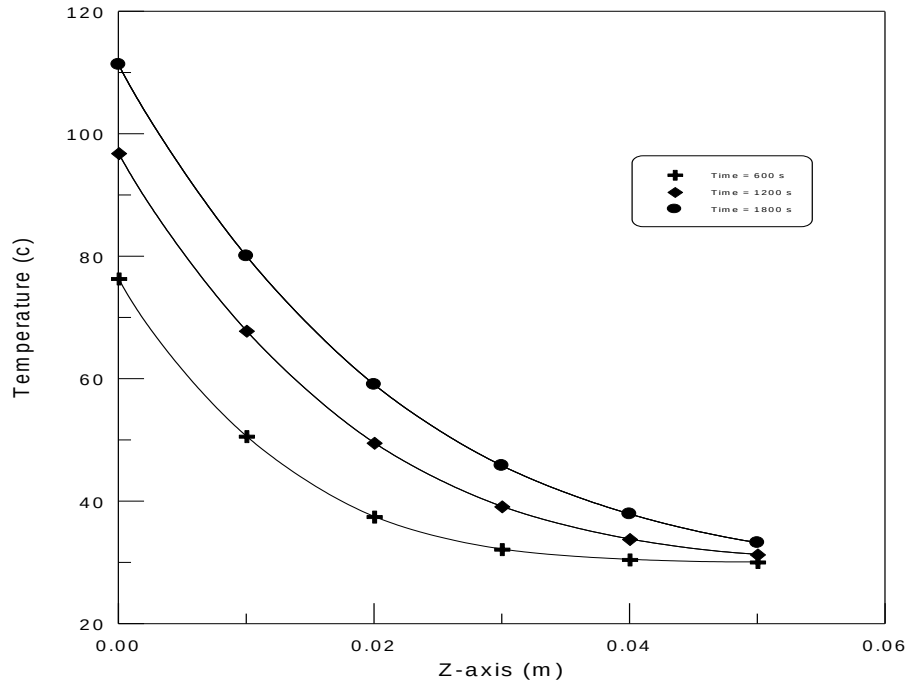

Figure (5-24) temperature distribution through z- axis in steel-air ($\phi = .416$) system with heat flux of 40000 W/m^2 at different times, according to method No2 of calculating k_e

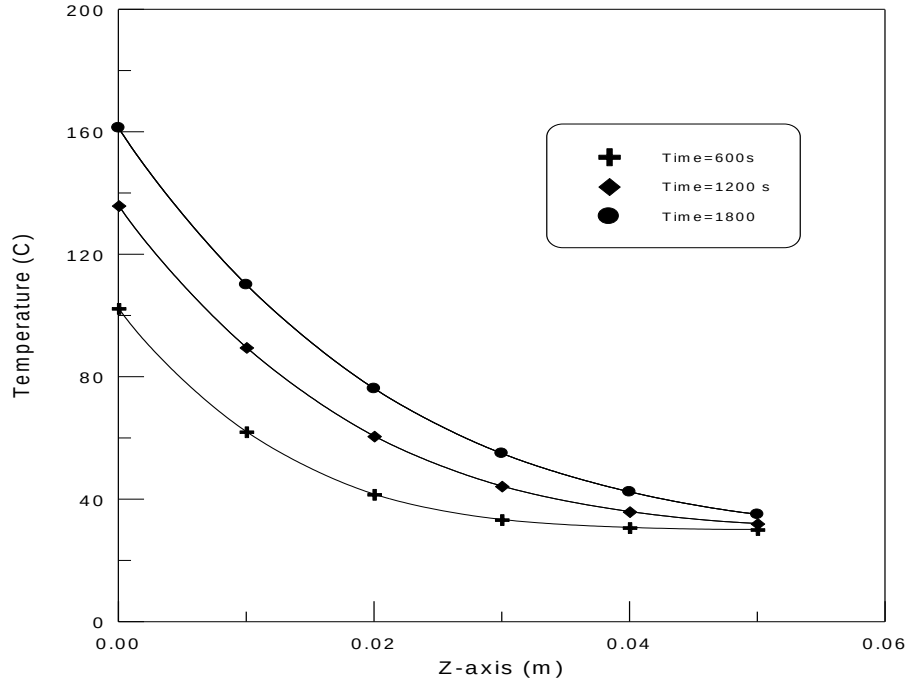

Figure (5-25)temperature distribution through z- axis in steel-air ($\phi = .416$) system with heat flux of 70000 W/m^2 at different times, according to method No2 of calculating k_e

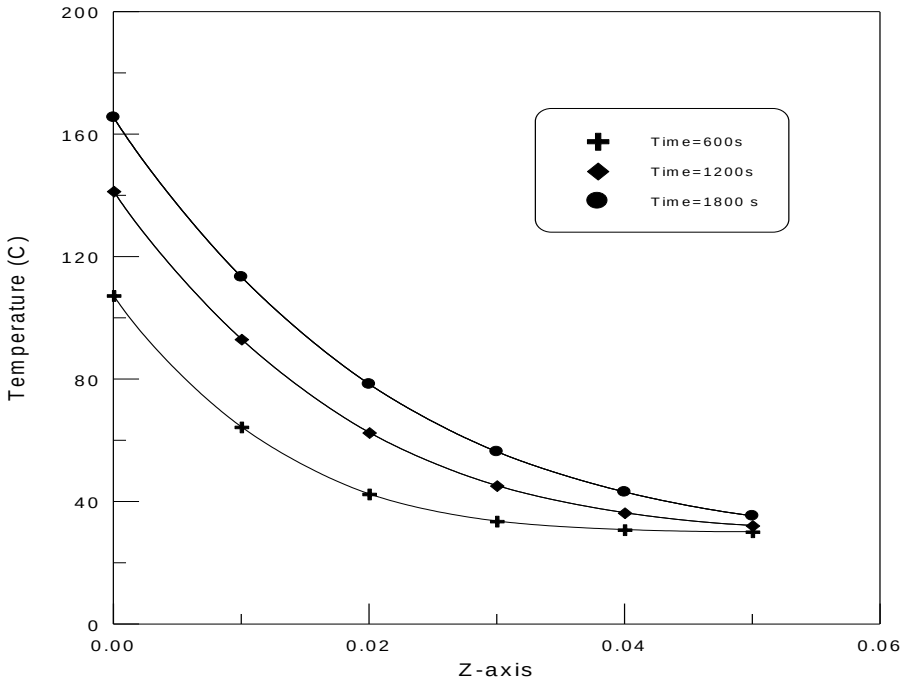

Figure (5-26) temperature distribution through z- axis in steel-air ($\phi = .416$) system with heat flux of 70000 W/m^2 at different times, to method No2 of calculating k_e

(a)

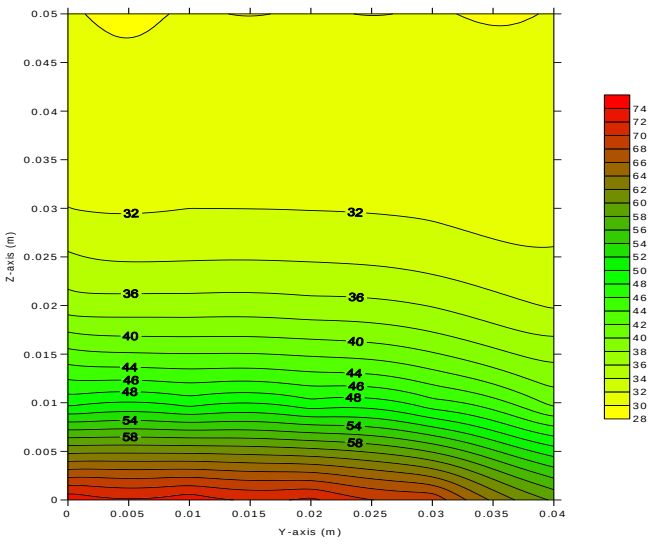

(b)

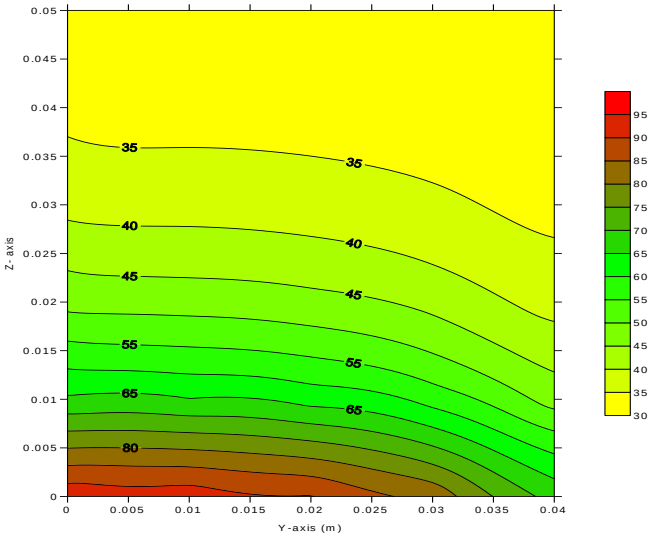

(c)

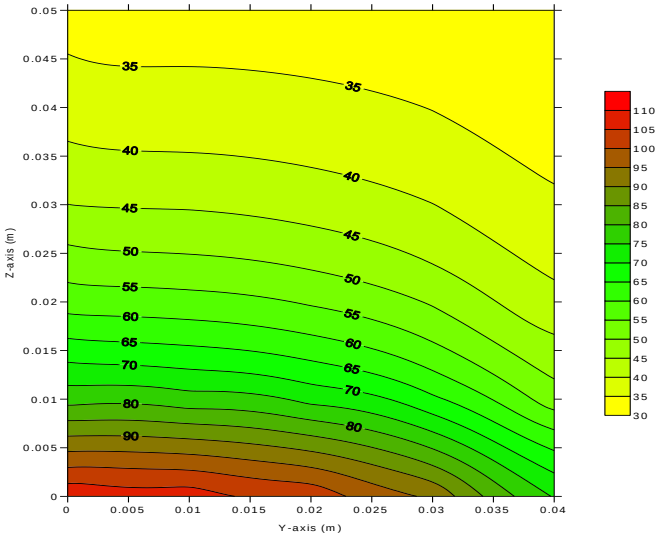

Figure (5-27)isothermal contour map for (y-z) plane in Chrome steel-air system with $\phi = .416$ and heat flux of 40000 W/m^2 at different times (a-time =600s ,b-time=1200 s and c- time=1800)according method No1 of calculating k_e

(a)

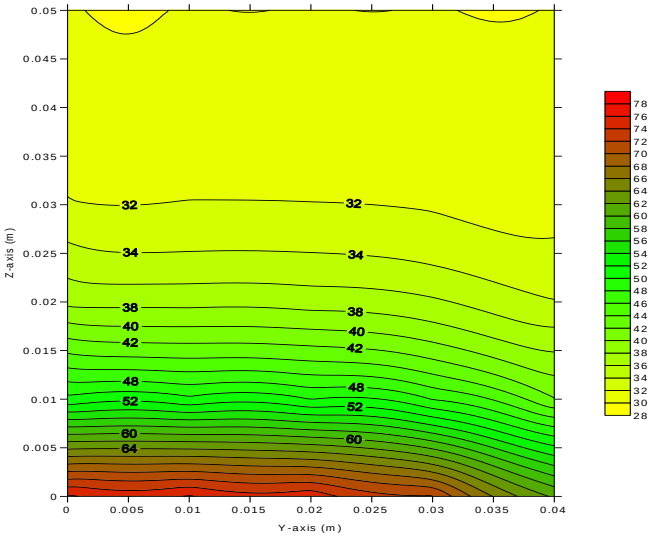

(b)

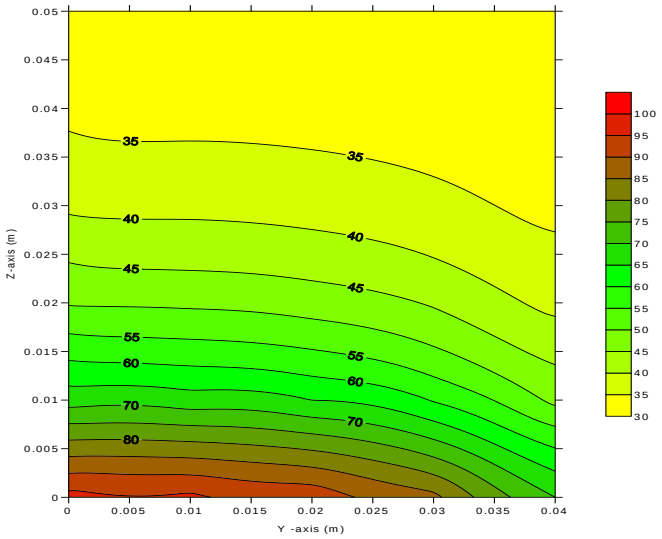

(c)

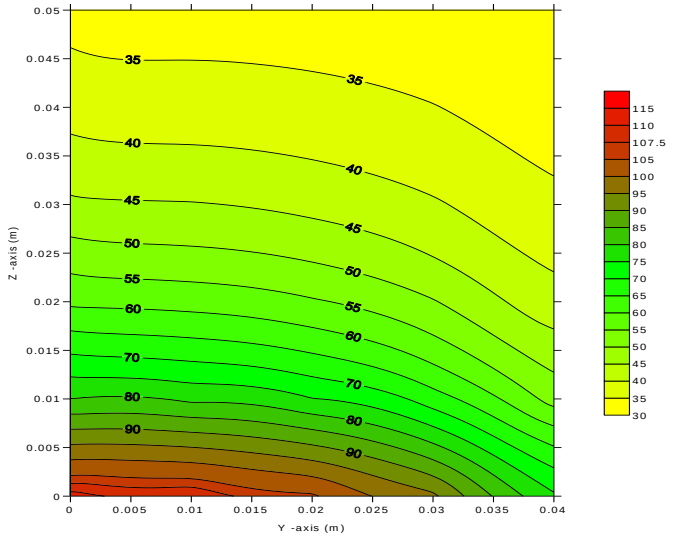

Figure (5-28)isothermal contour map for (y-z) plane in Chrome steel-air system with $\phi = .416$ and heat fluof 40000 W/m^2 at different times (a-time =600s ,b-time=1200 s and c- time=1800) according method No2 of calculating k_e

(a)

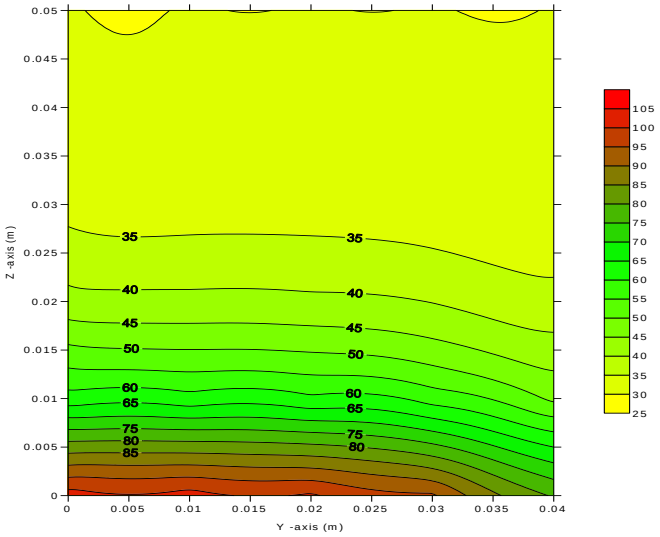

(b)

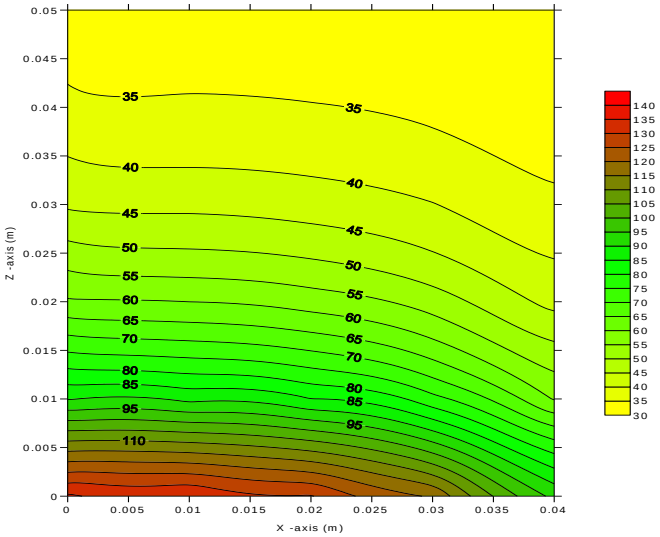

(c)

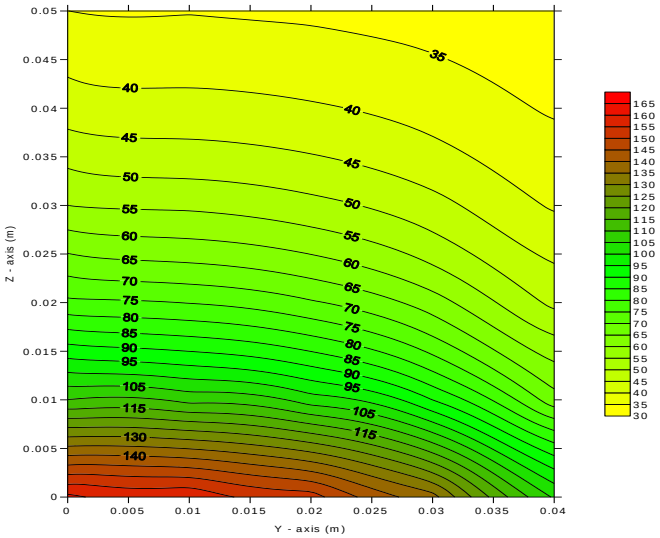

Figure (5-29) isothermal contour map for (y-z) plane in Chrome steel-air system with $\phi = .416$ and heat flux of 70000 W/m^2 at different times (a-time =600s ,b-time=1200 s and c- time=1800) according method No 1 of calculating k_e

(a)

(b)

(c)

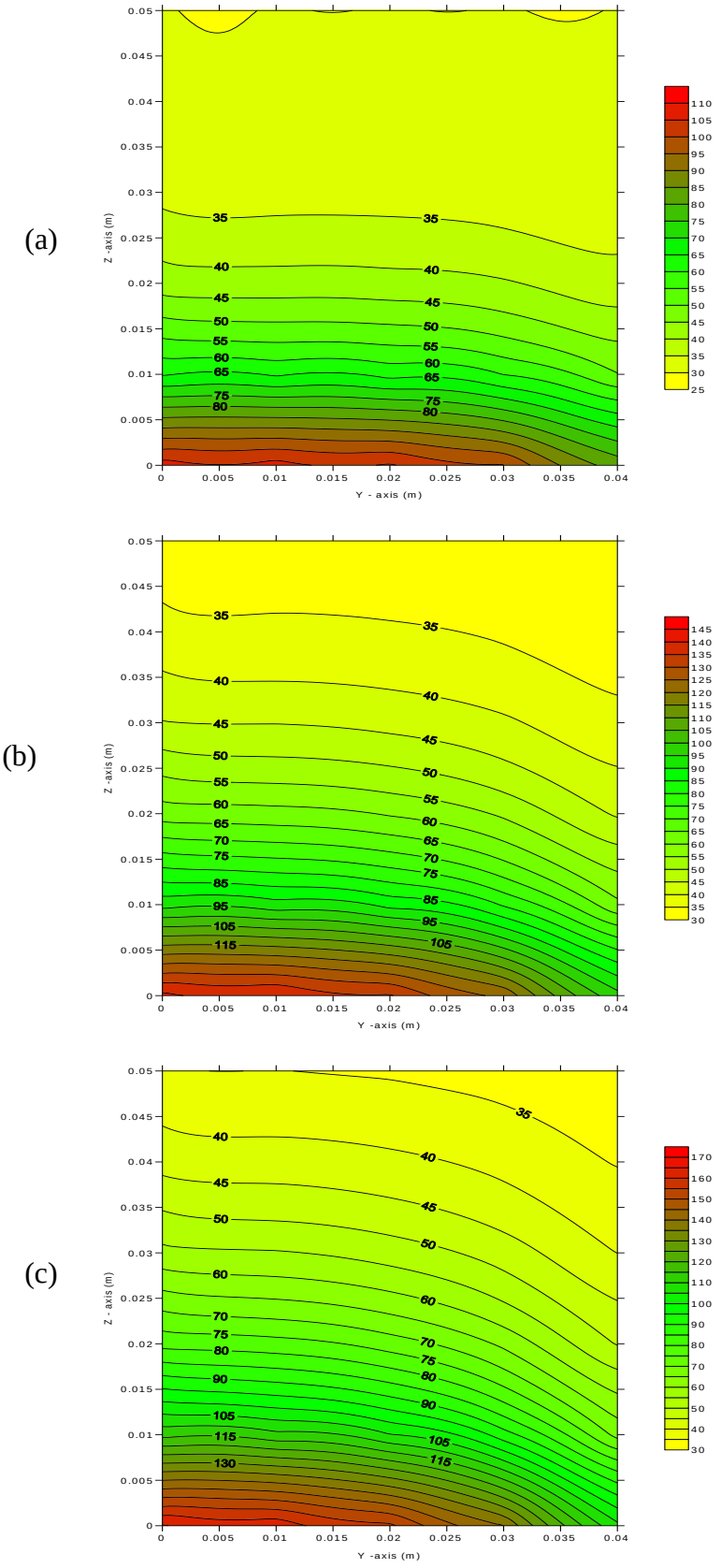

Figure (5-30) isothermal contour map for (y-z) plane in Chrome steel-air system with $\phi = .416$ and heat flux of 70000 W/m^2 at different times (a-time =600s ,b-time=1200 s and c- time=1800) according method No2 of calculating k_e

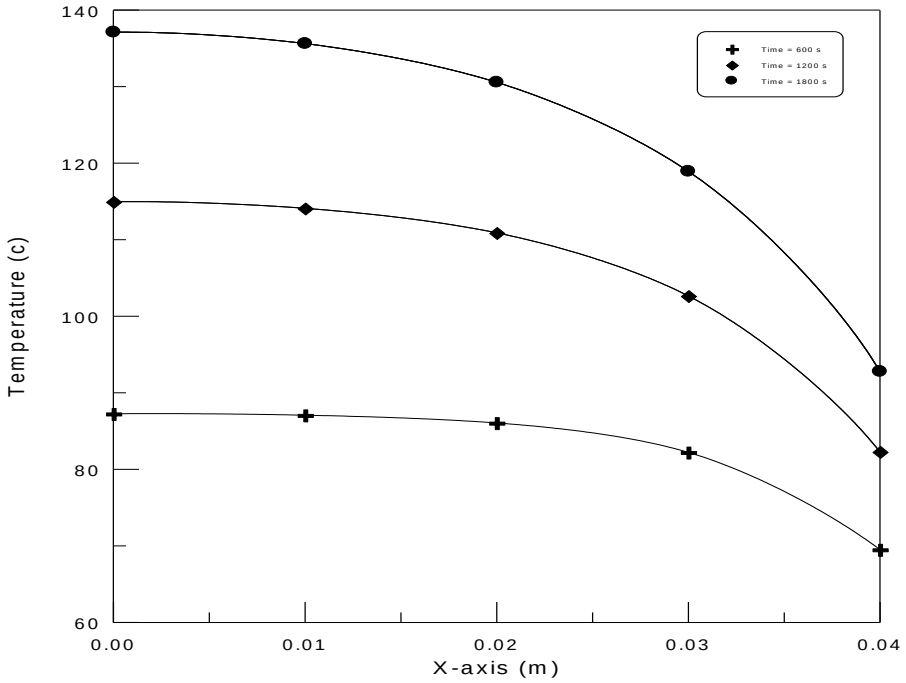

Figure (5-31) temperature distribution through x- axis in steel-air ($\phi = 0.313$) system with heat flux of 40000 W/m^2 at different times, according to method No1 of calculating k_e

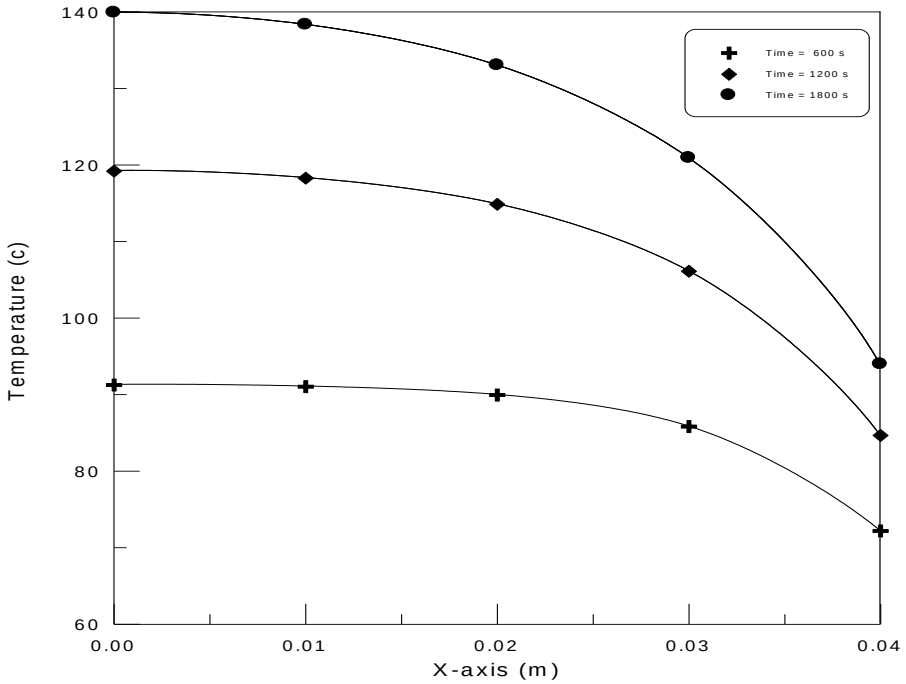

Figure (5-32) temperature distribution through x- axis in steel-air ($\phi = .313$) system with heat flux of 40000 W/m^2 at different times, according to method No2 of calculating k_e

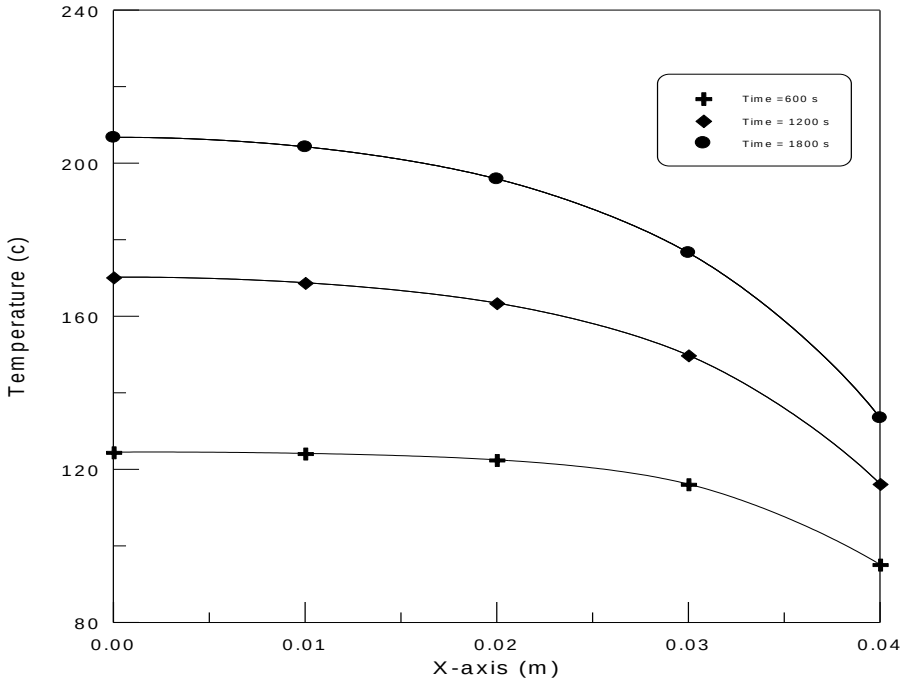

Figure (5-33) temperature distribution through x- axis in steel-air ($\phi = .313$) system with heat flux of 70000 W/m^2 at different times, according to method No1 of calculating k_e

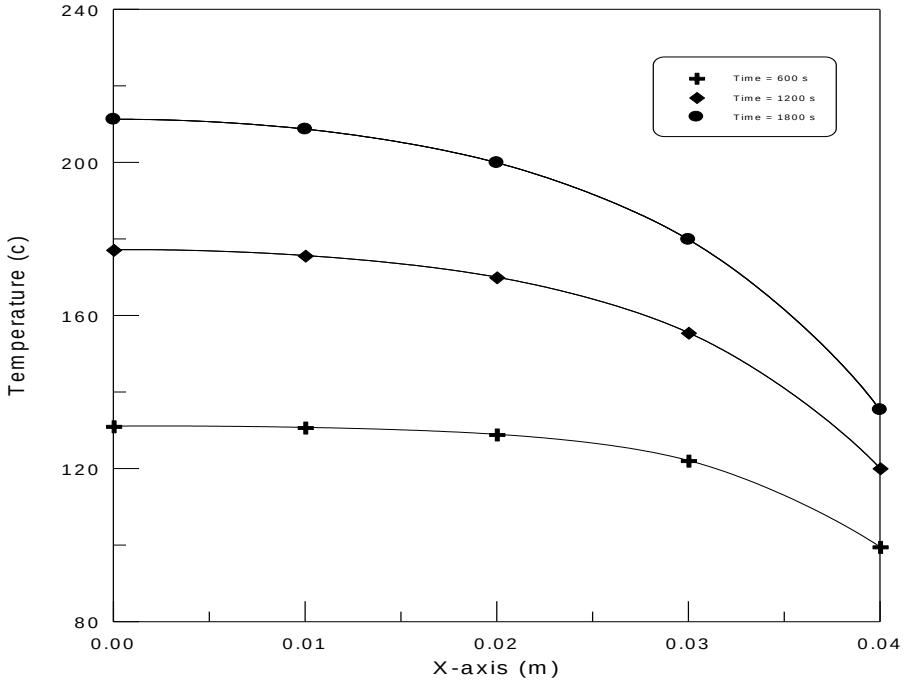

Figure (5-34) temperature distribution through x- axis in steel-air ($\phi = .313$) system with heat flux of 70000 W/m^2 at different times, according to method No2 of calculating k_e

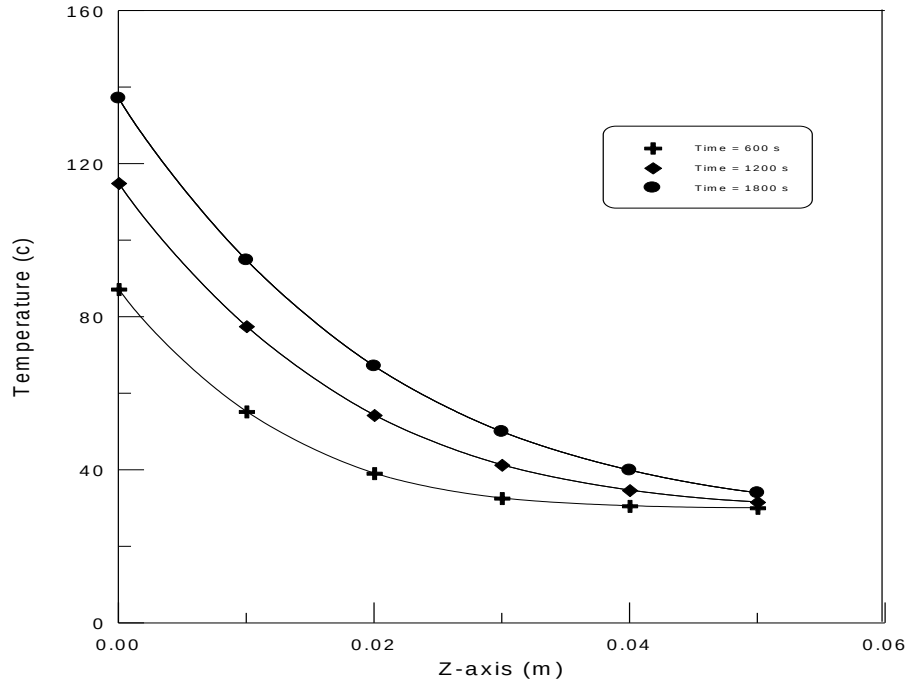

Figure (5-35) temperature distribution through z- axis in steel-air ($\phi = .313$) system with heat flux of 40000 W/m^2 at different times, according to method No1 of calculating k_e

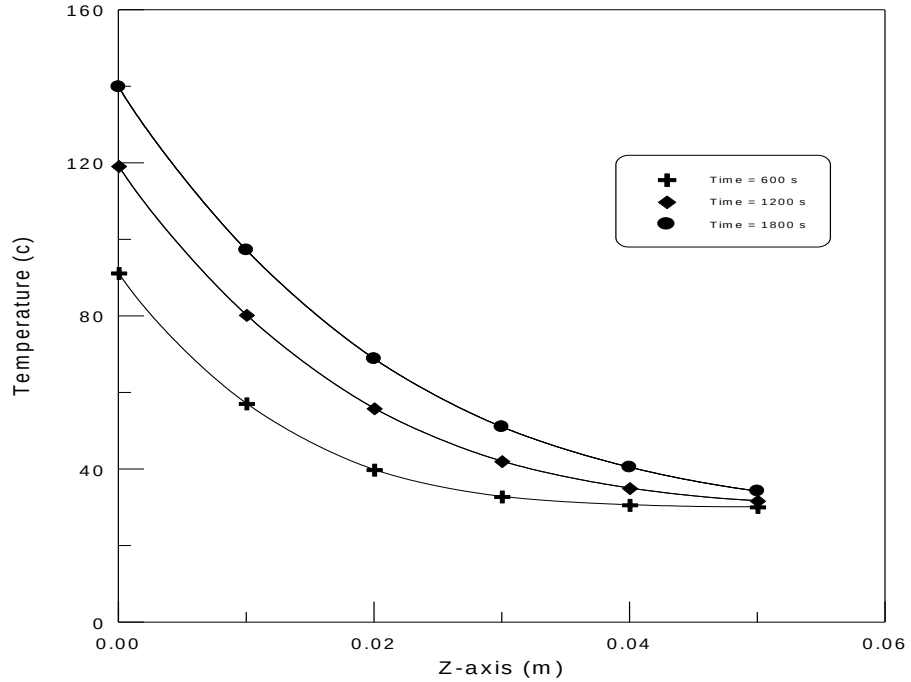

Figure (5-36) temperature distribution through z- axis in steel-air ($\phi = .313$)

system with heat flux of 40000 W/m^2 at different times, according to method No2 of calculating k_e

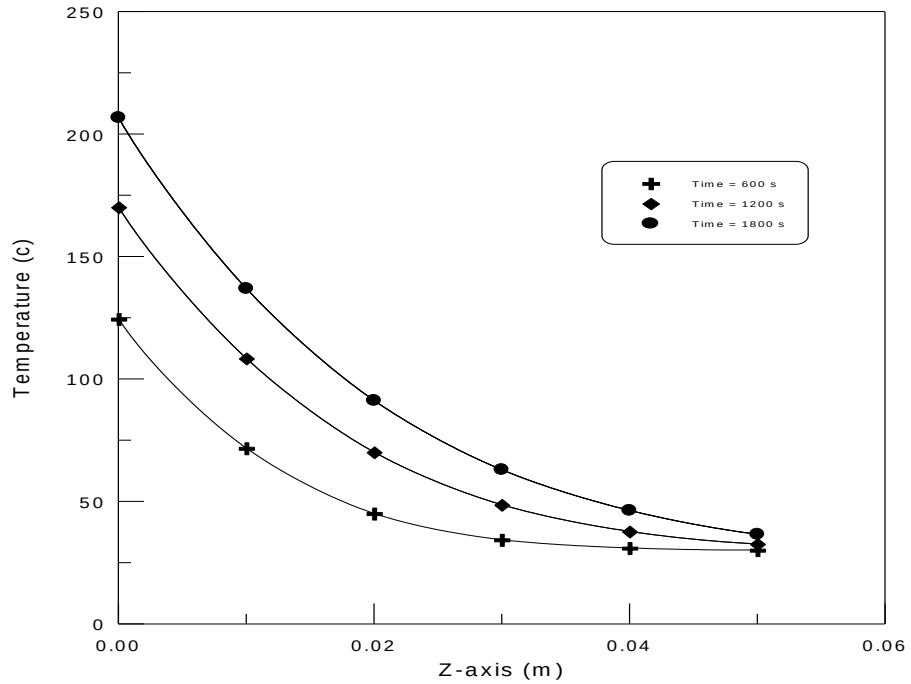

Figure (5-37) temperature distribution through z- axis in steel-air ($\phi = .313$)

system with heat flux of 70000 W/m^2 at different times, according to method No1 of calculating k_e

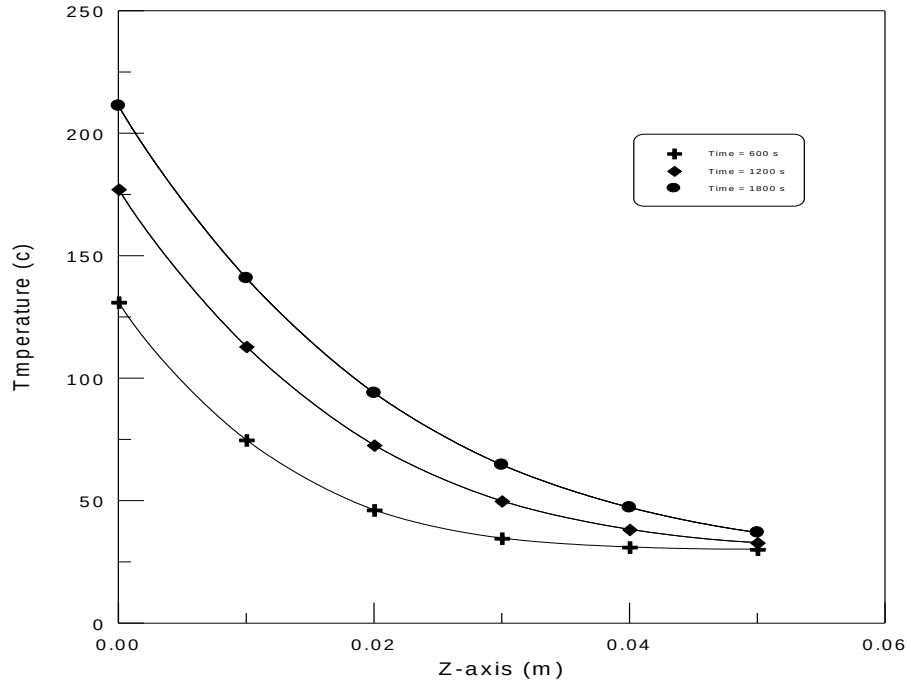

Figure (5-38) temperature distribution through z- axis in steel-air ($\phi = .313$) system with heat flux of 70000 W/m^2 at different times, according to method No2 of calculating k_e

(a)

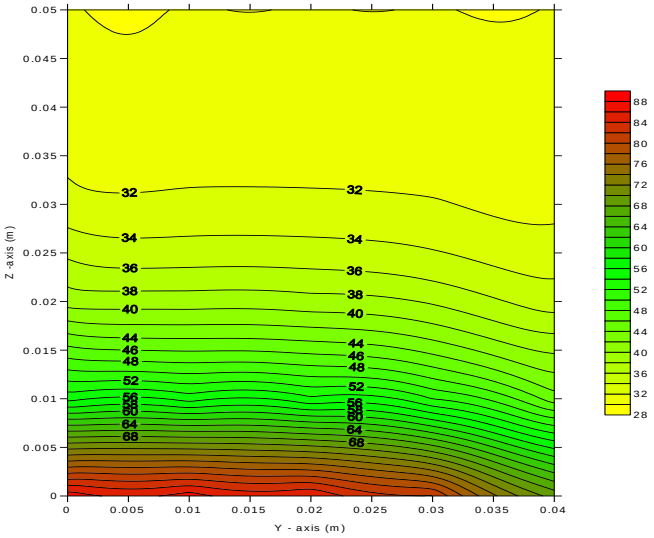

(b)

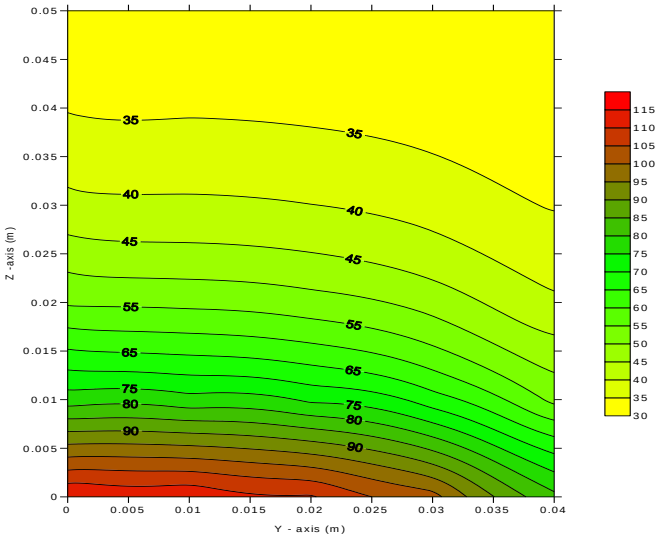

(c)

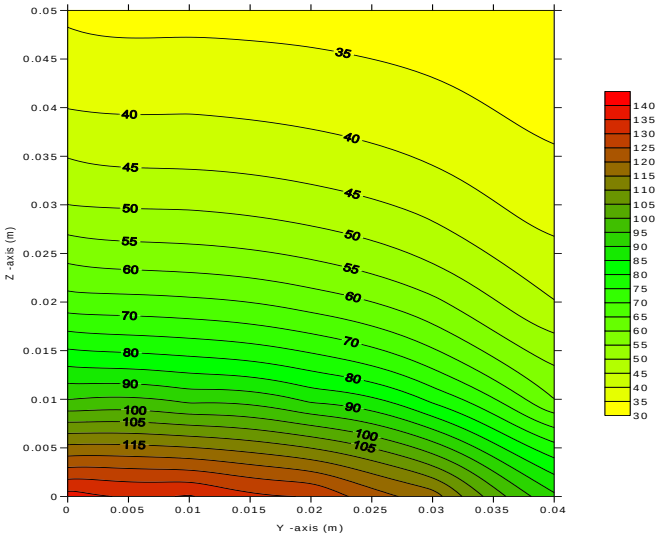

Figure (5-39) isothermal contour map for (y-z) plane in Chrome steel-air system with $\phi = .313$ and heat flux of 40000 W/m^2 at different times (a-time =600s ,b-time=1200 s and c- time=1800) according method No 1 of calculating k_e

(a)

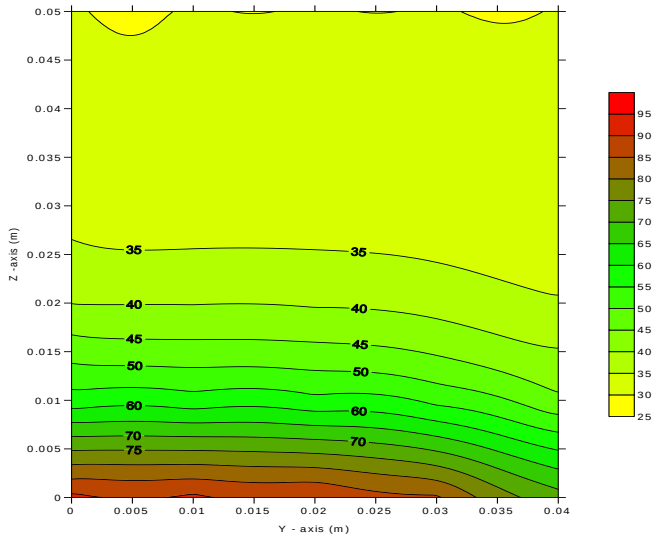

(b)

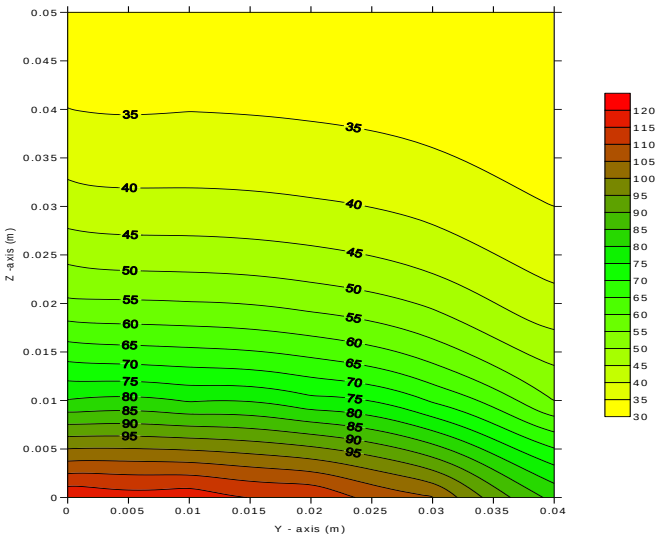

(c)

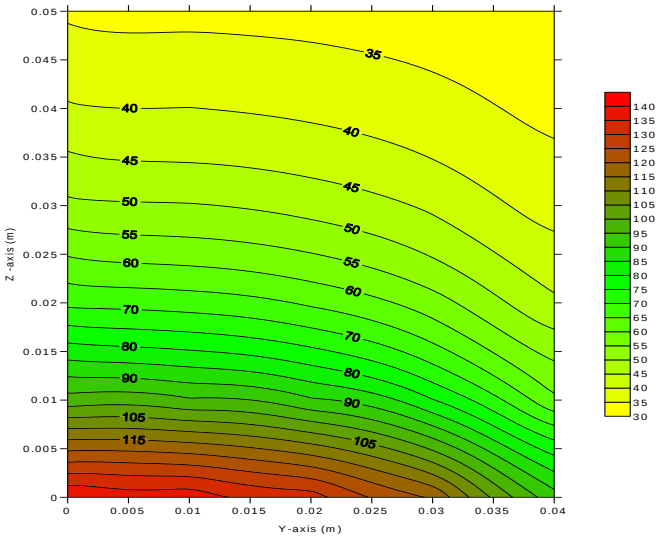

Figure (5-40) isothermal contour map for (y-z) plane in Chrome steel-air system with $\phi = .313$ and heat flux of 40000 W/m^2 at different times (a-time =600s ,b-time=1200 s and c- time=1800) according method No 2 of calculating k_e

(a)

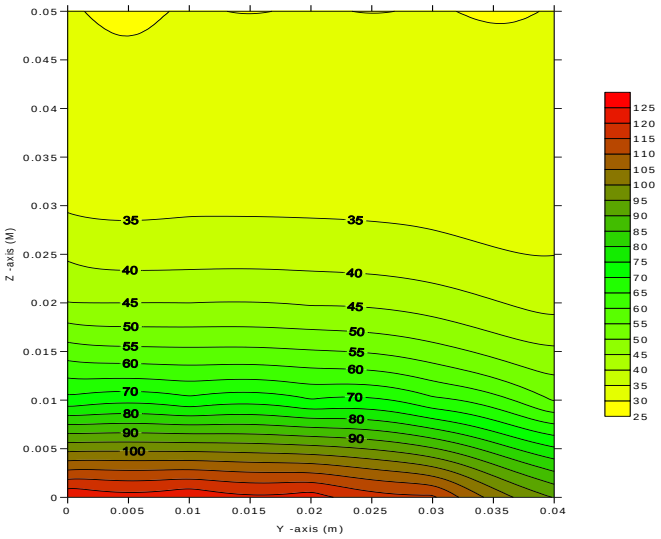

(b)

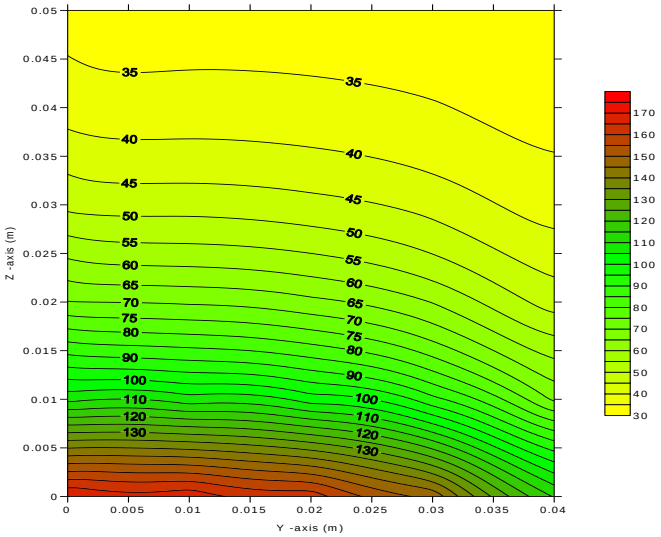

(c)

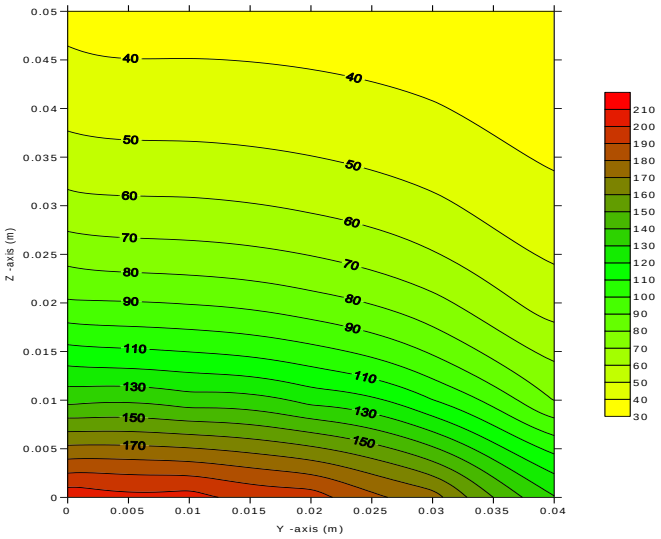

Figure (5-41) isothermal contour map for (y-z) plane in Chrome steel-air system with $\phi = .313$ and heat flux of 70000 W/m^2 at different times (a-time =600s ,b-time=1200 s and c- time=1800) according method No 1 of calculating k_e

(a)

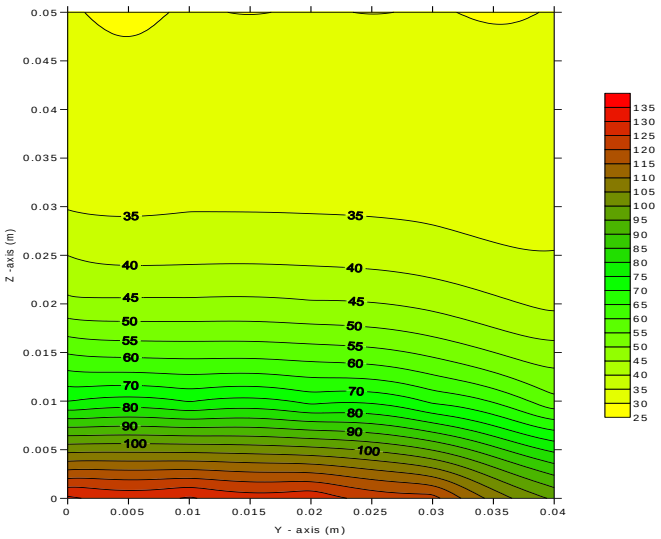

(b)

(c)

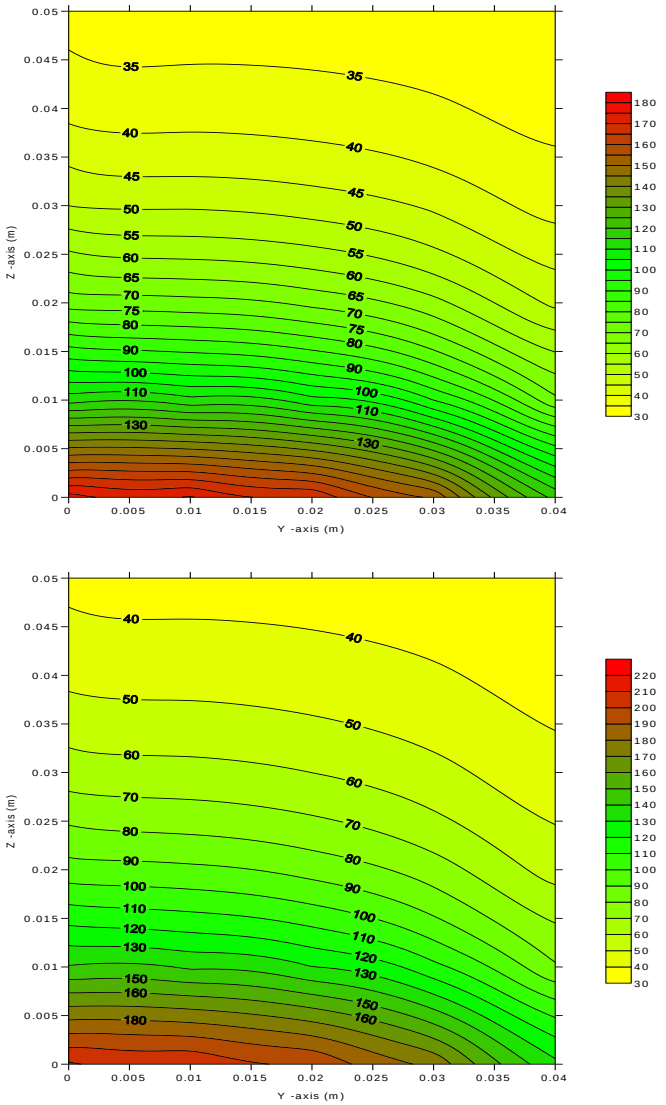

Figure (5-42) isothermal contour map for (y-z) plane in Chrome steel-air system with $\phi = .313$ and heat flux of 70000 W/m^2 at different times (a-time =600s ,b-time=1200 s and c- time=1800) according method No 2 of calculating k_e

Part (II) Experimental work:

Figures (5-43) to (5-54) represent the temperatures variation of MgO-air system and Chrome steel-air matrix with different heat flux and porosity values These were measured by using a new technique equipment (interface) with computer software.

Figures (5-43) and (5-44) show the temporal variation of temperature of MgO-air at heat flux values of 40000 W/m^2 and 70000 W/m^2.These figures show the temperature increased with increasing the time and with heat flux .

Figures (5-45) and (5-46) show the temperature variation with time at center point of Chrome steel-air matrix at value of the porosity 0.416.These figures indicated fast temperature variation with increasing time and heat flux values .This ensured the dependence of heat transfer rate on the solid phase thermal conductivity when the fluid phase is stagnant .

Figures (5-47) and (5-48) represent the temperature variation with time of Chrome steel-air matrix at value of porosity is 0.313 with different values of heat flux These figures show that temperature value increased compared with increasing the time and heat flux value .That was indicated that the porous media behavior become close to as solid phase of thermal conductivity and it was increased and the porosity decreased at increasing the heat flux value.

Figures (4-49) to (4-54) represent the experimental of temperature distribution through z and x- axis for the two test samples at different time intervals for two values of heat flux.

Figures (5-49) and (4-50) show the experimental temperature distribution through z-axis of MgO at three time interval when heat flux subjected of 40000 and 70000 W/m^2 These figures indicated that temperature variation increased with increasing the heat flux value . These figures indicated as in prediction model the temperature value at center is high .It was decreased at layer depth of material .That was due to the heat flux subjected at the lower surface of material and heat diffusion to inside depth of material.

Figures (5-51) to (5-54) illustrate the relationship between the temperature distribution of samples of Chrome steel –air system with spatial distance in x-axis. These samples materials have difference values of measured porosity .It was shown that the temperature profile was responded with time interval increasing and also with increasing the value of heat flux. It was also indicated that the temperature decreased when far away from center point in x-axis .A minimum temperature was measured at the wall of the material sample.

Figures (5-55) to (5-60) give another description of spatial temperature distribution with different time intervals for two materials .These results illustrate the comparison between the experimental and theoretical prediction results for two material samples at different values of heat flux .It was shown that there is very little difference between these results .This was due to the advanced equipments ,which were used to measure the temperature distribution .

Figures (5-55) and (5-56) show the comparison between the theoretical prediction result of MgO –air system using a new model in Three-dimensional and unsteady state with experimental work. These figures represented by using two methods of calculating the effective thermal conductivity and all results with different time interval and values of heat flux .

Figures (5-57) to (5-60) show same behavior of responsing the prediction results with measuring temperature at different values of heat flux for two Chrome steel-air systems with different values of measured porosity .These figures explain the difference between experimental and theoretical work which was marked a little bit than previous results in MgO-air system

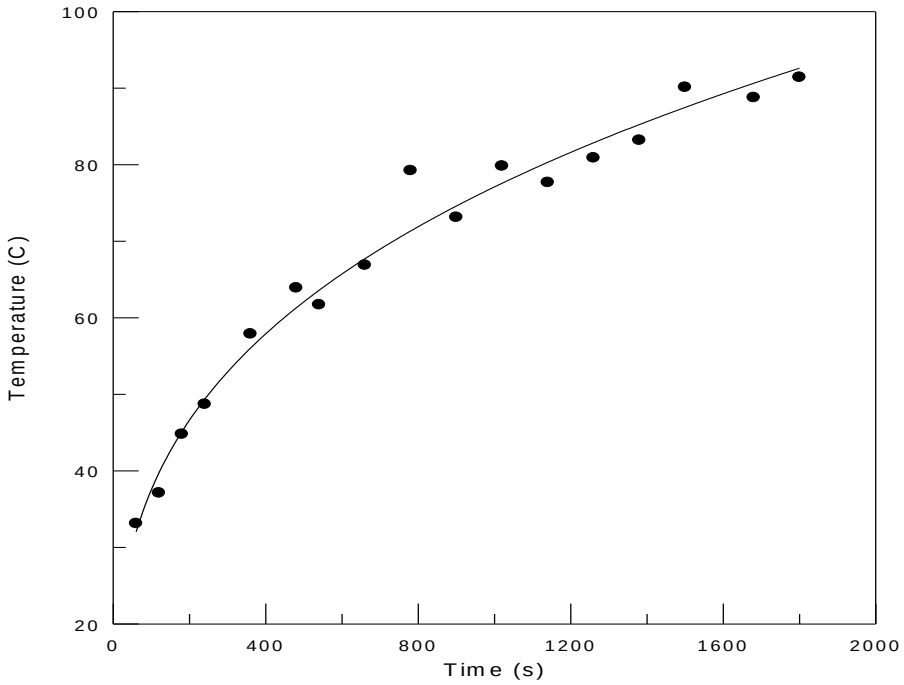

Figure (5-43) temperature variation with time at center point for MgO-air system at heat flux of 40000 W/m^2

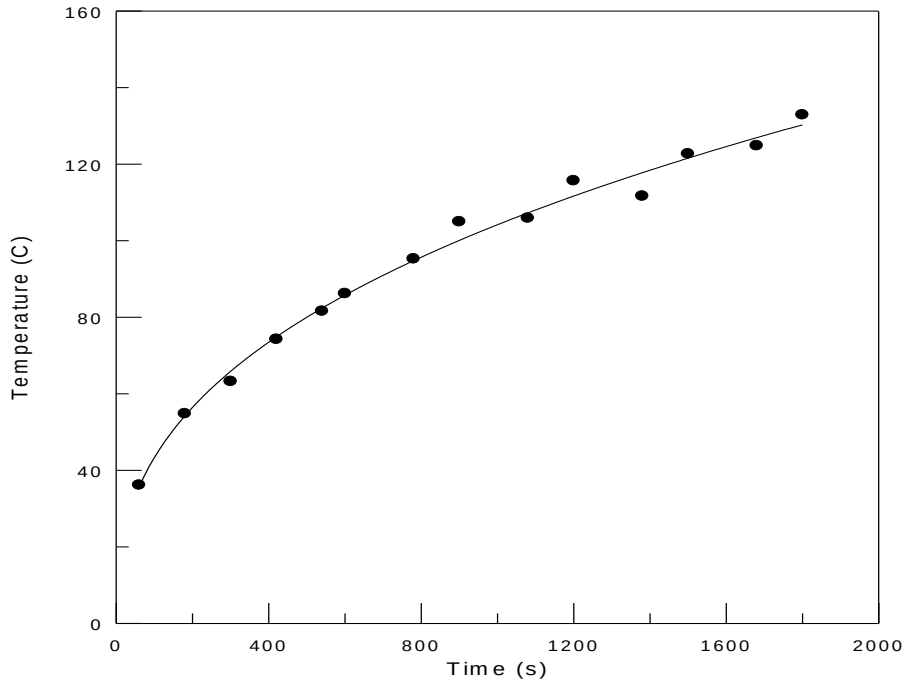

Figure (5-44) temperature variation with time at center point for MgO-air system at heat flux of 70000 W/m^2

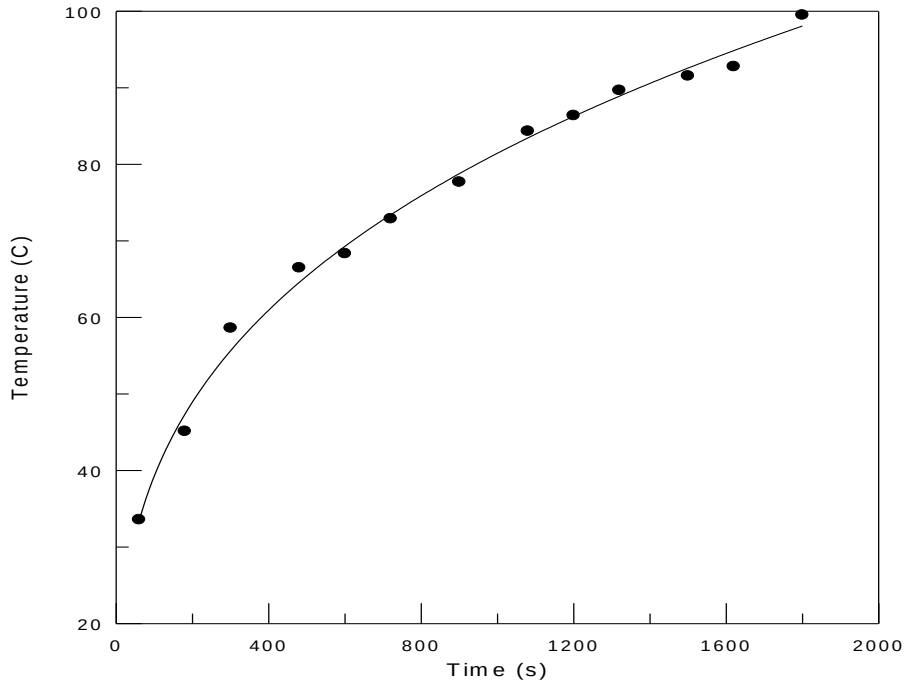

Figure (5-45) temperature variation with time at center point for steel-air ($\phi = .416$)system at heat flux of 40000 W/m^2

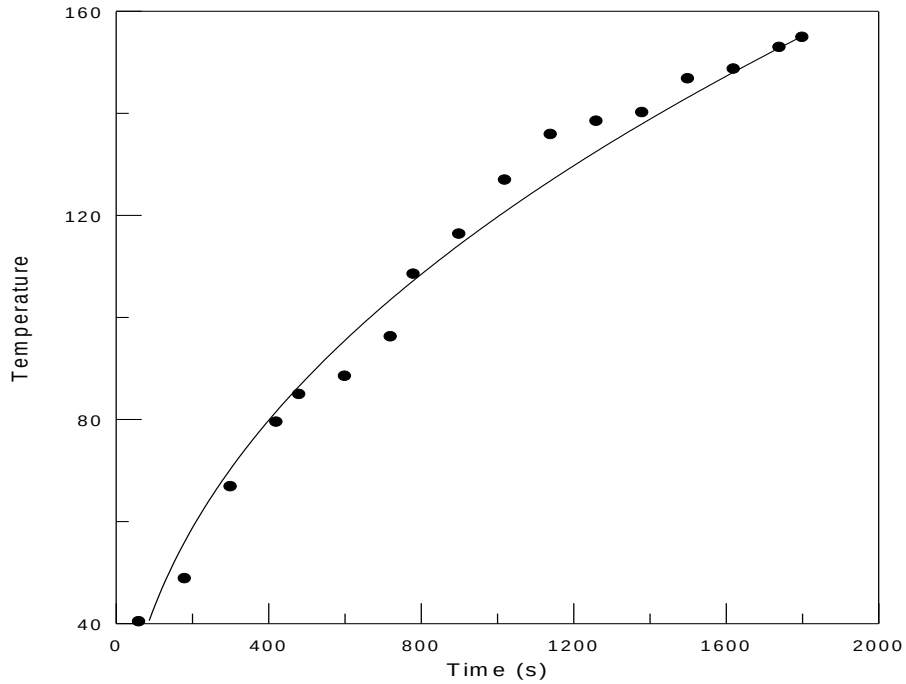

Figure (5-46) temperature variation with time at center point for steel-air ($\phi = .416$)system at heat flux of 70000 W/ m^2

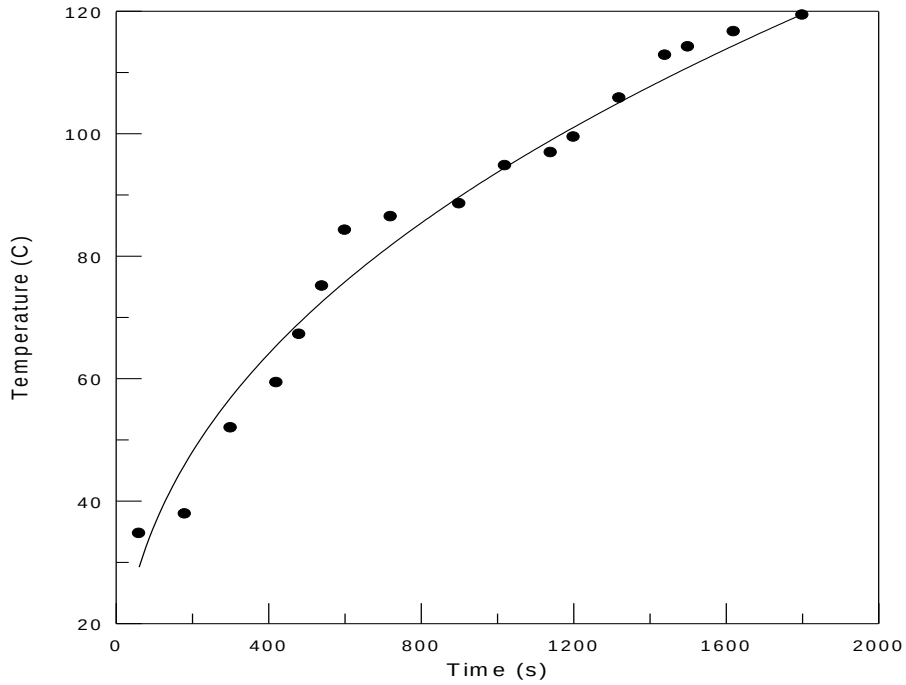

Figure (5-47) temperature variation with time at center point for steel-air ($\phi = .313$)system at heat flux of 40000 W/m^2

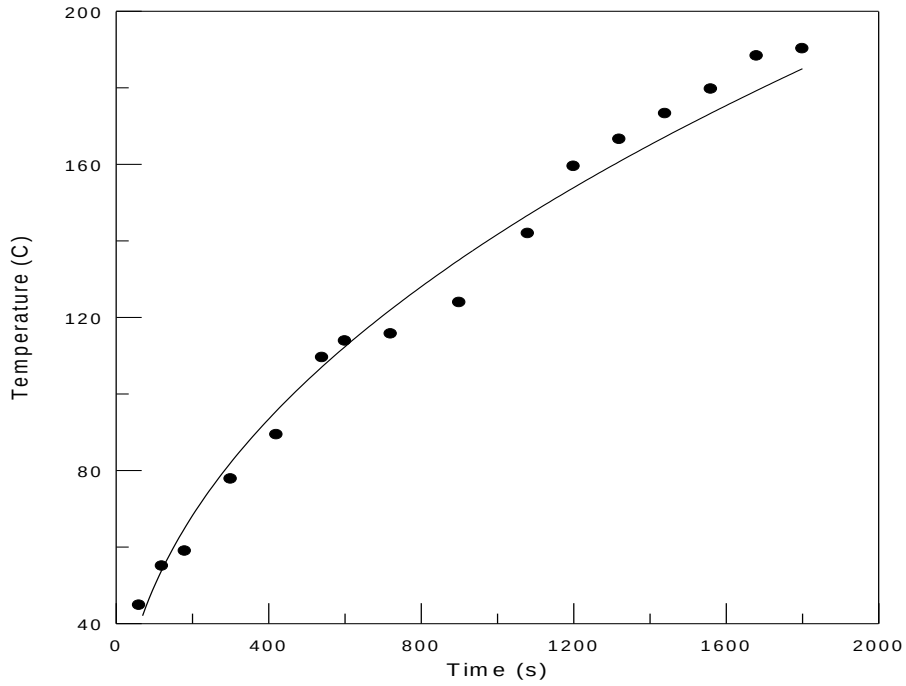

Figure (5-48) temperature variation with time at center point for steel-air ($\phi = .313$)system at heat flux of 70000 W/m^2

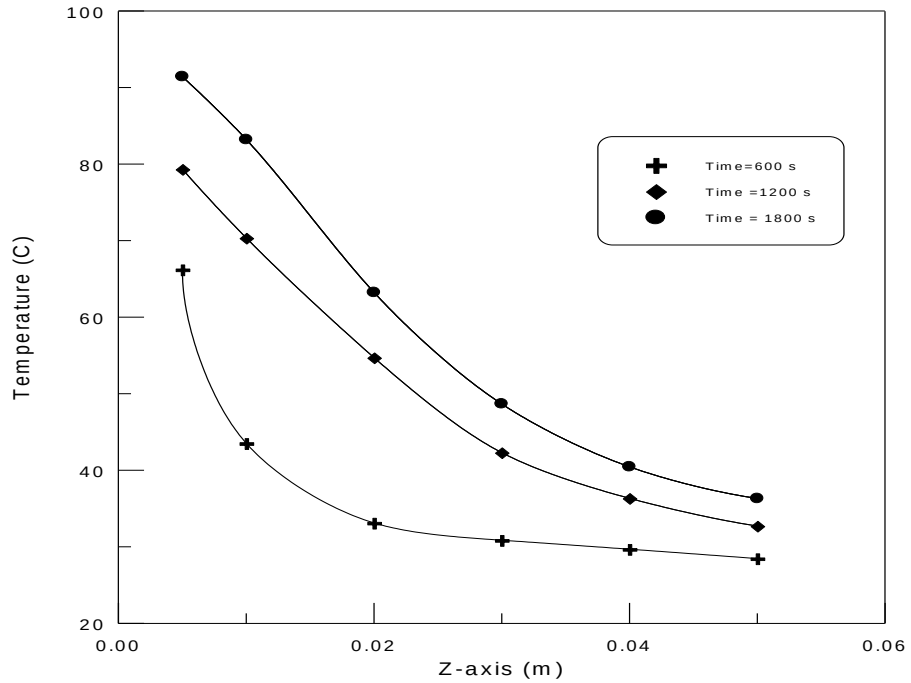

Figure (5-49) temperature distribution through z- axis in MgO –air system at different times at heat flux of 40000 W/m^2

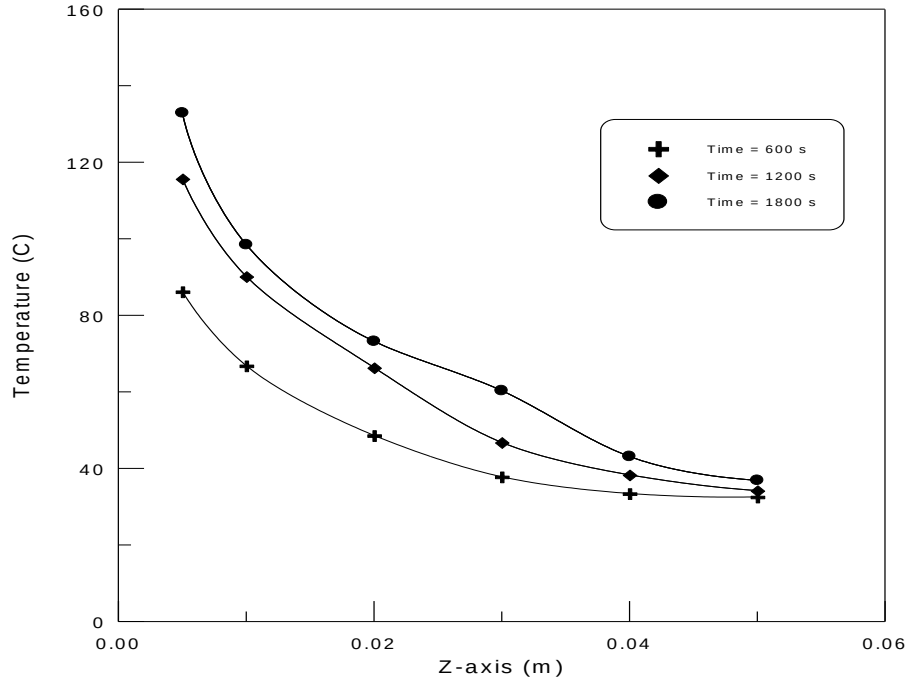

Figure (5-50) temperature distribution through z- axis in MgO –air system at different times at heat flux of 70000 W/m^2

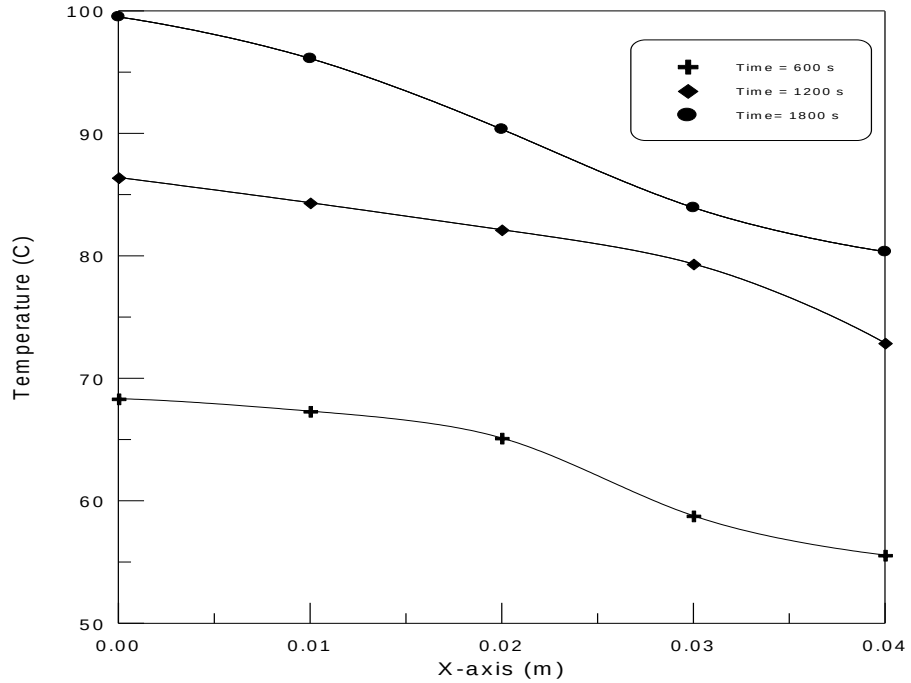

Figure (5-51) temperature distribution through x- axis in steel-air ($\phi = .416$) system at heat flux of 40000 W/m^2 at different times

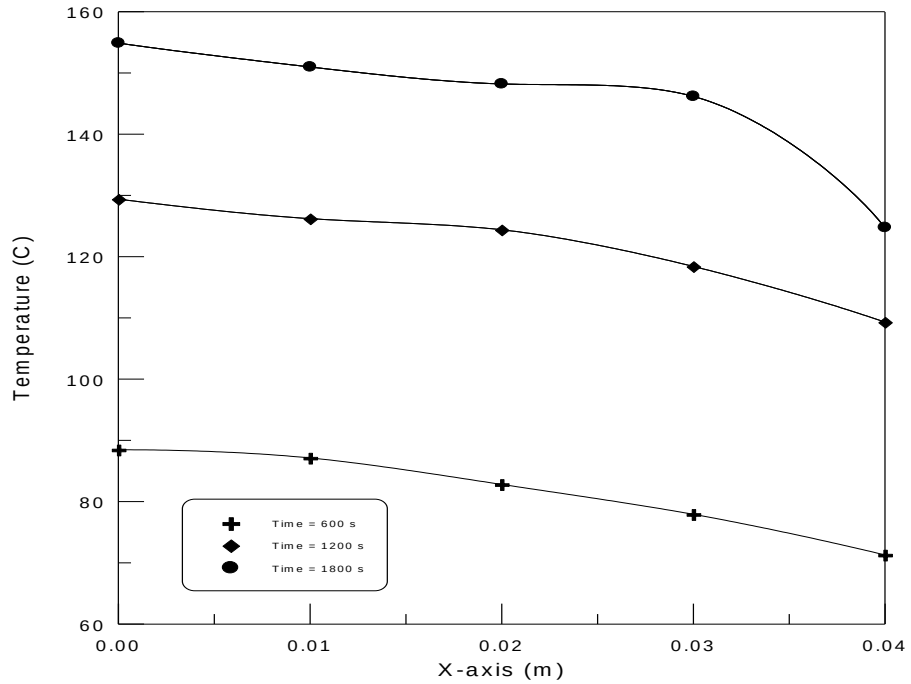

Figure (5-52) temperature distribution through x- axis in steel-air ($\phi = .416$) system at heat flux of 70000 W/m^2 at different times

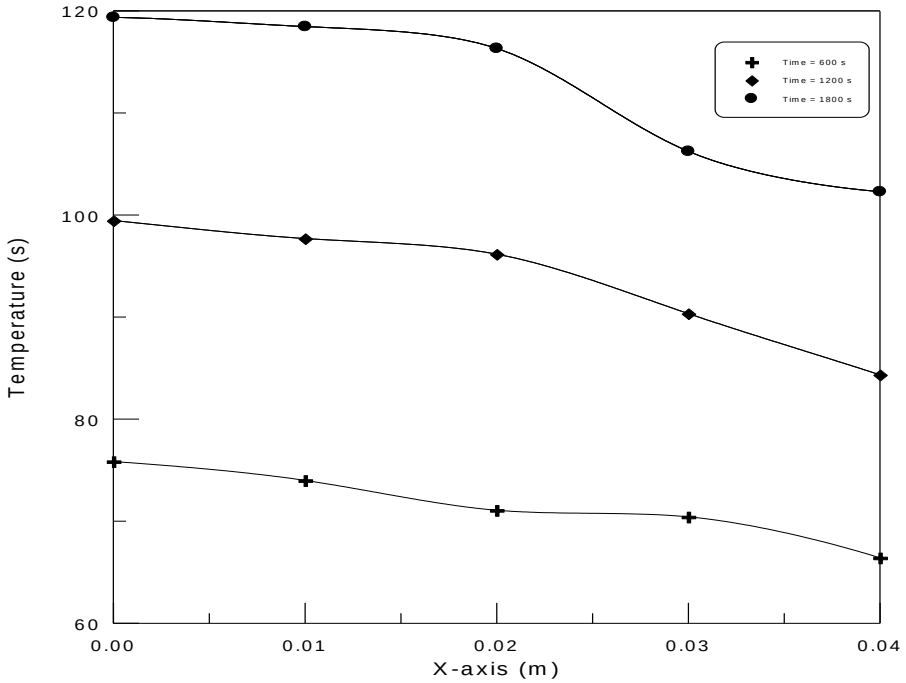

Figure (5-53) temperature distribution through x- axis in steel-air ($\phi = .313$) system at heat flux of 40000 W/m^2 at different times

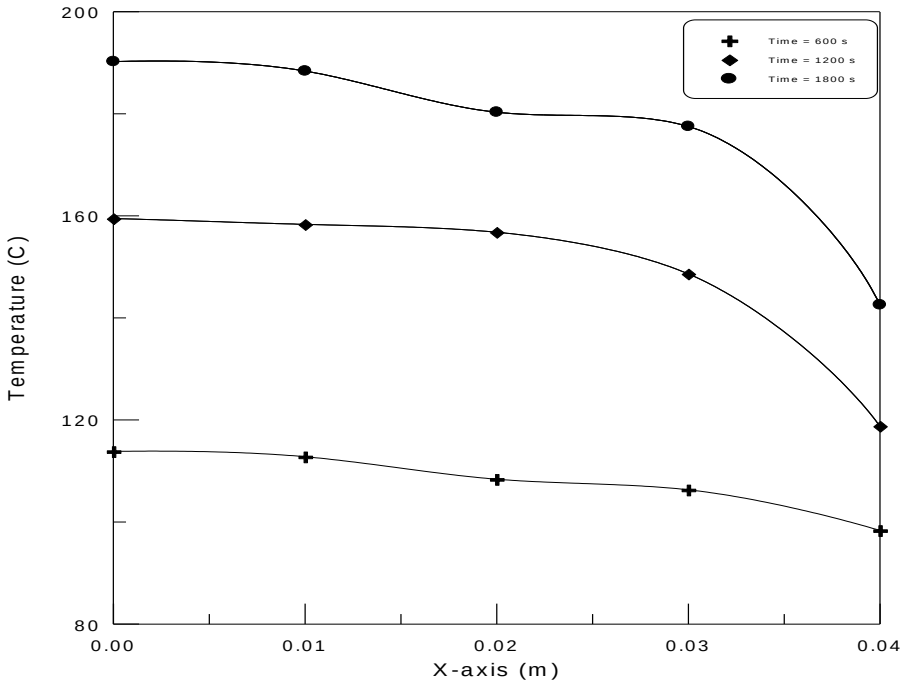

Figure (5-54) temperature distribution through x- axis in steel-air ($\phi = .313$) system at heat flux of 70000 W/m^2 at different times

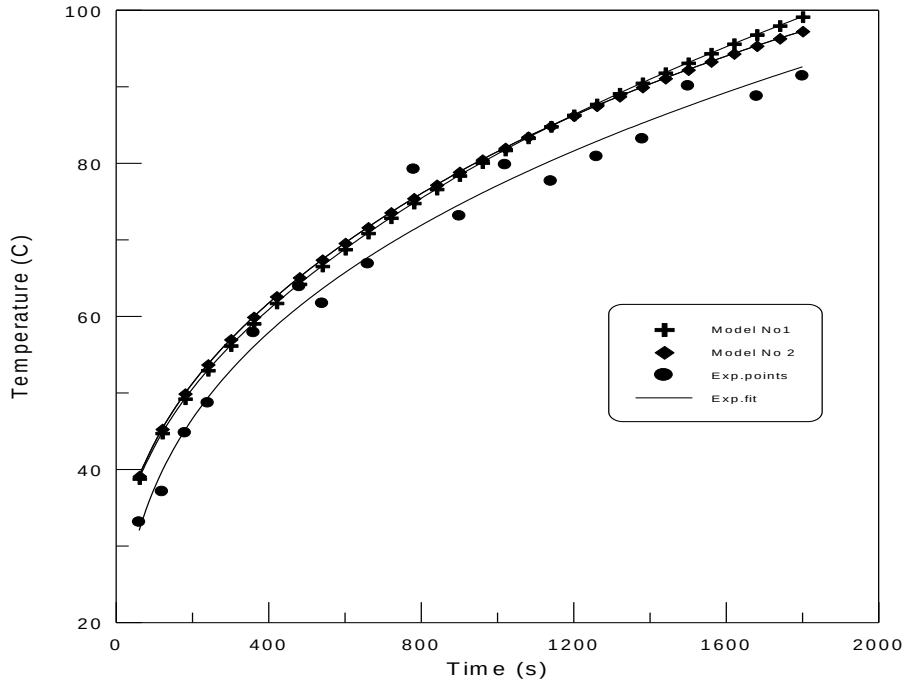

Figure (5-55) comparison of temperature variation with time at center point for MgO-air system at heat flux of 40000 W/m^2

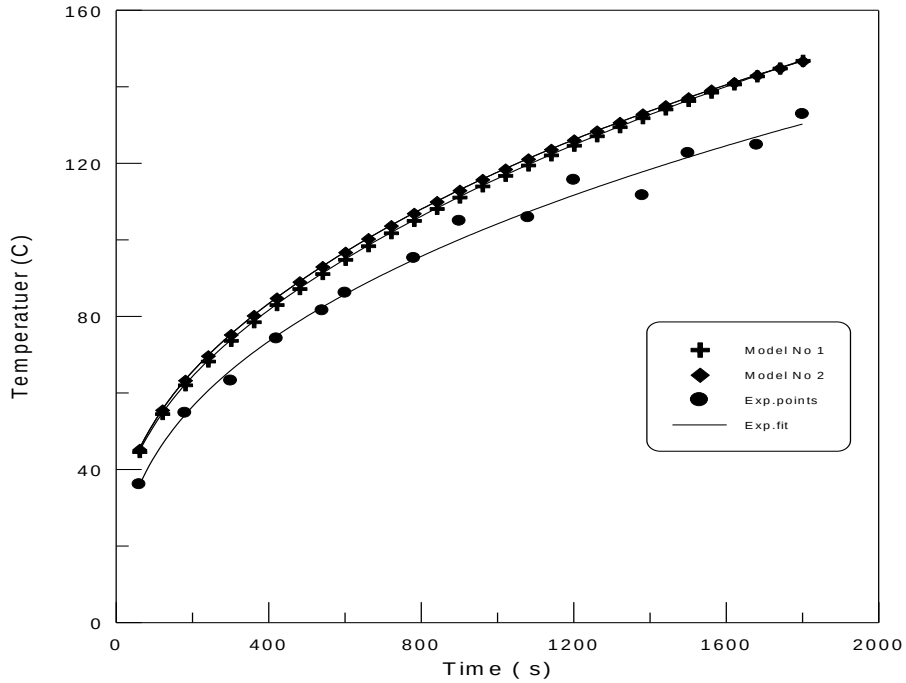

Figure (5-56) comparison of temperature variation with time at center point for MgO-air system at heat flux of 70000 W/m^2 .

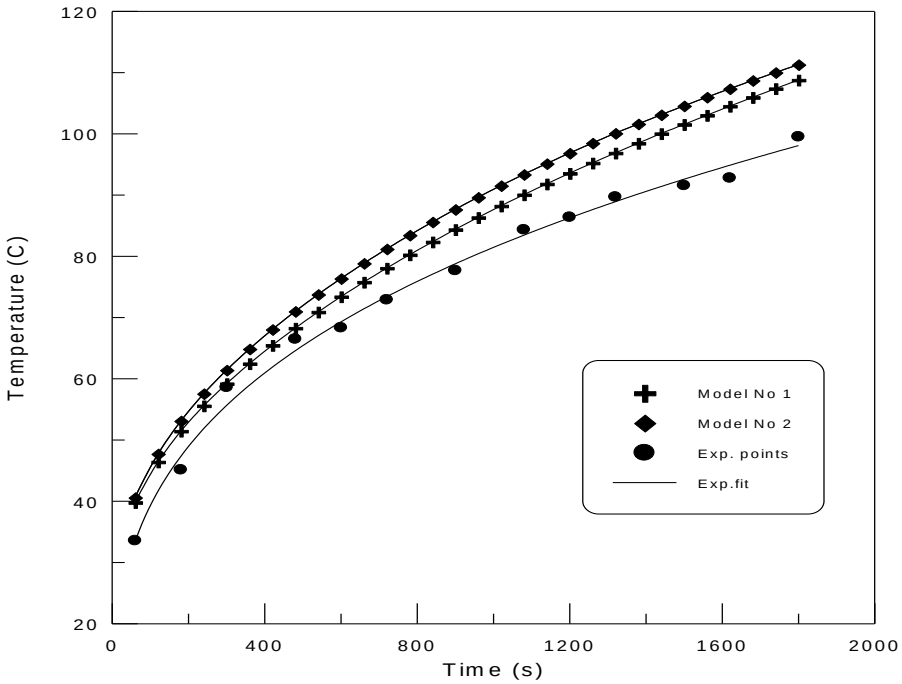

Figure (5-57) comparison of temperature variation with time at center point for steel-air ($\phi = .416$)system at heat flux of 40000 W/m^2

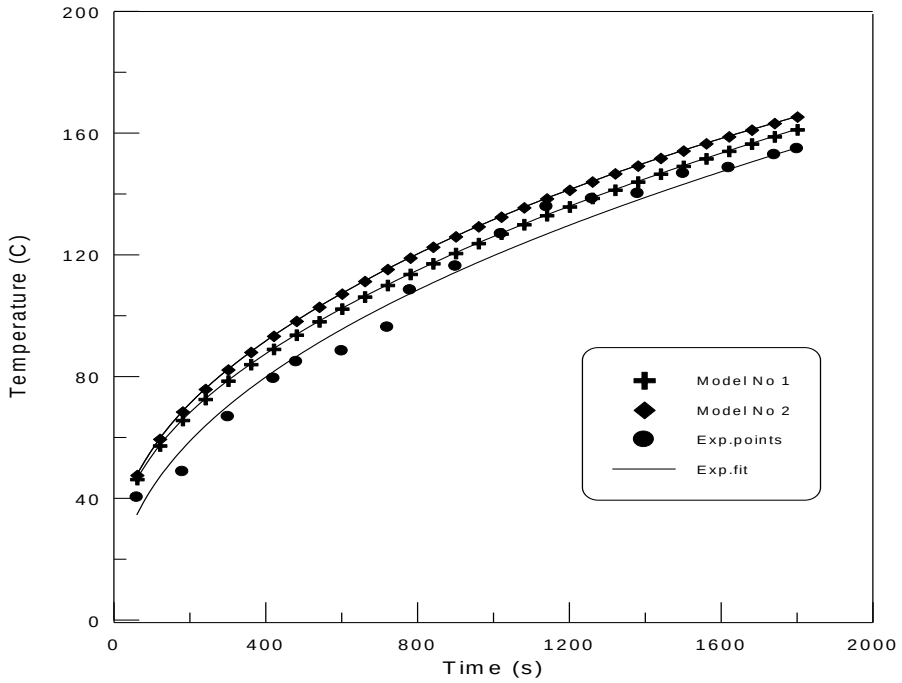

Figure (5-58) comparison of temperature variation with time at center point for steel-air ($\phi = .416$)system at heat flux of 70000 W/m^2

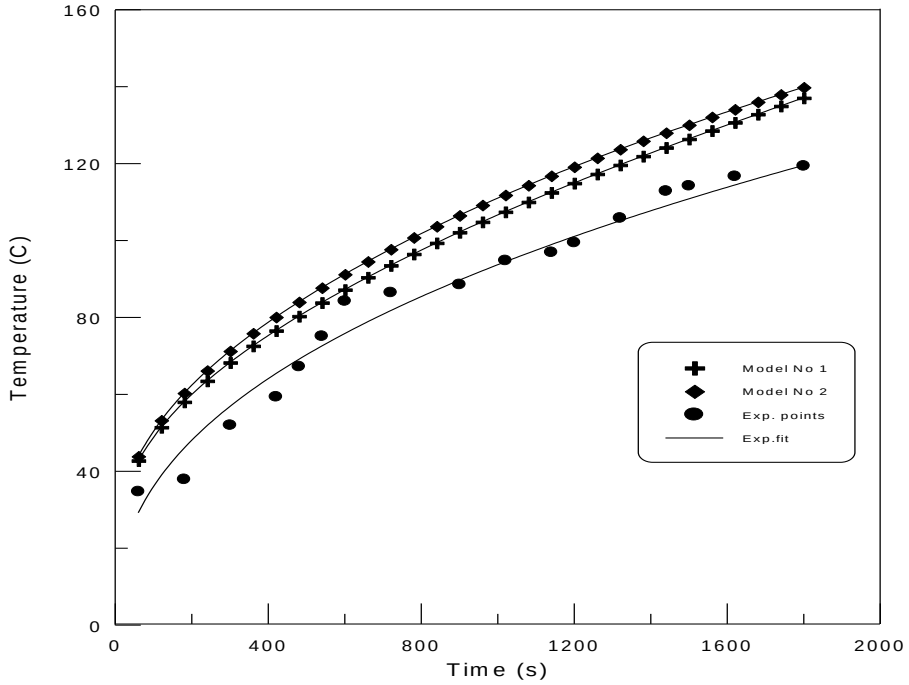

Figure (5-59) , comparison of temperature variation with time at center point for steel-air ($\phi = .313$)system at heat flux of 40000 W/m^2

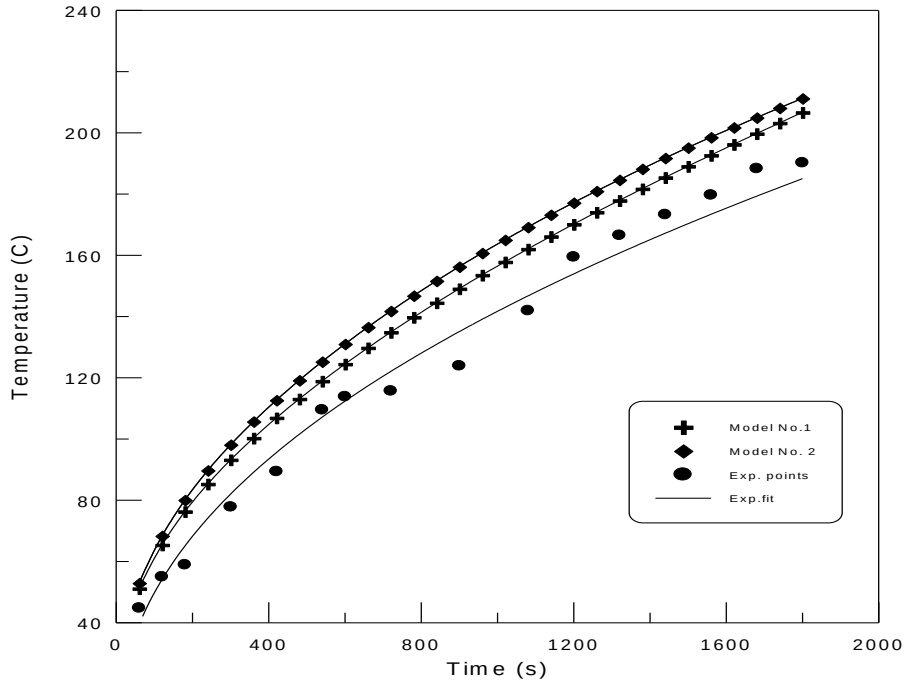

Figure (5-60) comparison of temperature variation with time at center point for steel-air ($\phi = .313$)system at heat flux of 70000 W/m^2

5.2.Effective Thermal conductivity

Figures (5-61) and (5-62) present the relationship between the calculated effective thermal conductivity and temperature distribution of MgO at two values of heat flux .These results of effective thermal conductivity were calculated by equation number (4.19) depending on the measuring temperature distributing over selected thickness for material sample. It was shown that the effective thermal conductivity increased as temperature increased .Then after period of time the response was changed , it was shown that the effective thermal conductivity start decrease when temperature increasing .This due to the properties of porous media material .It should be know that the material contain two phases solid and fluid. This response of result was represented the range values between the solid phase and fluid phase .Also it was shown these values decreasing with increasing the heat flux that was due to the same reason of geometrical and structure of porous material shape .

Figures (5-63) and (5-64) describe another relation between thermal conductivity ratio ($k = \frac{k_s}{k_f}$) and temperature distribution of MgO material at different value of heat flux .These results was estimated upon two assumption published methods of calculating the effective thermal conductivity .These methods were Zhner [11] and Hadley [14].It was shown that the thermal conductivity ratio(k) response as a parabola .That was more indicated with heat flux of 70000 Wm^2 .That were estimated upon two methods of calculating the effective thermal conductivity.

Figure (5-65) shows a relationship between dense thermal conductivity (k_{dense}) and temperature of MgO sample .The values depended on equations (4.21) and (4.22) and effective thermal conductivity calculation methods were given by Hadely[14] and Zhner[11] .These results were estimated upon different methods of calculating dense thermal conductivity (k_{dense}) .These were published by many authors such as

Klumens [38] and Maxwell- Garnett [7].It was shown that the better method of calculating dense thermal conductivity by Zhner [11] and Maxwell [7] .This due to calculated values are more close to the standard values presented in Appendix (A).

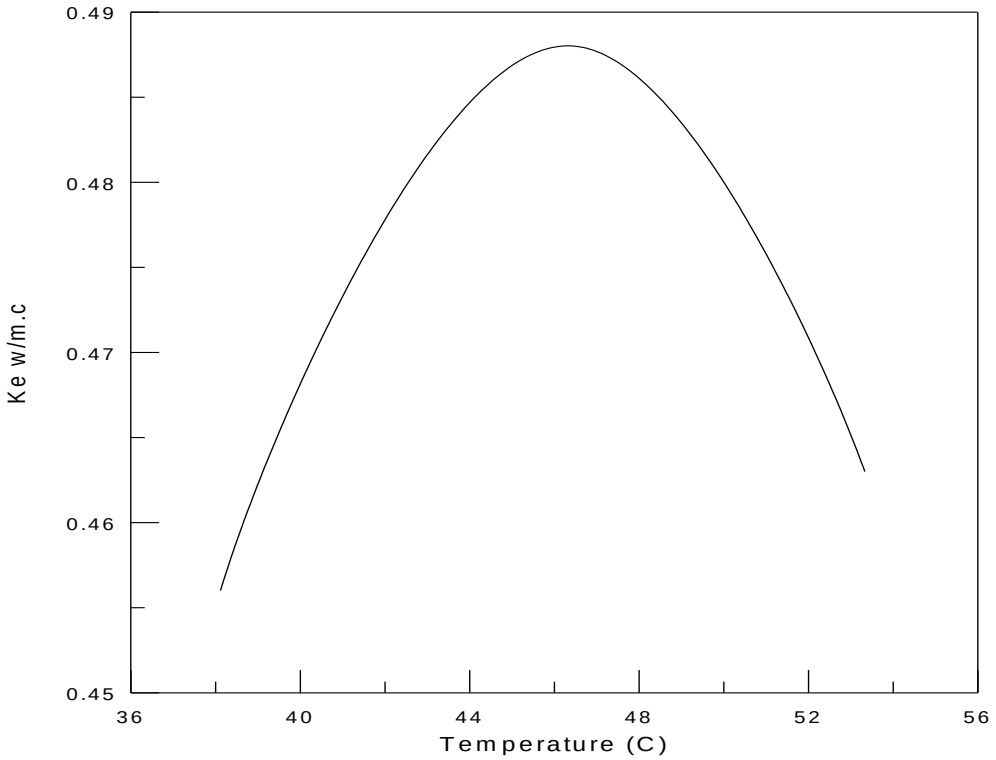

Figure (5-61) effective thermal conductivity variation with temperature of MgO at heat flux of 40000 W/m^2

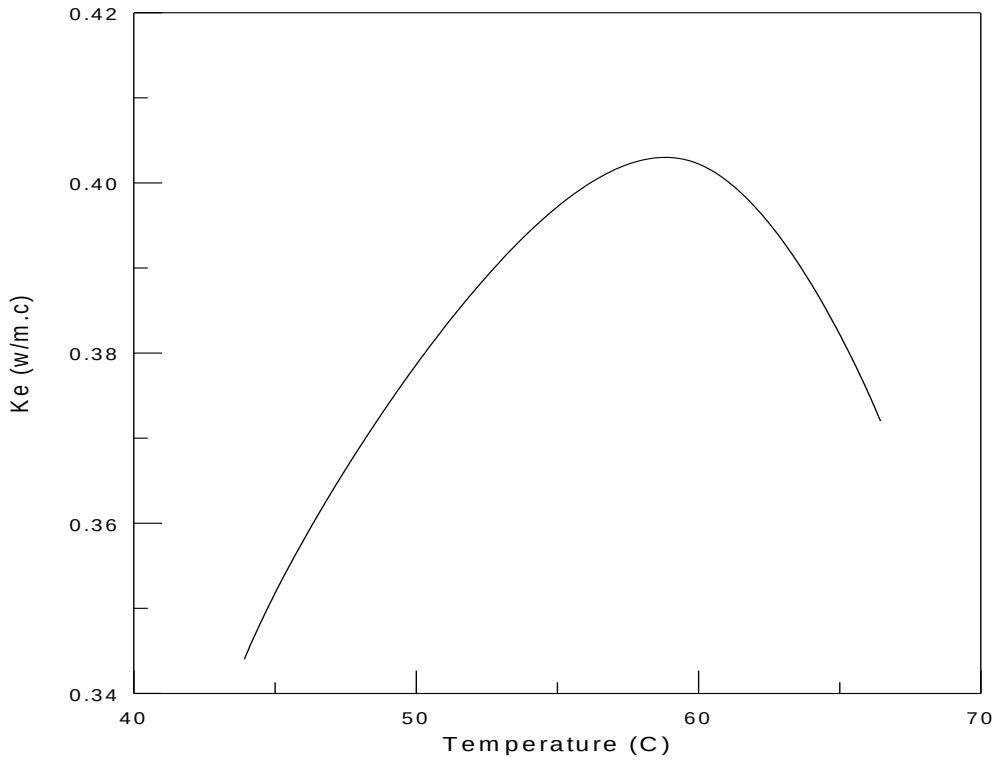

Figure (5-62) effective thermal conductivity variation with temperature of MgO at heat flux of 70000 W/m^2

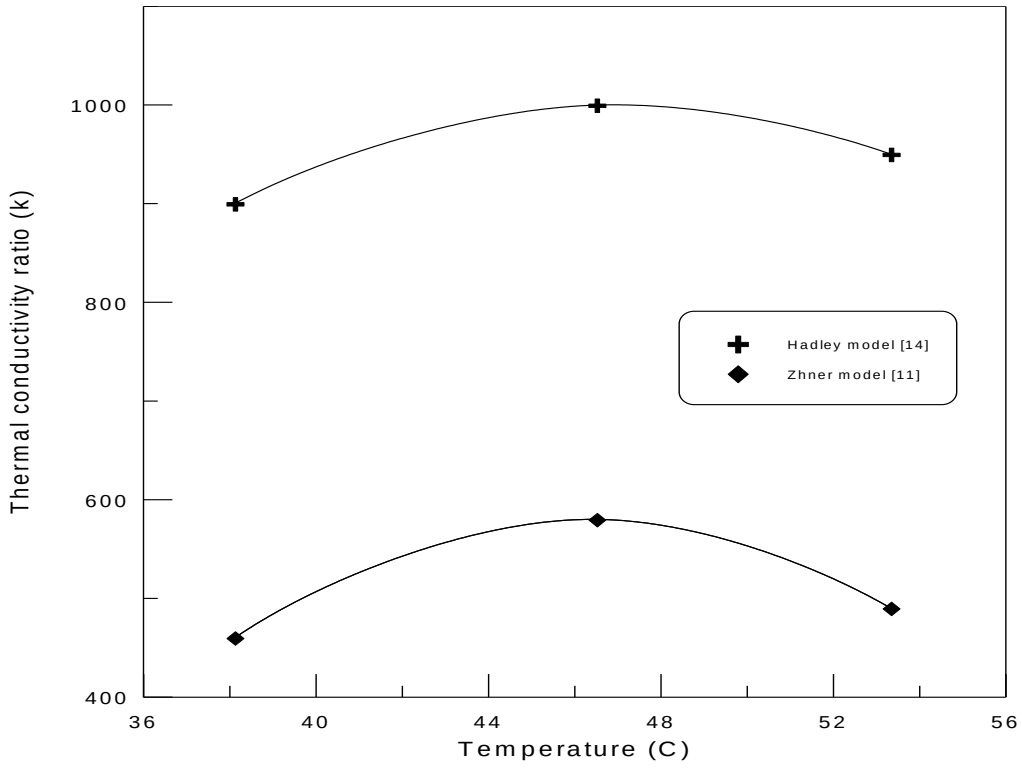

Figure (5-63) thermal conductivity ratio variation with temperature of MgO at heat flux of 40000 W/m^2

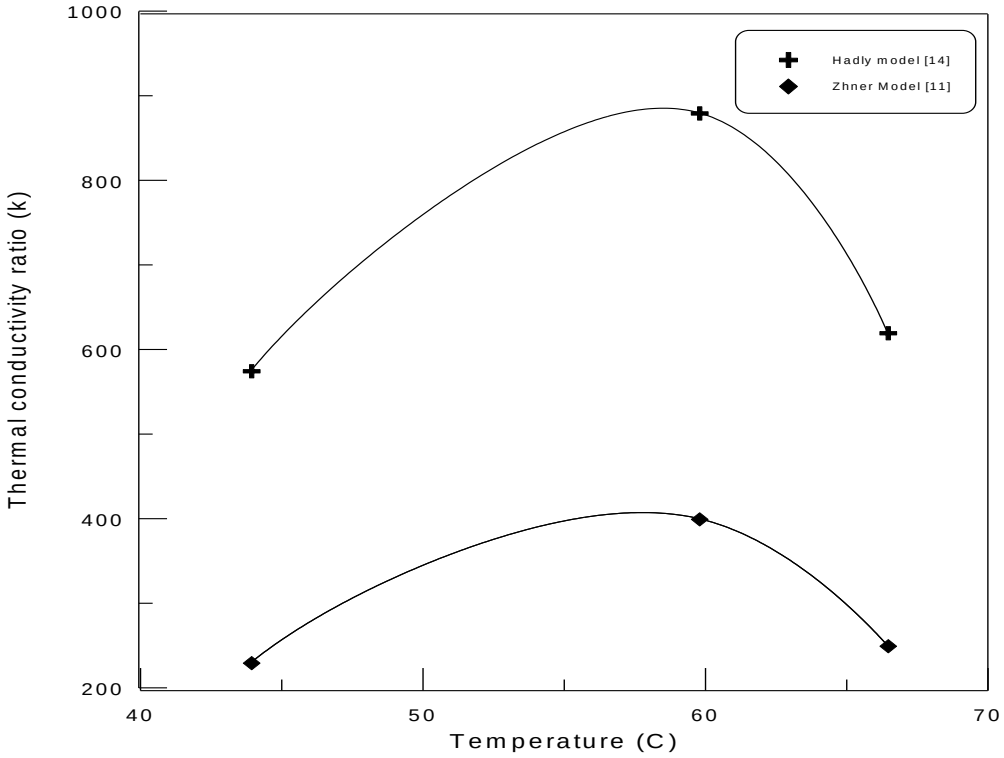

Figure (5-64) thermal conductivity ratio variation with temperature MgO at heat flux of 70000 W/m^2

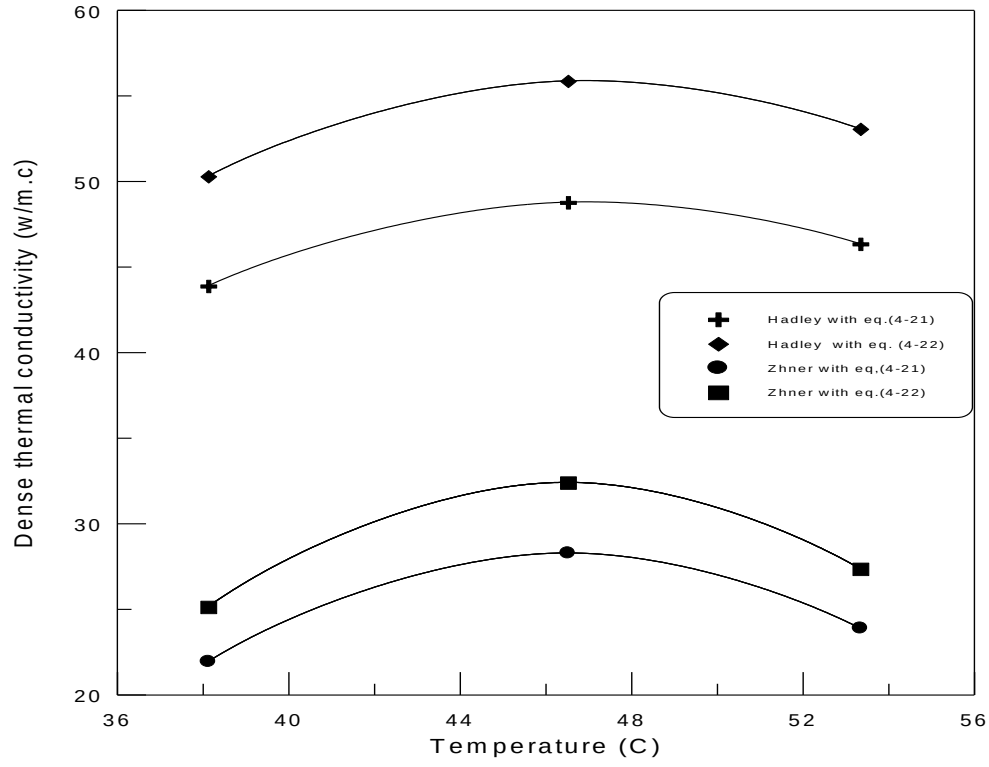

Figure (5-65) dense thermal conductivity of MgO variation with temperature

at heat flux of 40000 W/m^2

Conclusions and Suggestions for Future Work

6.1. Conclusions

In theoretical part of this study the three-dimensional heat conduction model was developed to find temperature distribution in porous media and predicts two methods of calculating the effective thermal conductivity derived from the previous studies . The simulation on a three samples of porous media with an idealized composite structure showed the anisotropic material properties (thermal conductivity) effect on the heat transport porous media .The following points were recorded from this study.

1-Therotical investigation of the energy transport in porous media materials caused by constant heat flux ,which was subjected at the top of these materials. A new model which was assumed that these materials in stagnation case between two phases of porous media material structure .This model gave more reliability to explain the temperature distribution .A new assumption was used in this model by calculating the effective thermal conductivity (k_e) ,which was estimated the thermal conductivities of two phases (solid and fluid) of material structure.

2-The new model of heat conduction has predicted the possibility of heat diffusion inside the porous material .This model gives a better conderstanding of that mechanism and minimize the round error .The present work may the first work analyze the mechanism in three dimension and unsteady state .Also it was used a numerical solution technique ,while many authors using analytical solutions with one dimension.

3-Experimental work was done by using advanced equipments in order to measure the temperature distribution through these samples .A computerize temperature meter (CTMO1) was used to record the temperature readings at different positions on the materials .These equipments have facilities to read the spatial and temporal distribution of temperature by special software ,which was built .This interface equipment gave more reliable and minimize error through the measurements.

4-Comparision between experimental and theoretical work was done .It was shown that the experimental measurement of temperature distribution more close with the prediction results of present model which was built in the present work. Experimental results were consistent with the results of a present model .This was due to the advance equipment which was used.

5- It was found that heat transferred in the x-direction different with the z direction due to the heat flux direction . It was found that the temperature gradient was higher near the area of heat flux surface . The difference of the temperature was decreasing with time.

6-Another work was done to calculate the effective thermal conductivity by using equation (4.19) .This method of calculating was different from traditional methods ,used by many authors .This method depend upon the measurement of temperature difference between selected thickness of material .That was done by using advance equipment (CTMO1).This predicted a good results compared with published tables .

6.2.Suggestions for Future Work

As related to the present work the following suggestions for future developments forward:

1-The theoretical model can be used to study the effect of porosity variation with temperature (as a function of temperature) with thermal conductivities variations on heat transfer in porous media.

2- The theoretical model can be used with another boundary conditions such as constant wall temperature or fully insulated surfaces.

3-The experimental rig can be used to study the cooling rate in porous media at different values of heat flux and porosity.

Contents

Examining Committees Certificate

We certify that we have read this thesis, entitled "***Theoretical and Experimental Investigation of Conduction Heat Transfer in porous media",*** and as examining committee, examined the student ***"Hussein Mahmood Jassim "*** in its contents and in what is connected with it, and that in our opinion it meets the standard of a thesis for the degree of Master of Science in Mechanical Engineering.

Signature:
Name: Asst. Prof.
Dr. **Adil A. Al- moosawy**
(Supervisor)
Date: / /2008

Signature:
Name: Asst. Prof.
Dr**. Alaa Abbas Mahdi**
(Member)
Date: / /2008

Signature:
Name: Asst. Prof.
Dr**. Emad S. Ali**
(Member)
Date: / /2008

Signature:
Name: Asst. Prof.
Dr**. Mohammed Idris Mohsin**
(Chairman)
Date: / /2008

Approval of the Mechanical Engineering Department.

Head of the Mechanical Engineering Department

Signature:
Name: Asst. Prof.
Dr. Adil A. Al- moosway
Date: / /2008

Approval of the Deanery of the College of Engineering.

Dean of the College of Engineering.

Signature:
Name: Asst. Prof.
Dr. Salah Tawfeeq Al- Bazzaz
Date: / /2008

Nomenclature

The following symbols are used generally through the text. Others are defined locally

LATIN SYMBOLS

A	Area (m^2)
A^o	Dimensionless empirical parameter
B	Dimensionless empirical shape parameter
B^O	Dimensionless empirical parameter
C_p	Specific heat (J/kg. K)
f_o	Parameter from Hadley (1986) correlation.
h	Convection heat transfer coefficient (W/m^2. °C)
I	Current (amp.)
k_{dense}	Dense thermal conductivity (W/m. °C)
k_{porous}	Thermal conductivity of porous material (W/m. °C)
k_e	Effective thermal conductivity (W/m. °C)
k_s	Solid Phase Thermal conductivity (W/m. °C)
k_f	Fluid Phase Thermal conductivity (W/m. °C)
k	Thermal conductivity ratio $\frac{k_s}{k_f}$
k_{sf}	Solid-fluid layer effective thermal conductivity
P	Parameter (m)
R	Radial dimension in the model of Zehner and Schlunder[11] or Hsu et al [17], (mm).
$q''_{(t)}$	Heat flux ($watt/m^2$)
T	Temperature (°C)
T_∞	Ambient temperature (°C)
t	Time (second)
V	Voltage (volt)
V_i	Initial volume (m^3)
V_d	Displaced volume (m^3)

GREEK SYMBOLS

α_e	*Thermal diffusivity (m^2/s)*
α_o	*Dimensionless particle deformation*
α_p	*Degree of consolidation parameter*
β	*Non-dimensional geometry parameter*
γ	*Non-dimensional geometry parameter*
γ_a	*Dimensionless parameter in the lumped square cylinder model*
γ_c	*Dimensionless parameter particle-to-particle contact parameter*
λ	*Convergence factor*
ρ	*Density (kg/m^3)*
ϕ	*Porosity*
ψ	*Non-dimensional geometry parameter*

SUBSCRIPTS

e	*Effective*
f	*Fluid Phase*
s	*Solid phase*
sf	*Solid fluid*
dense	*Pure Dense material*
porous	*Porous material*
h	*Hadley Method*
z	*Zhner Method*

ABBERVIATION

CTMO1	*Computerize Temperature Meter*
ETC	*Effective Thermal Conductivity*
REV	*Representative Elementary Volume*
FDTD	*Finite difference time domain methods*
PDEs	*Partial differential equations*

References

[1] Hans T. Aichlmayr **"The Effective Thermal Conductivity of Saturated Porous Media"** M.Sc.thesis University of Minnesota ,September 1999.{inter}

[2]Poulikakos and F. Zwick **"Metal foams as compact high performance heat exchangers "** Laboratory of Thermodynamics in Emerging Technologies, Institute of Energy Technology, Swiss Federal Institute of Technology, ETH Center, ML J 36, 8092 Zurich, Switzerland Received 1 June 2002; received in revised form 30 January 2003.{inter}.

[3]S.J. Kim, S.P. Jang, **"Effects of the Darcy number, the Prandtl number, and the Reynolds number on the local thermal non-equilibrium",** International Journal of Heat Mass Transfer Vol. 45 pp.3885–3896,2002.

[4] Judy Brewer**" Ceramics Windows To The Future"** materials science and Technology Teacher's ,Workshope Department of Materials Science and Engineering ,University of Illinois (UIUC) ,1995.

[5] L. Braginsky, V. Shklover, and G. Witz **"Laboratory of Crystallography**,, **Thermal conductivity of porous structures "**,Alstom (Schweiz) AG, Brown Bovery Strasse 7, 5401 Baden, Switzerland Received 21 July 2006; revised manuscript received 24 December 2006; published 12 March 2007 {inter}.

[6] Deissler and Eian **"The Effective Stagnant Thermal Conductivity of Porous Media with Periodic Structures ",**journal of porous media Vol. 2 issue,1952.

[7] J.C. Maxwell **"A Treatise on Electricity and Magnetism",** book, Vol. 1. Clarendon. London, Ser. A,204 , 385 Press, Oxford, 3rd .edn. October 1904.

[8] R. G. Deissler and J. S Boegli , **"An investigation of effective thermal conductivities of powders in various gases"** Journal, ASME Transactions, Vol. 80, pp. 1417-1425,1958.

[9] Kunii, D. and Smith **"Heat transfer characteristics of porous rocks "** AIChE Journal, Vol. 6, No. 1, pp. 71-78,1960. Cited in Ref.[1]

[10] Krupiczka **"Analysis of thermal conductivity in granular materials."** J. International Chemical Engineering, Vol. 7, Vo. 1, pp. 122-144,1967. Cited in Ref.[1]

[11] Zehner, P. and Schlunder, **"Thermal conductivity of granular materials at moderate temperatures."** J.Chemie -Ingr- Tech , vol. 42, pp. 933-941, 1970 Cited in Ref.[1]

[12] Batchelor, G. F. and O'Brien, R. W., **"Thermal or electrical conduction through a granular material."** J.Proc. R. Soc. London. A, vol. 355, pp. 313-333 , 1977.

[13] Nozad, I., Carbonell, R. G., and Whitaker, S., **"Heat conduction in multiphase systems theory and experiment for two-phase systems."** J.Chemical Engineering Science,Vol. 40, No. 5, pp. 843-855 , 1985. Cited in Ref.[1]

[14] Hadley, G. R.,. **"Thermal conductivity of packed metal powders."** International Journal of Heat and Mass Transfer, vol. 29, No. 6, pp. 909-920, 1986.

[15] Prasad, V., Kladias, N., Bandyopadhaya, A., and Tian, Q. **"Evaluation of correlation's for stagnant thermal conductivity of liquid-saturated porous beds of spheres."** International Journal of Heat and Mass Transfer, Vol. 32, No. 9, pp. (1793-1796). 1989.

[16] Nield, D. A., **"Estimation of the stagnant thermal conductivity of saturated porous media."** International Journal of Heat and Mass Transfer, Vol. 34, No. 6, pp. 1575-1576, 1991**.** Cited in Ref.[1]

[17] Hsu, C. T., Cheng, P., and Wong, K. W., **"Modified Zehner-Schlunder models for stagnant thermal conductivity of porous media."** International Journal of Heat and Mass Transfer, Vol. 37, No. 17, pp. 2751-2759, 1994**.**

[18] Hsu, C. T., Cheng, P., and Wong, K. W.,**." A lumped parameter model for stagnant thermal conductivity of spatially periodic porous media."** Journal

of Heat Transfer Transactions of the ASME, Vol. 117,No. 2, pp.264-269 , 1995. Cited in Ref.[1]

[19]A .V. Kuznetsov. **."An Investigation of a Wave of Temperature Difference Between Solid and Fluid Phases in a Porous Packed Beds".** International Journal of Heat Mass Transfer, Vol.37, p. 3030, 1994.

[20] M. Kaviany, **"Principles of Heat Transfer in Porous Media",** Book, second ed., Springer, Berlin, 1995 .

[21] Fu, X., Viskanta and R. Gore.**" Prediction of effective thermal conductivity of cellular ceramics** "Int. Comm. Heat Mass Transfer, Vol. 25, No. 2, pp. 151-160, 1998.

[22] X.G. Liang W. Qu **"Effective thermal conductivity of gas solid composite materials and the temperature difference effect at high temperature "** . Department of Engineering Mechanics. Tsinghua University. Beijing 100084. China International Journal of Heat and Mass Transfer Vol.32,pp.1885-1893,1999{inter}.

[23] K. Muralidhar and K. Suzuki. **"Analysis of Flow and Heat Transfer in a Re-generator Mesh using a Non-Darcy Thermally Non-equilibrium Model".** International Journal of Heat Mass Transfer, Vol. 44, p 2493 , 2001.

[24] Ramvir Singh **"Calculation of Effective Thermal Conductivity of Highly Porous Two-phase Materials"** J. Thermal Physics Laboratory, Department of Physics, University of Rajasthan, Jaipur ,No. 302 (INDIA),2002.

[25] C. Singh, R. G. Tathgir and K Muralidhar**. "Comparison of 1-equation and 2-equation Models for Convective Heat Transfer in Saturated Porous Media "** IE (I) Journal- MC Vol. 84, October 2003**.**

[26] Zhao, C.Y., Lu, T.J., Hodson, H.P. and Jackson, J.D.**"The Temperature Dependence of Effective Thermal Conductivity of Open-Celled Steel Alloy Foams**", International Journal of Heat and Mass transfer Vol. 367, pp. 123-131,2004.

[27] Z. Wang, A. Kulkarni, S. Deshpande, T. Nakamura, and H. Herman, Acta Mater. " **Thermal conductivity of porous structures** "Alstom (Schweiz) AG, Brown Bovery Strasse 7, 5401 Baden, Switzerland Received 21 July 2006; revised manuscript received 24 December 2006; published 12 March 2007 {inter}.

[28] Desmond "**Heat Transfer** ", book second edition ,west publishing company, Minnesota ,United Stats of America ,1982.

[29]Qijun Yu . **"A Unit Cube-Based Model for Heat Transfer and Fluid Flow in Porous Carbon Foam"** notes from Department of Mechanical and Materials Engineering, The University of Western Ontario, London, ON, N6A 5B8. Research for Natural Science and Engineering Research Council of Canada (NSERC)

[30]S. Torquato, S. Hyun, and A. Donev **"Optimal design of manufacturable three-dimensional composites with multifunctional characteristics"** Princeton Materials Institute and Department of Chemistry, Princeton University, Princeton, New Jersey 08544 ,Journal of Applied Physics ,Vol. 94 ,No. 9 ,November 2003.

[31] Johon Hernlund ,Kurt Leinenweber ,Darren Locke and James A.Tyburczy **"A numerical model for steady-state temperature distributions in solid-medium high-pressure cell assemblies** "American Mineralogist, Vol. 91, pp. 295-305, 2006.

[32] J.P .Holman **"Heat Transfer** " book,, fourth edition McGraw-Hill, Inc, 1976.

[33] D. Anderson ,J. Tennchill , and R. Pletcher ,"Computational Fluid Mechanics and Heat Transfer ",Book,McGraw-Hill,1984.

[34]Omega **,"The Temperature Hand Book** "book, Omega Engineering Inc., Stamford ,CT ,06907,Pg.z-18,1998 {inter}.

[35] Alwan,A.A., **"Surface Temperature Transient in Laser Machining of Metals** ,"M.Sc. Thesis ,University of Glasgow,1989.

[36] J. Ziman, , **"The Thermal Properties of Materials,"** J . Scientific American ,Vol.217, No. 3, pp. 180–188 , September 1967.

[37] Barry B. Spencer ,Hsin Wang and Kimberly K. Anderson "**Thermal Conductivity of IONSIV® IE-911™ Crystalline Silicotitanate and Savannah River Waste Stimulant Solutions"** Metals and Ceramics Division, ORNL Date Published , November 2000.

[38] P . G. Klumens, High Temps.-High Press. **Thermal conductivity of dense and porous yttria-stabilized zirconia"** journal of materials science Vol.36 pp.3003-3010 ,2001.

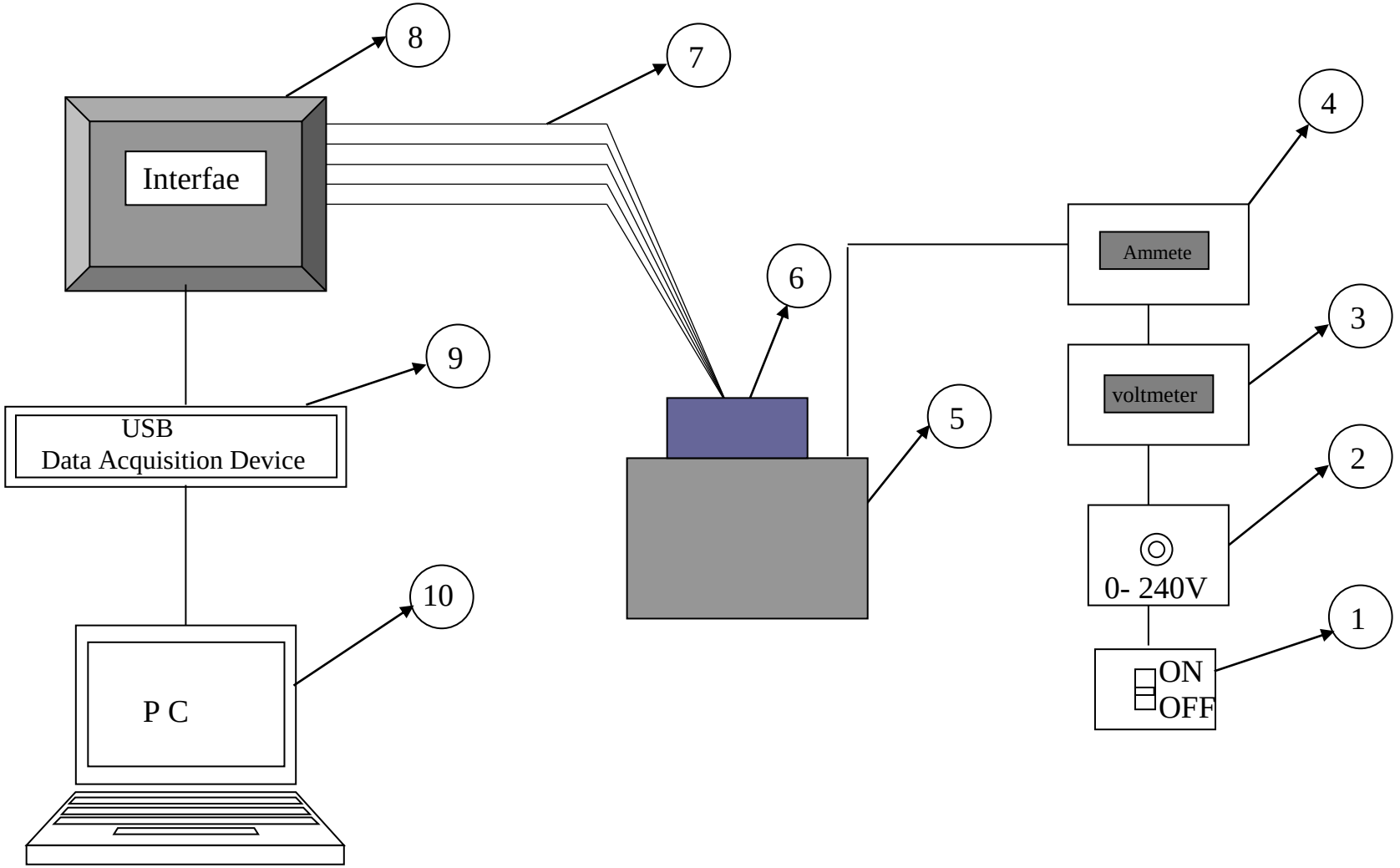

1	Power supply	2	Voltage control device	3	Voltmeter	4	Ammeter	5	Heater assembly
6	Test sample	7	Thermocouples	8	Interface	9	Data acquisition device	10	Computer

Figure (4-7) sechmatic digrame of rig

Chapter One

Introduction

Chapter Two

Literature Review

Chapter Three

Theoretical Work

Chapter Four

Experimental Work

Chapter Five

Results and Discussion

Chapter Six

Conclusions and Suggestions for Future Work

References

Appendences

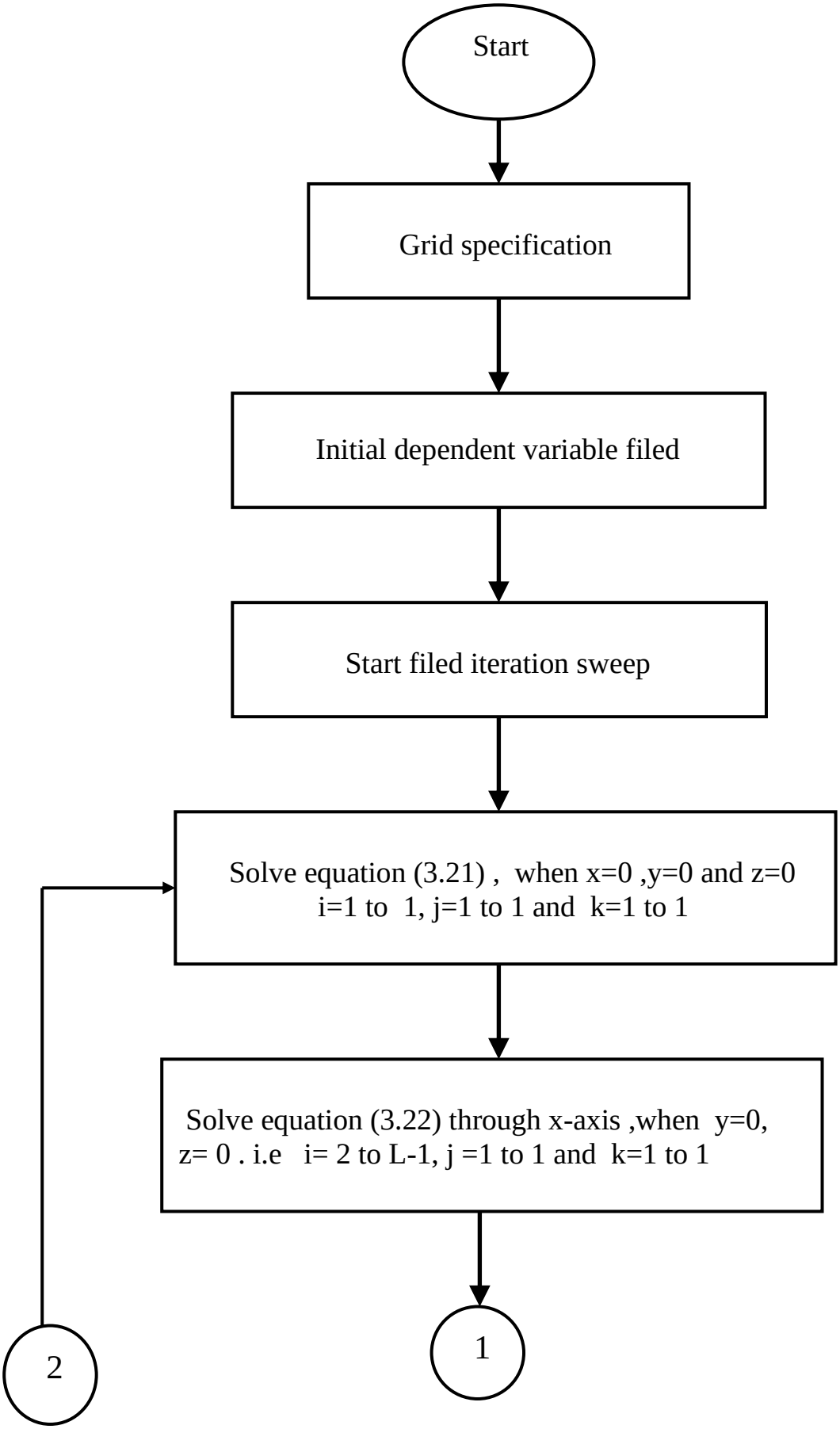

Figure (3-4) flowchart of the computer program of Cartesian model

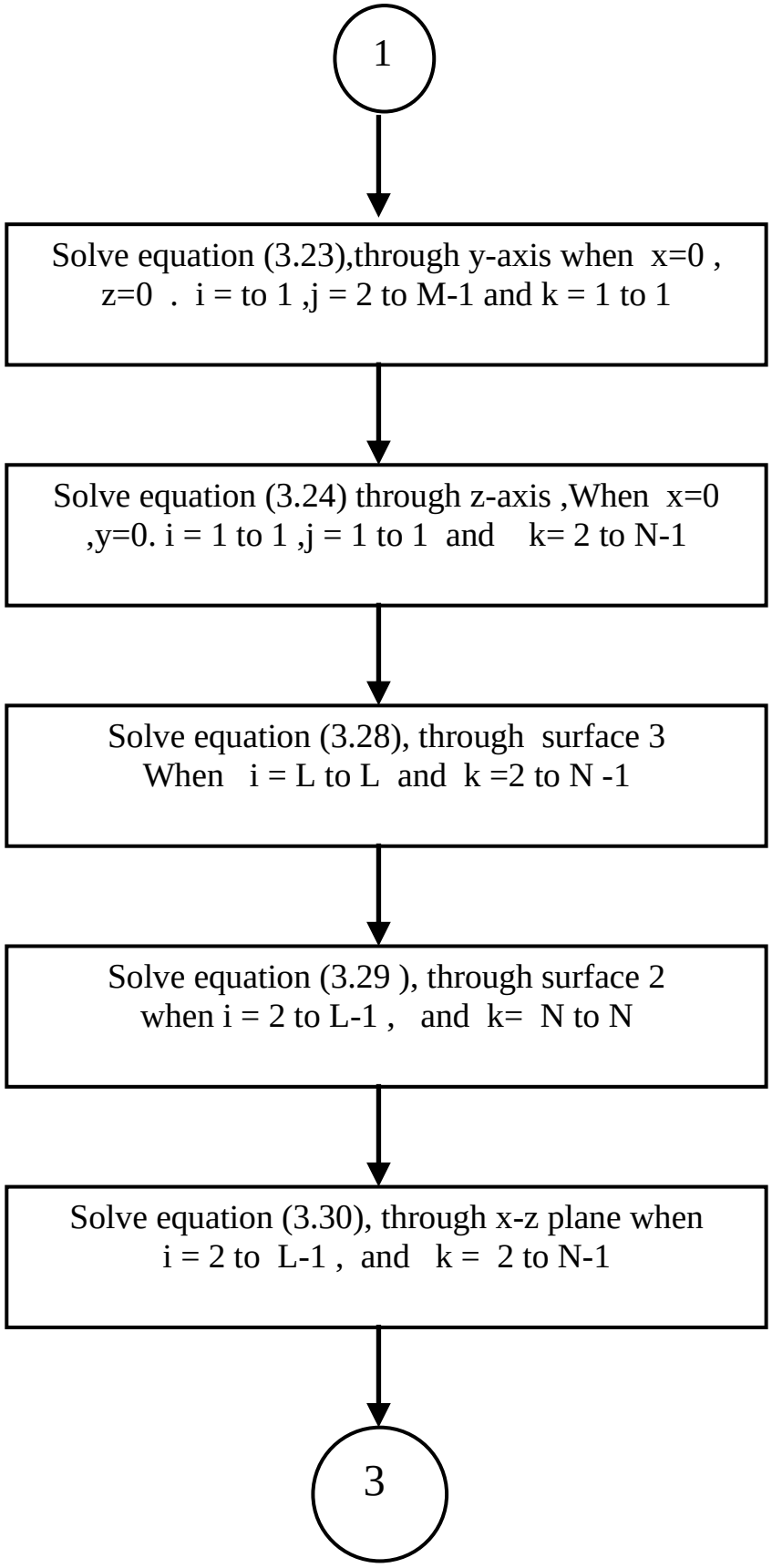

Figure (3-4) continued

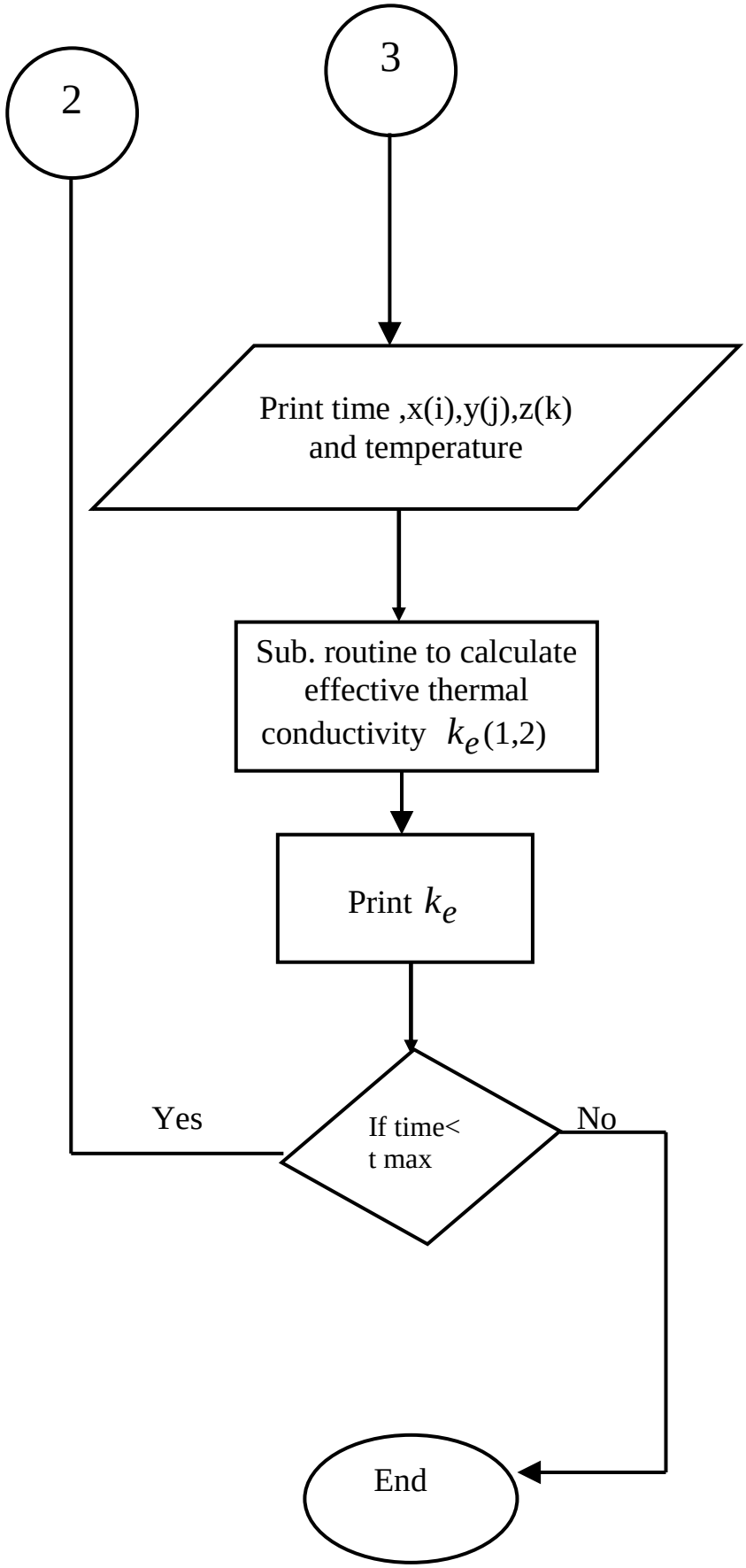

Figure (3-4) continued

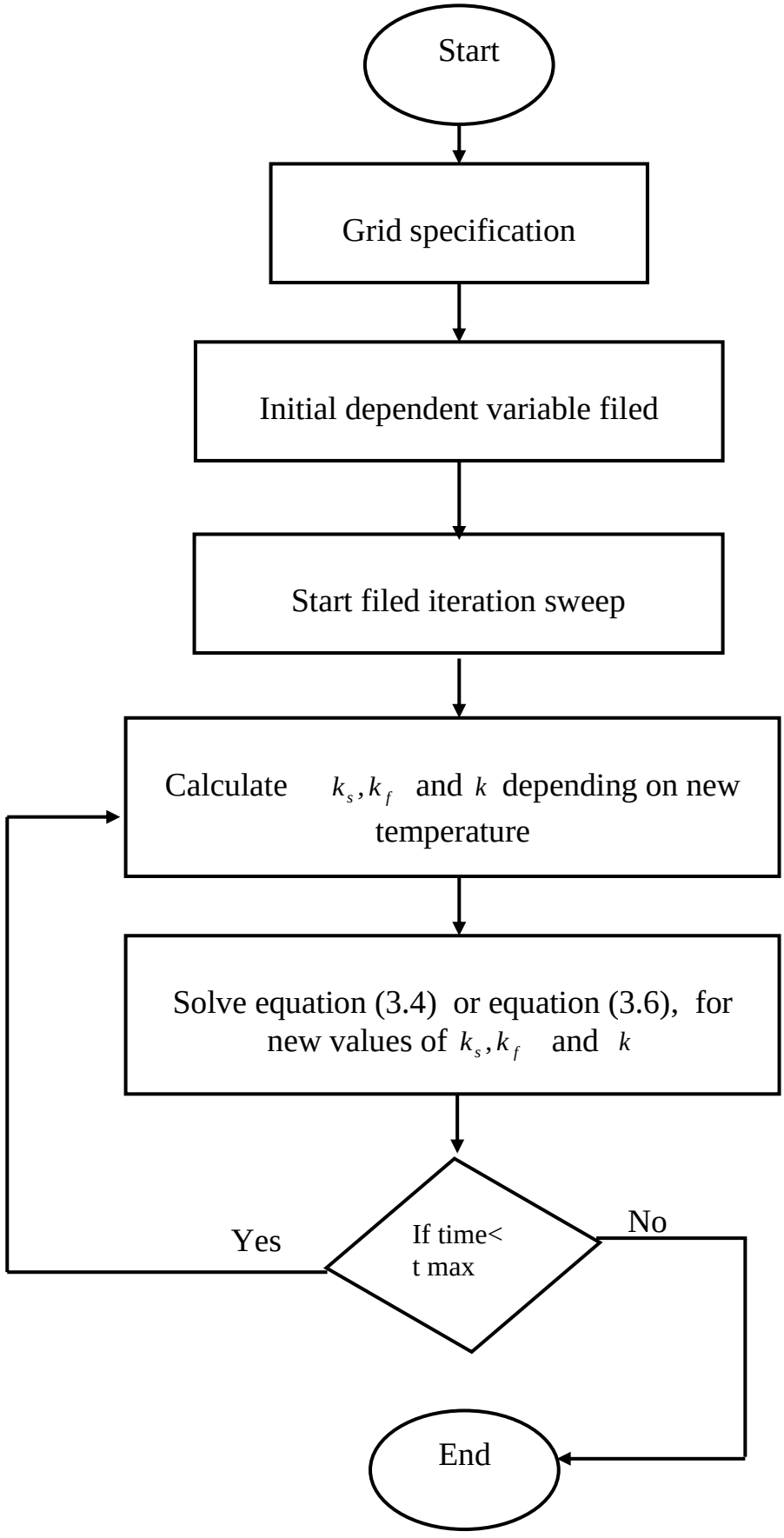

Figure (3-5) flowchart of subroutine computer program to calculate effective thermal conductivity according method number one or two